# CHAPTER I

# INTRODUCTION

## 1.1 DEVELOPMENT OF AN ENGINEERED SOFT TISSUE IMPLANT

An engineered oral mucosal tissue implant has the clinical potential to repair and/or replace tissues. Many of those in need of soft tissue transplants have suffered from disease, congenital genetic defects, and accidents. Soft tissue transplantation is an established and successful procedure that represents the causal and curative therapy for many of these diseases and conditions which lead to soft tissue failures.

The versatility of the oral mucosa for soft tissue transplantation has been clinically demonstrated in its use in vaginoplasty (Lin et al 2003). Further mechanical tests to determine mucosal tissue adaptability to other anatomical

areas is required for better understanding of the tissue properties and for successful long-term durability of the tissues within the transplanted area. The use of the scanning acoustic microscope (SAM) is one potentially effective tool to examine microscopic properties of tissues and test for mechanical effects. This includes examining the changes in the acoustic effects of natural oral muosal and comparing them to the engineered oral tissues. In the latter case, we are specifically examining and testing the currently designed *ex vivo* produced oral mucosa equivalents (EVPOME) used for intraoral surgical grafting procedures (Figure 1a) (Ward, et. al 2002). EVPOME is a composite human oral mucosa equivalent, which includes a dermal component consisting of an acellular allogenic dermal matrix under the patented brand name, AlloDerm® (LifeCell Corp., Branchburg, NJ, USA). AlloDerm® is a human dermis device that has been enzymatically decellularized to remove the risk of rejection and inflammation to patients who receive it as a transplant; a histology image of the AlloDerm® is seen in Figure 1b (Winterroth et al 2009). It is made from pathogen-screened cadaveric skin and freeze-dried through a patented process that does not damage the crucial elements of the tissue structure, including the distribution and architecture of the collagen bundles (Wagner, et. al 2010). To develop the EVPOME devices, AlloDerm® is seeded with autogenous human oral keratinocytes to form an overlying stratified parakeratinized epithelial layer. Further details of the seeding and development of the EVPOME are discussed under Chapters II - IV.

An engineered oral mucosal tissue implant has the clinical potential to repair and/or replace tissues. Many of those in need of soft tissue transplants have suffered from disease, congenital genetic defects, and accidents. Soft tissue transplantation is an established and successful procedure that represents the causal and curative therapy for many of these diseases and conditions which lead to soft tissue failures (Izumi et. al. 2003, Izumi et. al. 2004).

## 1.2 HISTOLOGICAL AND CHEMICAL COMPOSITIONS OF SKIN AND ORAL MUCOSAL TISSUES

### 1.2.1 Background on Skin and Oral Mucosa

Both the skin and oral mucosa are composed of multi-layered tissues; the former is the single largest organ of the human body, accounting for 16-20% of the total body mass. Both tissue types are comprised of stratified squamous cell layers, particularly at the apical surfaces (Hammersen, 1989).

A histology image of the human palate (Figure 2) provides an example of the stratified cells which typically comprise this tissue (Ward et al 2002). The superficial epidermis forms an uninterrupted barrier that ranges in thickness from 0.07 mm to 0.12 mm over much of the body surface and contributes little to the mechanical properties (Hammersen 1989). Below the epidermis is the dermis, which is between 1 mm and 4 mm thick: the dermis is composed of the papillary and reticular layers. The papillary dermis forms the upper layer, which comprises

about 10% of the full dermal thickness. It contains thin collagen fibrils 20–40 nm in diameter that are packed into thicker collagen fibers 0.3–3.0 nm in diameter. Below the papillary layer is found the reticular layer, which contains collagen fibrils 60–100 nm in diameter. Reticular collagen fibrils are composed primarily of type I collagen and have fiber diameters between 10 nm and 40 nm. Type III collagen accounts for only about 15% of the dermal collagen, much of which is found in the papillary layer. In the young adult, the collagen in the papillary dermis appears as a feltwork of randomly oriented fine fibers while that in the reticular dermis consists of loosely interwoven, large, wavy, randomly oriented collagen bundles. Increased collagen fiber density is observed with increased age, which is reported to reflect a decrease in the spaces between individual bundles. The mean fractional volumes of collagen fibers determined from stereological data is reported to be relatively constant for both papillary and reticular dermis and is between about 66% and 69% for all age groups studied. Collagen fibers are observed to be more compact with increased age and appear to unravel.

Elastic tissue in oral and vaginal mucosa and skin consists of superficial thin bundles of microfibrils that become associated with progressively larger amounts of amorphous elastin and increase in size from the papillary to reticular dermis. The relative volume of elastic fibers increases from about 0.7% to about 2.5% while the diameters increase from about 1 nm to 2 nm, going from the

papillary to the reticular dermis. The volume fraction increases with age up to about 1 year, then appears to plateau. The density of elastic fibers in the papillary dermis decreases from about 2.5% to about 2% for individuals older than 10 years. Elastic fibers of older individuals appear to fray and contain holes.

#### 1.2.1.1 Background on Oral Mucosal Anatomy

The oral mucosal epidermis is composed of a keratinized stratified squamous epithelium. Its cells, keratinocytes, are arranged into 4 (thin skin) or 5 (thick skin) layers. The outermost layer is always composed of non-living, highly keratinized (cornified) cells that function to reduce water loss (Warner et. al. 1988). After keratinocytes leave the germinal layer, they undergo a specialized form of cell death known as anoikis. Anoikis is initiated when cells detach from their surrounding environment and lose communication with it (Tortora et. al. 1993). In keratinocytes, this programmed cell death is accompanied by the accumulation of keratin to the exclusion of all other products and organelles (Broekaert et. al 1988, Holland et al 1997, Norlén et al 2004).

The stratified layers of natural oral mucosal cells and tissues lie in both the epidermis-dermis and include the following constituents:

1. Basement membrane complex at the dermal-epidermal junction

a. Type IV collagen

b. Laminin

c. Type VII collagen

i Fibrils

ii. Filaments: Ensure physical bonding between dermis and epidermis

d. Vascular plexus – found mostly in the dermis

2. Matrix components found within both epidermis and dermis tissues

a. Collagen fibrils

b. Elastin network

i. Elastin

ii. Microfibrillar fibers

iii. Proteoglycans

#### 1.2.1.2 Background on the Human Dermis and its Comparison to AlloDerm®

The dermis is the thick layer of connective tissue to which the epidermis is attached. Its deepest part continues into the subcutaneous tissue without a sharply defined boundary. Its thickness is for this reason difficult to determine but 1-2 mm is a good estimate for human skin. Figure 1 illustrates the histology of the human dermis and its principal components. The dermis may be divided into two sublayers (again without a sharp boundary):

1. The papillary layer: consisting of loose, comparatively cell-rich connective tissue, which fills the hollows at deep surface (dermal papillae) of the epidermis. Capillaries are frequent. Collagen fibers appear finer than in the reticular layer.

2. The reticular layer: appearing denser and containing fewer cells. Thick collagen fibers (5-10 µm) often aggregate into bundles (up to 100 µm thick). The fibers form an interlacing network, although their predominant direction is parallel to the surface of the skin. A preferred orientation of the collagen fibers is not visible in the sections, but the main orientation of the fibers differs in skin from different parts of the body. Usually, their main orientation will follow the "lines of greatest tension" in the skin (Kraissl lines). This is of some surgical importance since incisions parallel to these lines will heal faster and with less formation of scar tissue.

#### 1.2.1.3 Background on EVPOME

The development and use of an *ex vivo* produced oral mucosal equivalent (EVPOME) has demonstrated its clinical efficacy in intra-oral surgical grafts (Hotta et. al 2007, Izumi et. al. 2003). In addition, oral mucosa tissues have been clinically reported to be suitable for transplantation to treat vaginal agenesis (Lin et. al. 2003). The oral mucosa's histology resembles that of skin: as new cells are formed on the basal lamina, the more matured cells migrate toward the apex, undergoing apoptosis and keratinization they migrate (Izumi et. al. 2004); this same process occurs in the EVPOME tissues. Figure 1 provides an illustration comparing the EVPOME device with natural oral mucosa tissue; in

both cases, there is a basal layer of actively dividing and differentiating cells, followed by a uniformly keratinized apical layer. What is still unknown is EVPOME's effectiveness as a substitute tissue replacement for other soft tissues such as dermal, vaginal, or urethral; they have not been tested for non-linear elastic characteristics. Although the oral mucosa's histology resembles that of human epidermis and both tissue types are derived from ectodermal tissues, similarities in their physical properties have yet to be compared.

## 1.3 THE NECESSITY OF TISSUE RECONSTRUCTION AND ENGINEERED TISSUE MATRICES

One of the principal concerns among medical professionals is treating soft tissue injuries among soldiers -particularly victims of explosive devices. In a recent study analyzed by the Joint Theatre Trauma Registry database for maxillofacial battle-injuries (BI) experienced by U.S. soldiers in Iraq/Afghanistan, approximately 26% had maxillofacial BI. There were 4,783 maxillofacial BI among the 2,014 BI, which translates into 2.4 maxillofacial injuries per soldier (Jenkins, et. al. 2010). As a result, there is an immediate and significant need for an engineered soft tissue equivalent to rapidly and effectively treat BI maxillofacial victims.

Biomechanical studies suggest that the initial portion of the stress-strain curve of skin is highly viscoelastic with a high viscous dissipation occurring during collagen fibril alignment (Fung 1990). The stress-strain behavior of skin is

composed of three phases. Up to strains of about 0.3 the collagen network offers little resistance to deformation and the behavior is dominated by the elastic fibers. Between strains of about 0.3 and 0.6 the collagen fibrils begin to offer resistance to deformation. During the linear portion of the stress-strain curve, the elastic component dominates the deformation and appears to involve stretching of the flexible regions of cross-linked collagen molecules. In tendon, the viscous component of the stress-strain behavior is associated with fibrillar slippage. In the yield and failure region (strains above 0.6), fibril defibrillation occurs. While it is clear from inspection of stress-strain curves that the behavior of skin and tendon are quite different (Lieber, et al 2003, Fung 1990), it is not clear whether the elastic spring constant for collagen molecules in tendon (7 to 8 GPa) is different from that for collagen in skin.

## 1.4 BACKGROUND ON ULTRASOUND: INSTRUMENT IN NON-DESTRUCTIVE TESTING

Non-destructive testing utilizes various non-invasive measurement techniques. These include ultrasonic waves (sound waves above 20 kHz) and radiography to determine the integrity of a component, structure, or material without destroying the usefulness of the tissues.

A transducer produces high frequency sound waves which interact with the tissue sample. High frequency sound waves cannot propagate through air, hence a couplant is used to carry the high frequency sound waves. Water is the

most common couplant for immersion testing. Transducer frequencies are based on two basic groups – high and low - which provide opposite parameters:

1. Higher frequencies (usually > 50 MHz): Higher resolution, shorter focal lengths, less penetration

2. Lower frequencies (generally <15 MHz): Lower resolution, longer focal lengths, greater penetration

### 1.4.1 Characteristics of Ultrasonic Waves

Ultrasound waves propagate through liquids and solids. and reflect at boundaries of internal flaws and change of material. Ultrasound capabilities include the ability to be focused, straight transmission, suitable for real-time processing, essentially harmless to the human body, and non-destructive to material.

Whenever a sudden change in acoustic impedance is encountered, like at the boundaries of tissues, a portion of sound is reflected and the remainder propagates through the boundary. Ultrasound scans consist of the following waveforms:

1. RF (radiofrequency) Signal - The raw ultrasonic data. The presentation of unrectified signals on a display.

2. A-Scan**-** A display in which the received pulse amplitude is represented as a displacement along one axis (usually the y-axis) and the travel time of the ultrasonic pulse is represented as a displacement along the other axis (usually the x-axis).

3. B-Scan **-** The travel time of an ultrasonic pulse, represents a map of echo amplitude as a function of position in the region being scanned. The B-scan is in one axial & one lateral dimension.

4. C-Scan - Data from a specified depth over the entire scan area. (Horizontal cross-section); C-scan is in both lateral dimensions.

Ultrasonic waveforms consist of three principal signals. The first signal is commonly referred to as the initial pulse and occurs at zero microseconds. The second signal is commonly referred to as the front surface. This represents the first interface the sound encounters. The third signal would be considered the area of interest. A data gate would be positioned over this signal or group of signals for evaluation. Ultrasonics includes acoustic reflections, acoustic waveforms, and image display. Further details on ultrasound background, with specific emphasis on acoustic microscopy is discussed in Chapter II.

### 1.4.2 Focusing the Transducer

Focusing an ultrasonic transducer is similar to focusing an optical microscope. When the focus is reached, the signal will reach a maximum value.

The ultrasound beam can be focused on or within the specimen at a fixed distance from the transducer called the focal zone. Further details on focusing the transducer on tissues is discussed under Chapters II and III

### 1.4.3 Background: Utilization of the SAM

The SAM produces images with resolution similar to a good optical microscope using ultrasound, typically in the 50 MHz to 1 GHz range; specifically 61MHz for the in-house model used for most of the experiments conducted in this study. Ultrasonic focusing has the opposite curvature of optical focusing: to get the same type of focusing from a convex optical lens you need a concave acoustic lens. However, because the images come from an acoustic signal, contrast arises from variation in the acoustic properties of the material and features may be revealed that are not visible in an optical microscope. In cells and tissues, such changes in acoustic features may derive from different anatomical tissues. The advantages to using SAM include its potential to examine various cells and tissues based on differences in their properties, providing a better understanding of the comparisons between tissues (ie: soft tissues which are anatomically similar, but found in different regions of the human body). Acoustic microscopy complements conventional optical microscopy, but does not necessarily replace it. Additionally, the SAM will be used to examine the elastic properties of mucosal tissues (both oral and uterine) and compare both natural and engineered tissue elastic characteristics. These

aims include the following studies: Based on earlier SAM experiments on the cornea, similar techniques will be applied toward *in vitro* soft tissue measurements of the oral mucosa tissues (both natural and engineered) and subsequently toward the vaginal tissues and the uterine lining. Additionally, The SAM will be used to produce high-resolution strain images of mucosal tissues (oral and vaginal) – both engineered and natural. This will lead to determining linear elastic properties of these tissues. SAM images would be compared to histology sections examined using a standard optical scope.

## 1.5 BACKGROUND ON ULTRASONIC METHODS TO ESTIMATE ELASTICITY

Ultrasound does not image tissue elasticity (shear or Young's modulus) directly because the contrast mechanism is primarily related to changes in bulk modulus, rather than shear elastic modulus. Ultrasound imaging systems can indirectly estimate and image elastic properties of tissue using ultrasonic measurements of externally or internally induced internal tissue motion. The ultrasound elasticity microscope was developed to image tissue stiffness at high resolution (Cohn et al 1997).

The hypotheses tested on this experimental system have direct application to an eventual real-time, clinical system. This experiment is a critical initial test in the development of the ultrasound elasticity microscope for understanding the physical characteristics of soft tissues.

The tissues are deformed by a flat plate with a narrow slit (approximately 20.0 mm in length and 2.0mm wide) machined in it. For controlled deformation, the plate is coupled by an arm to a precision sled and stepper motor. Poor acoustic impedance matching between water and the metal plate would cause most of the ultrasonic signal to be reflected from this boundary. To avoid this signal loss, the transducer produces the images through the 2.0-mm wide slit within the center of the compression plate. To avoid reflection of side lobes from either side of the slit, 1-mm wide images were acquired in the center of the slit. This geometry reduces out-of-plane motion. Tissue in contact with the plate undergoes compression, whereas tissue in the middle of the slit bulges into it, producing tissue deformation. Out-of-plane motion along the slit is confined by adjacent tissues; differences in the tissue composition (such as stratified cells and the presence of subcellular components) could potentially amplify this out-of plane motion (Hollman et al 2002).

### 1.5.1 Additional Compression Testing

Further compression tests involve using an in-house built compressor with a cylindrical piston to indent the tissue sample at steps of a known equal length, registering as increasing changes in mass (in grams) on an electronic scale. This will provide different degrees of surface displacement on the tissue specimens.

The tissue sample is cylindrical in shape with an area (A) slightly larger than that of the piston. The piston is mounted directly over the center of the sample and pushes on the sample, producing a known amount of force at each of the indentation steps. This force plus knowing the degree of surface displacement provides the stiffness characteristic for the given samples. This set-up is derived from the experiments originally performed by Erkamp (Erkamp et. al.1998) in which a tissue phantom was indented while mounted on top of a glass slide.

### 1.5.2 Measurement of Young's Modulus in Soft Tissues

Young modulus (E) measures the elasticity as one mechanical property of a tissue: the stress – strain relationship. However, Young's modulus is but one tissue property and it remains to be seen whether it will be the parameter best predictive of erosion rate. These measurements for natural tissues will also be examined for the acellular dermal grafts and will be compared to both oral mucosal and uterine tissues).

## 1.6 EXAMINATION OF BIOENGINEERED SOFT TISSUES

Biologic substitutes of human skin and mucosa have a common set of requirements for the duplication of anatomic structures and physiologic functions that they are to emulate. For use in wound closure, the first definitive requirement is reestablishment of the epidermal barrier to fluid loss and microorganisms as

well as alleviating pain and enhancing wound healing. In full-thickness skin loss, replacement of both the epidermis and dermis is the preferred approach. Replacement of these tissue compartments must also minimize scar formation and restore acceptable function and cosmesis. A major advantage of the use of substitutes in wound closure is to reduce or eliminate the donor site for skin and mucosa grafts. If one is successful in the elimination or minimization of donor site morbidity this could shorten recovery time and reduce the length of operative procedures.

Approaches that have been used in the fabrication, manufacturing, and tissue engineering of skin and mucosa substitutes can be classified as *in vitro* culturing of autologous and allogeneic keratinoctyes, *in vitro* tissue engineering of dermis composed of either artificial (collagen, glycosaminoglycans, polymers of polyglycolic and polylactic acid) or allogeneic acellular dermis, and a bilayer of skin or mucosa. Three essential components are known to be necessary to engineer human skin and mucosa: cells, an extracellular matrix, and cytokines.

When examining the structure and function of related soft tissues (namely the natural and engineered oral mucosa), we need to determine:

1. What are the subcellular components of its matrix?

2. What is natural tissue composed of (the characterization of oral and vaginal mucosal tissues)?

3. What are the linear elastic properties?

4. Can these measurements be done on engineered tissues?

5. What are the mechanical properties of AlloDerm®/EVPOME (with comparisons to natural oral mucosal tissues)?

6. Strength to failure of EVPOME; what is the pliability of the matrix?

As EVPOME is derived from a foundation containing AlloDerm®, it should contain similar concentrations of matrix seen in human dermis. EVPOME contains an additional seeding of oral mucosal cells on the basal surface of the AlloDerm® matrix. This addition of cells has been shown experimentally to affect the elastic properties of the AlloDerm®.

### 1.6.1. Brief Overview on the Biomechanical Properties of the Skin and Mucosal Tissues

Because there are no previous stress-strain models for either natural or engineered oral mucosal tissues to compare our studies to, we examined the stress-strain models of skin for the comparisons to natural and engineered oral tissues (Silver et. al. 2001).

Biomechanical studies suggest that the initial portion of the stress-strain curve of skin is highly viscoelastic with a high viscous dissipation occurring

during collagen fibril alignment. The stress-strain behavior of skin is composed of three phases (Kvistedal et. al. 2004, 2009). Up to strains of about 0.3 the collagen network offers little resistance to deformation and the behavior is dominated by the elastic fibers. Between strains of about 0.3 and 0.6 the collagen fibrils begin to offer resistance to deformation. During the linear portion of the stress-strain curve, the elastic component dominates the deformation and appears to involve stretching of the flexible regions of cross-linked collagen molecules. While it is clear from inspection of stress-strain curves that the behavior of skin and tendon are quite different, it is not clear whether the elastic spring constant for collagen molecules in tendon (7 to 8 GPa) is different from that for collagen in skin.

Further SAM-based tests will be performed to correlate the evolution and differentiation of EVPOME determined with changes in its cellular morphology. These would include examining and comparing how the cells and tissues look over certain time points (ie: 1-day, 2-days, 4-days, 7-days, and 11-days post-seeding); all work performed under sterile conditions. Current and future studies to better understand soft tissues' physical and biological properties require studying these principal factors:

1. Examining whether regenerated mucosal tissues come close to mimicking natural tissues
2. Need to determine what the cell turnover rates are in the skin and compare them to the oral cavity

3. Examining the normal mucosal tissues of the uterus and comparing the deformation characteristics
4. Future studies will consider the mechanical properties of other comparable soft tissues (ie: ureter, vaginal mucosal tissues)

## 1.7 OVERVIEW OF THE DISSERTATION

This work describes applications of an in-house built SAM to examine the morphologies of EVPOME and the unseeded AlloDerm® device and compare them to histology counterparts, to quantify and compare the mean surface irregularities on AlloDerm® and on developing and fully mature EVPOME from both SAM and histology images. Additional studies involve examining using SAM to examine the surface characteristics of EVPOME which have undergone thermally stressed conditions compared to unstressed controls. Examining the stiffness properties of the AlloDerm® - the degree of stress as a result of increasing strain – and comparing it to EVPOME and natural mucosal tissues are also considered.

In Chapter II, details of the overall experimental setup and the methods to quantify the aforementioned surface irregularities on both AlloDerm® and EVPOME are discussed. This includes a general description on the benefits and limitations of using a single-element focused ultrasound in the experiment set-up and execution. Included are materials on acoustical characterization of the

transducer, methods for quantifying the degree of surface irregularities on the tissue specimens, and statistically correlating the quantifying methods used, both with SAM and optical microscopy.

Chapter III amends the methods used in the Introduction and in Chapter II, examining the surface characteristics of the EVPOME after being subjected to a thermally elevated environment for a brief period of its development (stressed), then comparing its results to those of EVPOME developed under standard physiological conditions (unstressed) and to unseeded AlloDerm®.

Chapter IV further examines the thermal stress studies on EVPOME, specifically using an analyses algorithm to fit and subtract the planar surfaces of the aforementioned three tissue specimens, followed by using filtering methods to improve the surface images of each specimen. This is done to more accurately image and reproduce the surface conditions of each specimen detected using SAM.

Examining the tissues elastic properties are the main focus of Chapter V. These include experimental measurements of internal displacement and strain using both SAM and an in-house compressor unit. SAM is also used to examine the thickness and stratifications of the tissues, in particular mature EVPOME, along with natural oral tissues. The stiffness of the AlloDerm® is examined and compared to EVPOME and natural tissues as are the latter tissues' incompressibility. Further, 3D reconstructions of the individual tissues and their respective deformations during compression are mapped out. Measurements of

Young's modulus for each tissue are taken into account, including limitations of the SAM as a means to qualitatively analyze strain.

Conclusions and future studies are considered in Chapter VI, including the aforementioned possibility of using SAM to monitor cell/tissue growth and development under aseptic conditions. The non-destructive/non-invasive qualities of ultrasound serve as a vehicle to image and assess biological materials more accurately as they appear *in vitro*. Finally, long-term studies will consider SAM imaging and monitoring cell and tissues *in situ* to better understand and assess their functions in living systems. Such cases would provide strong support for SAM as an effective tool for any biological/medical laboratory involved in microscopy.

## REFERENCES


Broekaert, D., Van Oostveldt, P. Nuclear Differentiation During Epidermal Keratinization. *Arch. Dermatol. Res.* 1988. 280:188-189.

Cohn, N.A., Emelianov, S.Y., Lubinski, M.A., O'Donnell, M. An Elasticity Microscope. Part I: Methods. *IEEE Trans. Ultrason. Ferr. Freq. Ctrl.* 1997. 44(6): 1304-1319.

Erkamp RQ, Wiggins P, Skovoroda AR, Emelianov SY, O'Donnell M. .Measuring the Elastic Modulus of Small Tissue Samples. *Ultrasonic Imaging*. 1998; 20(1):17-28.

Fung, Y.C. *Biomechanics: Motion, Flow, Stress, and Control.* NY. Springer-Verlag. 1990. 569pp.

Hammersen, F. *Histology Color Atlas of Microscopic Anatomy, 3rd ed*. Baltimore: Urban and Schwartzenberg. 1989. 260pp.

Holland, M.R., Hall, C.S., Lewis, S.H., Handley , S.M., Finch-Johnston, A.E., D'Sa, A.P., Perez, J.E., Miller, J.G. Comparison of Integrated Backscatter Values Obtained with Acoustic Densitometry with Values Derived from Spectral Analysis of Digitized Signals from a Clinical Imaging System. *J. Amer. Soc. Echocardio.* 1997. 10(5): 511-517.

Hotta, T., Yokoo, S., Terashi, H., Komori, T. Clinical and Histopathological Analysis of Healing Process of Intraoral Reconstruction with *Ex Vivo* Produced Oral Mucosa Equivalent. *Kobe J. Med. Sci.*, 2007. 53(1): 1-14.

Izumi, K., Feinberg, S.E., Iida, A., Yoshizawa, M. Intraoral Grafting of an *Ex Vivo* Produced Oral Mucosa Equivalent: A Preliminary Report. *Int. J. Oral Maxillofac. Surg.* 2003. 32: 188–197.

Izumi, K., Song, J., Feinberg, S.E. Development of a Tissue-Engineered Human Oral Mucosa: From the Bench to the Bed Side. *Cells Tissues Organs.* 2004. 176:134–152.

Jenkins, D.H., Bolenbaucher, R.M., Cotner-Pouncy, T. Trauma System Development in a Combat Theater. 2010. *www.amtrauma.org/courses/article_combatTheater.doc*

Kvistedal Y.A., Nielsen P.M. Investigating Stress-Strain Properties of in-vivo Human Skin using Multiaxial Loading Experiments and Finite Element Modeling. *Conf Proc IEEE Eng Med Biol Soc*. 2004;7:5096-9.

Kvistedal Y.A., Nielsen P.M. Estimating Material Parameters of Human Skin in vivo. *Biomech Model Mechanobiol.* 2009 Feb;8(1):1-8.

Lieber, R.L., Burkholder, T.J. Musculoskeletal Soft Tissue Mechanics. In: Schneck, D.J., Bronzino, J.D. *Biomechanics Principles and Applications.* NY: CRC Press 2003. pp. 99-106.

Lin, W.C., Chang, C.Y.Y., Shen, Y.Y., Tsai, H.D. Use of Autologous Buccal Mucosa for Vaginoplasty: A Study of Eight Cases. *Human Reproduction*. 2003. 18(3): 604-607.

Norle´ n, L., Al-Amoudiz, A. Stratum Corneum Keratin Structure, Function, and Formation: The Cubic Rod-Packing and Membrane Templating Model. *J Invest Dermatol*. 2004. 123:715 –732.

Silver, F.H., Freeman, J.W., DeVore, D. Viscoelastic Properties of Human Skin and Processed Dermis. *Skin Res. and Tech.* 2001; 7: 18–23.

Tortora, G.J. & Grabowski, S.R. *Principles of Anatomy and Physiology (7th Edition)*. NY: Harper-Collins College Publisher. 1993. 1050 pages.

Wagner CT., Owens RT., Harper JR, McQuillan DJ. Human-derived acellular matrices for dermal replacement. 2009; page 142-173 in *Biomaterials for Treating Skin Loss*; CRC Press; Editors D. Orgill and C. Blanco.

Ward, R.B., Feinberg, S.E., Friedman, C.D.. Tissue Matrices for Soft Tissue and Mucosal Augmentation and Replacement**.** *Facial Plast Surg* 2002; 18: 003-012.

Warner, R.R., Myers, M.C., Taylor, D.A. Electron Probe Analysis of Human Skin: Determination of the Water Concentration Profile. *J. of Invest. Dermatol.* 1988. 90: 218–224.

Winterroth, F., Hollman, K.W., Izumi, K., Feinberg, S.E., Fowlkes, J.B., Hollister S.J.. Examination and Comparisons of EVPOME/ AlloDerm® Compositions with Natural Mucosal Tissues Using Scanning Acoustic Microscopy. *Society for Biomaterials Annual Meeting and Exposition*. April 2009.

## FIGURES

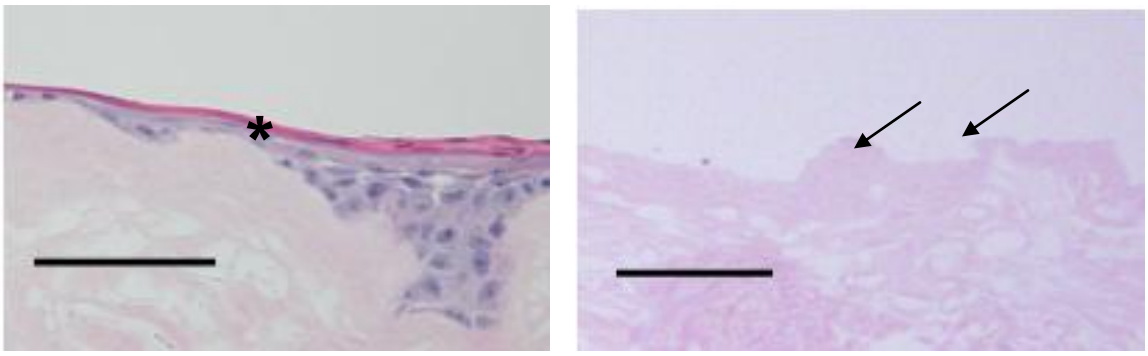

a b

**Figure 1.1. Histological representations of a mature EVPOME (a) and an unseeded AlloDerm® scaffold (b). For the former, there is a smoother surface (asterisk), the result of the space filling and keratinization properties of the seeded cells. The latter shows greater surface irregularities (arrows). Scale bars represent 100 μm.**

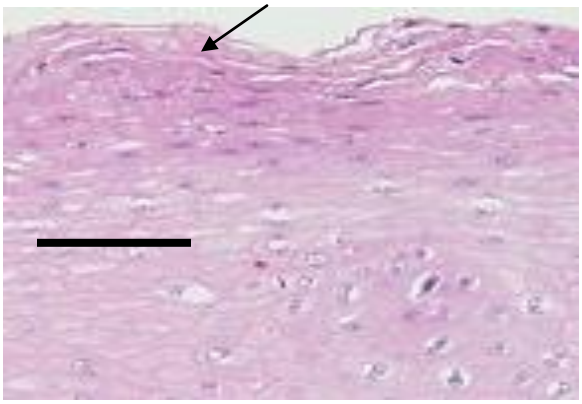

**Figure 1.2. Histology image of human palate tissue. Like the mature EVPOME, the surface shows less presence of nuclei - the result of keratinization - and the cells are more squamous in appearance (arrow). Scale bar equals 100 μm.**

# CHAPTER II

# EXAMINATION AND CHARACTERIZATION OF HUMAN MUCOSAL TISSUE DIFFERENTIATION USING SCANNING ACOUSTIC MICROSCOPY

## 2.1 INTRODUCTION

Ultrasound in the frequency range of 20-100 MHz has been shown to detect changes in cells and tissues undergoing apoptosis (Czarnota, et. al. 1997, Kolios,, et. al. 2002, Taggart, et. al. 2007). However, the changes in backscatter ultrasound intensity in epithelial cells undergoing apoptosis followed by keratinization have not yet been examined. Keratinized cells of the oral mucosa are histologically and physiologically similar to skin and are derived from the

same ectodermal tissues during embryologic development (Alur, et. al. 2001, Dill-Müller, et. al. 2007, Hoogstraate, et. al. 1998). The mechanical properties of both tissues have yet to be tested and compared, neither has there been any comparisons with other similar ectoderm-derived tissues such as the ureter and vaginal mucosal tissues.

Our overall objectives are testing engineered tissues *in vitro* - specifically an *ex vivo* produced oral mucosal equivalent (EVPOME), and for assessing tissue performance after their grafting, *in situ*. EVPOME had been successfully developed and applied to patients in clinical studies (Izumi, et. al. 2004). This can be performed using non-invasive and non-destructive testing procedures. For the former study, it is first critical to assess the structures of the tissues, which will be followed by testing any similarities to their functions. The comparisons of the tissues' similarities to natural mucosal tissues will be performed using methods which do not alter either the physical or chemical compositions of the tissues, thus more closely mimicking their structures *in situ*.

### 2.1.1 Background on the Oral Mucosal Epidermis and Keratinization

Keratinized oral mucosa consists of basal, spinous, and granular layers plus one keratinized layer without cells for keratinized mucosa; basal, intermediate, and superficial layers for non-keratinized mucosa (Presland, et. al. 2000). The outermost layer is always composed of non-living, highly keratinized (cornified) cells that function to reduce water loss (Warner, et. al. 1988). After

keratinocytes leave the germinal layer, they undergo a specialized form of cell death known as anoikis. Anoikis is initiated when cells detach from their surrounding environment and lose communication with it (Tortora, et. al. 1993). In keratinocytes, this programmed cell death is includes the formation of keratohyalin granules which produce keratin filaments within the cell body to the exclusion of all other products and organelles (Broekaert, et. al. 1988, Holland, et. al. 1997, Tu, et. al. 2009). Figure 2.1 provides an illustration of the oral mucosal lining, showing the principal cell layers – base to apex: stratum basale, stratum spinosum, stratum granulosum, and stratum corneum - above the basal lamina and the accumulation of keratin. Figure 2.2a shows a histology micrograph of healthy oral mucosa, showing the features of the aforementioned cell layers. Cells on the basal layer are more cuboidal in shape and mitotic. As these cells migrate toward the surface layer, they undergo differentiation, losing their water content, becoming more squamous in appearance, and accumulating keratin. When they reach the surface of the mucosal tissue, these keratinocytes have undergone anoikis and are more fully integrated into a uniform keratinized layer.

### 2.1.2 Background on EVPOME

The development and use of EVPOME has demonstrated its clinical efficacy in intra-oral surgical grafts (Hotta, et. al. 2007, Izumi, et. al. 2003, Izumi,

et. al. 2004). In addition, oral mucosa tissues have been clinically reported to be suitable for transplantation to treat vaginal agenesis (Lin, et. al. 2003). The oral mucosa's histology resembles that of skin: as new cells are formed on the basal lamina, the more matured cells migrate upward, undergoing apoptosis and keratinization as they migrate (Izumi, et. al. 2004); this same process occurs in the EVPOME tissues. Figure 2.2b provides a histology micrograph of EVPOME, comparing it with the aforementioned histology image of natural oral mucosa tissue. In both cases, there is a basal layer of mitotic and differentiating cells, followed by post-mitotic, differentiated cell layers, then an uppermost keratinized layer (Izumi, et. al. 2003, Izumi, et. al. 2004). What is still unknown is EVPOME's effectiveness as a substitute tissue replacement for other soft tissues such as dermal, vaginal, or urethral; they have not been tested for non-linear elastic characteristics. Although the oral mucosa's histology resembles that of human epidermis and both tissue types are derived from ectodermal tissues, similarities in their physical properties have yet to be compared.

We had earlier compared EVPOME's morphology to a commercially available acellular cadaver epidermis (AlloDerm®) and natural oral mucosa (Izumi, et. al. 2003, Winterroth, et. al. 2005). AlloDerm® comes from tissue donors; just after death, technicians remove a thin layer of skin and use antibiotics and other substances to remove cells and DNA that may cause rejection. We examined and compared the morphologies of EVPOME at different stages after seeding – 4 days, 7 days, 11 days, and 14 days - using scanning

acoustic microscopy (SAM). By comparing the radiofrequency (RF) backscatter at different stages of growth and development of the oral mucosal tissue, we can better understand changes in their physical compositions when it comes to contrasting their physical properties (Srivastava 2007). We can then quantify the cellular constituents among each of the tissue types and correlate how each contributes to the physical behavior of their respective tissues.

Although there are different biological tests to determine if cells undergo apoptosis or necrosis (Norle´ n, et.al 2004, Vermes, et. al. 1995), there is no method to noninvasively test cell death in tissues or organs. Further, there are no studies which microscopically record the maturation and development of any cells and tissues, either *in vitro* or *in vivo.*

### 2.1.3 Background on SAM

Acoustic microscopy has been used for decades, mostly to non-invasively assess the structures and properties of engineered materials (Quate, 1976). It is just in the last several years that such technology has also been applied to examine biological materials such as cells and tissues. SAM has been proven an effective tool to study both the morphology and non-linear elastic characteristics of natural and engineered oral mucosal tissues. The advantages of using SAM over conventional optical and electron microscopy include being able to image the cells and tissues without doing any preparations which could potentially kill or alter the tissues; this provides a more accurate representation of

the tissues' natural properties. It will also provide evidence as to the degree of differentiation which the cells are undergoing without chemically affecting its properties (Kolios, et. al. 2003, Saijo, et. al. 2004). The reflectivity off the top will analyze the degree of surface roughness: a strong linear correlation between the optical and SAM imaging results to quantify the surface characteristics.

The transducer's parameters are: 15 μm scanning step size in both the transverse and horizontal directions; a lateral resolution ($R_{lat}$) of 37μm; an axial resolution ($R_{ax}$) of 24μm; a depth of field of 223μm; the f-number is 1.5. Z-axis was sampled at 300 mega samples/second. $R_{ax}$ is the resolution in the direction of propagation and is determined by the length of the ultrasound pulse propagating in the tissue; $R_{lat}$ is the resolution orthogonal to the propagation direction of the ultrasound wave. Table 1 provides further details of the SAM's operating mechanisms, including axial and lateral resolutions, depth of field, and acoustic impedance.

#### 2.1.3.1 Sound Reflection and Backscatter

Whenever a sudden change in acoustic impedance is encountered, like at a material boundary, a portion of sound is reflected and the remainder propagates through the boundary. Acoustic material properties include:

- density (ρ)
- velocity of sound in material (c)

- acoustic impedance (Z)

The backscatter coefficient is the method by which material scatters energy from a sound wave. It was earlier hypothesized that the structural changes within apoptotic cells were responsible for the increase in backscatter observed (Kolios, et. al. 2002, Kolios, et. al 2003). However, the source of increased backscatter could also be due, in part, to changes in the spatial rearrangement of cellular and sub-cellular structures responsible for the scattered sound (Strohm, et. al. 2010). Acoustic backscatter results from the presence of acoustic impedance inhomogeneities in a tissue. Because transducers emit acoustic energy over a usually Gaussian-shaped spectrum about a nominal center frequency, the frequency dependence of backscatter can be determined from echo data by comparing the received backscatter spectrum to that emitted by the transducer (Huang et. al. 2010). Scattering theory shows that the size, concentration and relative impedance of impedance inhomogeneities affects the power spectrum of acoustic backscatter (Silverman et. al. 2009, Lizzi et al. 1983).

The mechanical property calculations were completed using established methods (Quate 1976) . The thickness, $d$, and the sound velocity, $c$, of the cell can be calculated using time resolved methods. The time of the echoes from the top of the cell, $t_1$, the substrate-cell interface, $t_2$, and a reference measurement from the substrate, $t_0$, are used in the following equations:

$$d = c_w /2 \, (t_0 - t_1),$$

$$c = c_w \, [(t_0 - t_1)/( t_2 - t_1)]$$

where $c_w$ is the sound velocity in the water.

Given the sound velocity travelling through the water and the acoustic impedance, the density $\rho$, and bulk modulus $K$ can be calculated:

$$\rho = Z/c$$

$$K = cZ = \rho c^2.$$

Previously, we used SAM to compare any changes in the RF data to the EVPOME and natural human oral mucosal cells in general undergoing differentiation, apoptosis, and keratinization (Winterroth, et. al. 2009b, Zuber, et. al. 1999). The spectral analysis results from SAM can be compared to histological images of the EVPOME tissues at different stages of growth and development. By correlating changes in the RF data to the EVPOME (and mucosal cells in general) undergoing differentiation, apoptosis, and keratinization, we can better understand the physiological processes of these cells as they evolve.

For this study, we examined, compared, and quantified surface irregularities in the apical morphologies of AlloDerm® - a commercially available acellular human cadaver dermis, and EVPOME – at different stages of

development - using SAM. By first comparing the morphologies of the oral mucosal tissues – both natural and engineered, we can establish a better understanding of the physical compositions when it comes to testing for similarities in the tissues' physical properties. We can then quantify the cellular constituents among each of the tissue types and correlate how each contributes to the physical behavior of their respective tissues. Correlating the changes in integrated backscatter to the differentiation of cells as they migrate and undergo apoptosis could lead to better methods to examine the stages of cellular differentiation.

## 2.2 Tissue Preparation – *Ex Vivo* Produced Oral Mucosal Equivalents (EVPOME)

The protocol for harvesting human oral mucosal tissue was approved by a University of Michigan Internal Review Board. All individuals signed informed consent before the tissue samples were procured. A keratinized oral mucosa sample was taken from an out-patient at the University of Michigan Oral and Maxillofacial Surgery Clinic. The methods for preparation have been described in greater detail previously (Izumi, et. al. 2004, Izumi, et. al. 2007). Briefly, oral mucosa keratinocytes were enzymatically dissociated from the tissue sample, and a primary cell culture was established and propagated in a chemically-defined, serum- and xenogeneic products-free culture medium, with a calcium

concentration of 0.06 mM. The AlloDerm® (acellular human cadaver dermis) was soaked in 5 $\mu g/cm^2$ human type IV collagen overnight prior to seeding cells to assist the adherence of cells, then approximately 1.5 x $10^5$ cells/$cm^2$ of oral keratinocytes were seeded onto the type IV collagen pre-soaked AlloDerm®. The composites of the keratinocytes and the AlloDerm® were then cultured, in the submerged condition, for 4 days with a calcium concentration of 1.2mM to form a continuous epithelial monolayer. At day 4, samples of the EVPOME were collected while in the submerged condition for SAM imaging. After 4 days, the equivalents were raised to an air-liquid interface to encourage epithelial stratification and cultured for up to 14 days, resulting in a fully-differentiated, well-stratified epithelial layer on the AlloDerm®. At Day 7 and Day 14 post-seeding, EVPOME samples were again collected for SAM imaging.

### 2.3 SAM Apparatus Set-up, Imaging, and Tissue Preparations

Details of the scanning and ultrasound system are similar to those described elsewhere (Cohen, et. al. 1982, Cohn, et. al. 1997a, Cohn, et. al., 1997b). AlloDerm®, EVPOME, and natural mucosal tissue samples were immersed in deionized water and imaged with a single element fixed focus transducer, producing ultrasonic B-scans. The transducer has an approximate frequency of 61 MHz, the element is 3 mm in diameter and focused to a depth of 4.1 mm, giving an f/number of approximately 1.4. The transducer was fastened

to an optical mount and the angular position was adjusted until the ultrasonic beam was normal to the deflecting plate. We scanned the surfaces of the AlloDerm® and EVPOME (at different days post-seeding) showing the acoustic signal between the interface of the sample and water on the sample's apical side. DC stepper motors accurately positioned the transducer above the specimen. B-scan images were obtained by stepping the transducer element laterally across the desired region. At each position, the transducer fired and an RF A-line was recorded. After repeated firings at one position, the transducer moved to the next position, where the image was constructed from A-lines acquired at all lateral positions. Because of low f/number, single element transducers have a short depth of field, a composite B-scan image was generated from multiple scans at different heights. The general SAM set up with the mounted tissue is illustrated in Figure 2.3. Differences in the acoustic patterns as they reflect off of the tissue and immersion tank boundaries (surface and base) include the phase shift in the sound waves when reflecting off the tissue as opposed to the base surface of the holder, the reflections off the surface and bottom of the tissue, and the sound speed through water and tissue (Hollman, et. al. 2002, Saijo, et. al., 1991, Winterroth, et. al 2009b). The tissue surface was determined by thresholding the magnitude of the signal at the first axial incidence of a value safely above noise; approximately 20-40 dB above the signal of the water (Figure 2.4). Approximately 4-5 scans were performed for each of the AlloDerm® and EVPOME engineered tissue specimens.

### 2.3.1 Signal Processing and Creating the 2D B-Scan Images

Before confocal image reconstruction, raw RF signals captured by the digitizing board were first basebanded to the center frequency of the transducer. Next 2D image planes at each vertical position were cleaned with two 2D filters, one for each horizontal slice in the transverse/vertical plane and one for each transverse slice in the horizontal/vertical plane. In the axial direction filter limits were determined by the transducer bandwidth. In the lateral directions filter limits were determined by examining a 2D Fourier transform of a typical speckle image. In the frequency domain the shape of the filter is an oval. In amplitude the filter follows the Butterworth design: flat in the passband with rolloff in the stopband. Next the data set is interpolated from a 15μm lateral sampling to 3μm. All image processing was performed using a code developed using MatLab (Mathworks, Inc., Natick, MA, USA).

### 2.3.2 Histology

Histology slides were prepared by the Histology Core at the University of Michigan School of Dentistry. AlloDerm® and EVPOME (at different stages of growth following seeding of cells) were fixed with 10% formalin, embedded in paraffin, cut in 5 μm sections, and stained with hematoxylin and eosin for examination under a brightfield microscope.

### 2.3.3 Statistical Analyses

Both one-way analysis of variance (ANOVA) and student t-tests were performed on the stages of growth, differentiation, and eventual apoptosis of the cells.

Comparing the surfaces of the AlloDerm® and EVPOME for both 2D B-scan SAM and histology images: In order to quantify the surface irregularities on both specimens using SAM and histology, a known area from each micrograph examined (300-1000μm x 100μm) divided into 12-40 even segments: 4 rows, 4-10 columns; the total area for each divided segment would be 2610$\mu m^2$. Each segment was then examined for the number of irregularities between the foreground (tissue and specimen) and background (empty slide). Surface irregularities were quantified by first finding the instance of threshold value, fitting and subtracting the planar surface, then counting the number of variations found above and below the planar height. The RMS value was computed over the surface and therefore a function of the transverse and lateral axes. The numbers for all rows were then added up, giving the total counts for the entire area. An illustration of this segmentation method is seen in Figure 2.5. The visible surface irregularities on each of the images were counted and a linear regression analysis was performed to correlate the surface profiles for both the AlloDerm® and EVPOME categories imaged by both SAM and optical microscopy. Both the AlloDerm® and EVPOME specimens were quantified in the same manner; it was not performed as a single-blind study.

## 2.4 EXAMINING SPACE-FILLING CHARACTERISTICS OF EVPOME

In the SAM 2D B-scan for the AlloDerm® and EVPOME specimens, the transducer is positioned at the top of the image, pointing downward. The top bright echo indicates the boundary between the coupling medium (water) and the apical surface of the AlloDerm®. Below this, the tissue specimen appears as uniform speckle. Based on this reflectivity (namely, the degree of the ultrasonic signal that it reflected back to the transducer; the greater the reflected signal from any given material will produce a brighter image in the B-Scan), there is a much brighter, more uniform surface layer in the SAM EVPOME (7 days and 11 days post-seeding) images; in contrast, the AlloDerm® images do not display this bright surface layer. Histology micrographs of the same tissues - AlloDerm® and the EVPOME at 11 days post-seeding - validate this finding.

The histology images of the AlloDerm® and EVPOME at days 4, 7, and 14 post-seeding showed similarities to the SAM 2D B-scans in the details of surfaces: the differentiation of the cells and the keratinized surface (Figure 2.6 a-d, respectively). The image of the EVPOME at 14 days showed greater space-filling of the surface than under Days 4 and 7, indicative of greater cellular differentiating activity at later days of EVPOME maturity. The complementary

SAM images of the AlloDerm® and EVPOME at these same days – 4, 7, and14 (Figure 2.6 e-h, respectively) - verify these differentiation patterns: there are less surface irregularities than visible on the AlloDerm®, with the numbers decreasing as the specimens are incubated for longer periods. Some bright spots indicate backscatter and are approximately 20-30μm in diameter (Figure 2.6e, circled). The irregular surface of the AlloDerm® results in higher presence of grayscale within the surface as compared to the EVPOME in the SAM 2D B-Scan images.

SAM experiments on both AlloDerm® and EVPOME at 11 days post seeding produced 3D B-scan images (Figure 2.7 a-b, respectively). Similar to the 2D B-scans, the 3D scans of the AlloDerm® showed distinct surface irregularities, resulting in changes in the SAM thresholding values. This rendered the surface image as appearing fractionated (Figure 2.7a). By contrast, the 3D image of EVPOME at 11 days post-seeding had the keratinized surface and differentiating cells fill in most of the surface irregularities resulting in minimum threshold changes and a more continuous appearance on the surface (rendered as blue; Figure 2.7b). The blue images on the surfaces were produced by creating a threshold of the acoustic signal; everything below the threshold is made transparent, everything above it is in grayscale. Every point at the threshold is part of the tissue surface. Some of the speckle signal dropped below this threshold, which was artificially rendered as blue surfaces inside the tissue. True

surfaces from the specular reflections are rendered at the threshold value, not at the peak; there is no second boundary between the tissue interface and the lower tissues. Because of greater surface irregularities on the AlloDerm® specimen, there is an increase in the amount of acoustic scatter, evident by the higher presence of grayscale on its surface. By contrast, there is significantly less scatter on the surface of the EVPOME; evident of the space-filling and keratinization of the cells seeded onto its surface.

For the EVPOMEs tested at 14-days post-seeding, the reflectivity was similar to the samples images at 11 days post-seeding from the previous study (Saijo, et. al. 1991, Somekh. et. al. 1985, Winterroth 2009a). Comparing these scans with the histology images there is a continuous layer of keratin on the apical side of the EVPOME specimen, indicative of the keratinocytes' space filling properties on the EVPOME.

### 2.4.1 Quantifying Surface Irregularities

The correlations for the number of irregularities versus the unseeded AlloDerm® and development of EVPOME at 4 Days, 7 Days, and 14 Days after seeding are similar for both histology and 2D SAM B-scan images (Figure 2.8a and 2.8b, respectively). The unseeded AlloDerm® averaged 12-13 surface changes per 400μm; the number of changes decreases to 2-3 per 400μm at 4 days and decrease further to 1-2 per 400μm at 7-14 days post-seeding. This

was verified by linear regression analyses (Figure 2.9).

## 2.5 COMPARISON OF ALLODERM®/ EVPOME ACOUSTIC SIGNALS

The 2D and 3D SAM scanned images of the EVPOME (7days to 11 days post-seeding) shows increased ultrasonic reflection on the surface; this is indicative of keratinocyte uniformity. Such uniformity results from the superficial keratinized layer of stratified epithelium formed by seeded oral mucosa keratinocytes. Histology images of the apical surfaces for the EVPOME verify the uniformity. The EVPOME's keratinized surface is set at the threshold of the acoustic signal; the images taken of this surface show a near seamless image of blue along the surface of the tissue – this is strongly evident of the space-filling characteristics of keratin and keratinocytes. The keratinocytes' adaptability to grow, proliferate, and differentiate on the AlloDerm® scaffold strongly supports EVPOME's potential as an ideal graft material (Izumi, et. al. 2003, Izumi, et. al. 2007).

The SAM images comparing the surfaces between the AlloDerm® and EVPOME show an average 6.5X – 13X decrease in the number of irregularities as the keratinocytes on the surface undergo maturation, proliferation, and keratinization. This aforementioned proliferation leads to the reduction in surface irregularities on the EVPOME. Water has low echogenicity (Taggart, et. al. 2007), therefore our speculation is that the echogenicity increases as the cells further differentiate and undergo keratinization, decreasing their water content

(De Mare, et. al. 1990, Saijo, et. al. 2004); this along with the reduction in irregularities enhances the acoustic reflection of the EVPOME's surface. This is indicative in the apices of the two-dimensional axial images when comparing the two specimens (namely, the engineered tissues AlloDerm® and EVPOME).

Additionally, all the SAM images were achieved immediately upon obtaining the specimens; the samples required no prior processing of any kind. This is a major advantage for using acoustics to image cells and tissues over current microscopy methods which often require processing methods which can affect the cells' and tissues' conditions.

We are currently using SAM to analyze both natural oral mucosa and EVPOME's potential as a surgical graft material; this includes applying ultrasonics to examine these same tissues' elastic properties. Although Lin, et. al. (2003) reported clinical success in treating vaginal agenesis with allografts of oral mucosa (specifically buccal mucosa), the study was limited to a small group and any long-term effects of the mucosal transplants' adaptability to the vaginal area are unknown. The buccal has been studied for its structure and efficacy in drug delivery (Alur, et. al. 2001, Hoogstraate, et. al. 1998) but its potential as a surrogate for soft tissue reconstruction is rather limited. Although the morphology of the EVPOME - in its early stages of development at least – shows great promise in its space-filling abilities, testing its functional similarities to natural tissues has yet to be performed. Further, both EVPOME and natural oral

mucosal tissues must tested be *in situ* to get the best results for their long-term adaptability and durability as an aforementioned replacement tissue.

Ultrasonic B-scans (and their corresponding histology images) are not detecting seeded cells filling in the irregularities of the specimen until cells have sufficiently stratified and differentiated between day 4 and day 7. The more maturely differentiated cells, present at days 7 and 14, showing brighter echogenicity and less surface variance are possibly due to cellular changes resulting from an increase in stratification – verified by the histology at these days. These initial results show that ultrasonic characterization may have the potential to monitor EVPOME development during its manufacturing process.

Testing for ANOVA within the group of engineered tissues shows differences between the scans within the experiment as a whole. The number of undulations between the mean AlloDerm® surfaces and the EVPOMEs were calculated: there is a 2.7 – 5.6 fold decrease in the surface irregularities between the two specimens as determined using both conventional histology and SAM (Figure 8a-b). The actively dividing oral mucosal keratinocytes have been shown to differentiate and show space-filling activity (Izumi, et. al. 2004), decreasing the number of irregularities on the specimen surface. The mean counts for the AlloDerm® alone ranged from 18.00 to 23.33, while the EVPOME range was between 4.15 and 6.67. The linear regression analyses comparing the AlloDerm® and EVPOME samples verifies this decrease between approximately

2-6 fold between the undulation counts for AlloDerm® and EVPOME when examining both SAM and histology (Figure 2.9). The standard error of the mean (namely, the standard deviation divided over the mean number of surface irregularities) was incorporated into the linear regression; correlating the number of irregularities in the 2D B-scan SAM to those found in the histology images shows a mean correlation coefficient of 1.09. This establishes a near 1:1 correlation between the mean counts between both microscopy tools. SAM demonstrates its ability to discern the differences in the surfaces between the two specimens. This further verifies acoustic microscopy as an effective imaging modality for cells and tissues and their subsequent evolution and differentiation.

### 2.5.1 Corrections and Improvements

We need to perform additional scans per specimen to increase samplings, followed by closer examination and correlations of the RF data contrasts to the cells' development and apoptosis. We may possibly change the coupling medium to increase echogenicity as cells differentiate and undergo apoptosis and will also consider different media (ie: 0.9% NaCl) as the prolonged immersion in deionized water may affect the condition of the apical surface.

### 2.5.2 Future Directions

Our upcoming studies will investigate the non-linear effects (Dill-Müller, et. al. 2007, Revell, et. al. 2003) of the aforementioned tissues using a compressor

system on the SAM (Cohn, et. al. 1997a). This will be followed by studying for any acoustic changes which may be present between the mitotic cells on the basal layer of the mucosal tissues (Cohn, et. al. 1997b, Winterroth, et. al. 2009b) – both for natural and EVPOME – and the keratinized apical layer. By correlating any possible changes in the RF data to the EVPOME (and mucosal cells in general) undergoing differentiation, apoptosis, and keratinization, we can better understand the physiological processes of these cells as they evolve and migrate toward the apical side of the tissue. Other future considerations will consider the use of apparent integrated backscatter (AIB). AIB is a measure of the frequency-averaged (integrated) backscattered power contained in some portion of a backscattered ultrasonic signal; it has been used extensively to study soft tissues (Winterroth, et. al. 2009b).

## REFERENCES


Alur, H.H., Johnson,T.P., Mitra, A.K.. Peptides and Proteins: Buccal Absorption. In: Swarbrick, J., Boylan, J.C., eds. 2001. *Encyclopedia of Pharmaceutical Technology: Volume 20 - Supplement 3*. Marcel Dekker. pp. 193-218.

Czarnota, G.J., Kolios, M.C., Vaziri, H., Benchimol, S., Ottensmeyer, F.P., Sherar, M.D., Hunt, J.W. Ultrasonic Biomicroscopy of Viable, Dead, and Apoptotic Cells, *Ultrasound in Med. Biol*, 1997. 23: 961-965.

Cohen, R.D., Mottley, J.G., Miller, J.G., Kurnik, P.B., Sobel, B.E. Detection of Ischemic Myocardium in Vivo Through the Chest Wall by Quantitative Ultrasonic Tissue Characterization. *Amer. J. Cardiol.* 1982. 61: 838-843.

Cohn, N.A., Emelianov, S.Y., Lubinski, M.A., O'Donnell, M. An Elasticity Microscope. Part I: Methods. *IEEE Trans. Ultrason. Ferr. Freq. Ctrl.* 1997. 44(6): 1304-1319.

Cohn, N.A., Emelianov, S.Y., O'Donnell, M. An Elasticity Microscope. Part II: Experimental Results. *IEEE Trans. Ultrason. Ferr. Freq. Ctrl.* 1997. 44(6): 1320-1331.

De Mare, S., Van Erp, P.E.J., Ramaekrs, F.C.S., Van De Kerkhof, P.C.M. Flow Cytometric Quantification of Human Epidermal Cells Expressing Keratin 16 *In Vivo* After Standardized Trauma. 1990. *Arch. Derm. Res*. 282: 126-130.

Dill-Müller, D., Maschke, J. Ultrasonography in Dermatology**.** *Journal der Deutschen Dermatologischen Gesellschaft***.** 2007.5:689–707.

Hollman, K.W., Emelianov, S.Y., Neiss, J.H., Jotyan, G., Spooner, G.J.R., Juhasz, T., Kurtz, R.M., O'Donnell, M. Strain Imaging of Corneal Tissue With an Ultrasound Elasticity Microscope. *Cornea.* 2002. 21(1): 68-73.

Hoogstraate, J.A.J., Wertz, P.W. Drug Delivery via the Buccal Mucosa. *Pharm. Sci. Tech. Tod*. 1998. 1(7): 309-316.

Hotta, T., Yokoo, S., Terashi, H., Komori, T. Clinical and Histopathological Analysis of Healing Process of Intraoral Reconstruction with *Ex Vivo* Produced Oral Mucosa Equivalent. *Kobe J. Med. Sci.*, 2007. 53(1): 1-14.

Huang, C-C. High-Frequency Attenuation and Backscatter Measurements of Rat Blood Between 30 and 60 MHz. *Phys Med Biol.* 2010 Oct 7;55(19):5801-15. Epub 2010 Sep 16.

Izumi, K., Feinberg, S.E., Iida, A., Yoshizawa, M. Intraoral Grafting of an *Ex Vivo* Produced Oral Mucosa Equivalent: A Preliminary Report. *Int. J. Oral Maxillofac. Surg.* 2003. 32: 188–197.

Izumi, K., Song, J., Feinberg, S.E. Development of a Tissue-Engineered Human Oral Mucosa: From the Bench to the Bed Side. *Cells Tissues Organs.* 2004. 176:134–152.

Izumi, K., Tobita, T., Feinberg, S.E. Isolation of Human Oral Keratinocyte Progenitor/Stem Cells. *J. Dent. Res.* 2007. 86(4):341-346.

Kolios, M.C., Czarnota, G.J., Lee, M., Hunt, J.W., Sherar, M.D. Ultrasonic Spectral Parameter Characterization of Apoptosis. *Ultrasound in Med. Biol*., 2002. 28(5): 589–597.

Kolios, M.C., Taggart, L., Baddour, R.E., Foster, F.S.., Hunt, J.W., Czarnota, G.J., Sherar, M.D. An Investigation of Backscatter Power Spectra from Cells, Cell Pellets, and Microspheres. *IEEE Ultrasonics Symposium*. 2003. 752-757.

Lin, W.C., Chang, C.Y.Y., Shen, Y.Y., Tsai, H.D. Use of Autologous Buccal Mucosa for Vaginoplasty: A Study of Eight Cases. *Human Reproduction*. 2003. 18(3): 604-607.

Lizzi, F.L., Greenebaum, M., Feleppa, E.J., Elbaum, M., Coleman, D.J. Theoretical Framework for Spectrum Analysis in Ultrasonic Tissue Characterization, *J Acoust Soc Am*. 1983. 73: 1366–1373.

Matsuyama, H., St. Goar, F.G., Tye, T.L., Oppenheim, G., Schnittger, I., Popp, R.L. Ultrasonic Tissue Characterization of Human Hypertrophied Hearts *In Vivo* with Cardiac Cycle-Dependent Variation in Integrated Backscatter. *Circul.* 1989. 80: 925-934.

Presland, R.D., Dale, B. A. Epithelial Structural Proteins of the Skin and Oral Cavity: Function in Health and Disease. *Crit Rev. Oral Biol Med*. 2000. 1(4): 383-408.

Quate, C.F.. Imaging Using Lenses. in. Wade, G., ed.. *Acoustic Imaging: Cameras, Microscopes, Phased Arrays, and Holographic Systems.* NY: Plenium Press. 1976. pp. 241-305.

Revell, J., Mirmehdi, M., McNally, D. Ultrasound Speckle Tracking for Strain Estimation. 2003. *http://www.cs.bris.ac.uk/~revell.*

Saijo, Y., Miyakawa, T., Sasaki, H., Tanaka, M., Nitta, S. Acoustic Properties of Aortic Aneurysm Obtained with Scanning Acoustic Microscopy. *Ultrasonics*. 2004. 42: 695–698.

Saijo, Y., Tanaka, M., Okawai, H., Dunn, F. The Ultrasonic Properties of Gastric Cancer Tissues Obtained with a Scanning Acoustic Microscope. *Ultrasound in Med. & Biol.* 1991. 17(7): 709-714.

Silverman RH, Patel MS, Gal O, Sarup A, Deobhakta A, Dababneh H, Reinstein DZ, Feleppa EJ, Coleman DJ. Effect of Corneal Hydration on Ultrasound Velocity and Backscatter. *Ultrasound Med Biol*. 2009 May;35(5):839-46. Epub 2009 Feb 5.

Somekh, M.G., Bertoni,H.L., Briggs, G.A.D., Burton, N.J. A Two-Dimensional Imaging Theory of Surface Discontinuities with the Scanning Acoustic Microscope. *Proceedings of the Royal Society of London. Series A, Mathematical and Physical Sciences*. 1985. 401(1820): 29-51.

Srivastava, R. *Apoptosis, Cell Signaling, and Human Diseases: Molecular Mechanisms.* NY: Humana Press, 2007. 402 pages. p. 157.

Strohm, E.M., Czarnota, G. J., Kolios, M.C. Quantitative Measurements of Apoptotic Cell Properties Using Acoustic Microscopy. *IEEE Transactions on Ultrasonics, Ferroelectrics, and Frequency Control,* 2010 57(10): 2293-2304.

Taggart, LR., Baddour, R.E., Giles, A., Czarnota, G.J., Kolios, M.C. Ultrasonic Characterization of Whole Cells and Isolated Nuclei. *Ultrasound in Med. & Biol*. 2007. 33(3): 389–401.

Tu, H-P., Chen, Y-T., Chiu, H-C., Chin Y-T., Huang S-M., Cheng L-C., Fu E., Chiang C-Y. Cyclosporine A Enhances Apoptosis in Gingival Keratinocytes of Rats and in OECM1 Cells via the Mitochondrial Pathway. *J. Periodontal Res.* 2009. 44(6):767-775.

Vermes, I., Haanen, C., Steffens-Nakken, H., Reutellingsperger, C. A Novel Assay for Apoptosis. Flow Cytometric Detection of Phosphatidylserine

Expression on Early Apoptotic Cells Using Fluorescein Labelled Annexin V. *J Immunol Methods*. 1995. 184(1):39-51.

Winterroth, F., Hollman, K.W., Izumi, K., Feinberg, S.E., Fowlkes, J.B., Hollister, S.J. Examination and Comparisons of EVPOME/ AlloDerm® Compositions with Natural Mucosal Tissues Using Scanning Acoustic Microscopy. *Society for Biomaterials 2009 Annual Meeting and Exposition*. 2009.

Winterroth, F., Fowlkes, J. B., Kuo, S., Izumi, K., Feinberg, S.E., Hollister, S. J., Hollman, K. W. High-Resolution Ultrasonic Monitoring of Cellular Differentiation in an *Ex Vivo* Produced Oral Mucosal Equivalent (EVPOME). *Proc. IEEE Bioultrasonics Conference.* 2009.

Zuber, M., Gerber, K., Erne, P. Myocardial Tissue Characterization in Heart Failure by Real-Time Integrated Backscatter. *Eur. J. Ultrasound* 1999. 9: 135–143.

## FIGURES

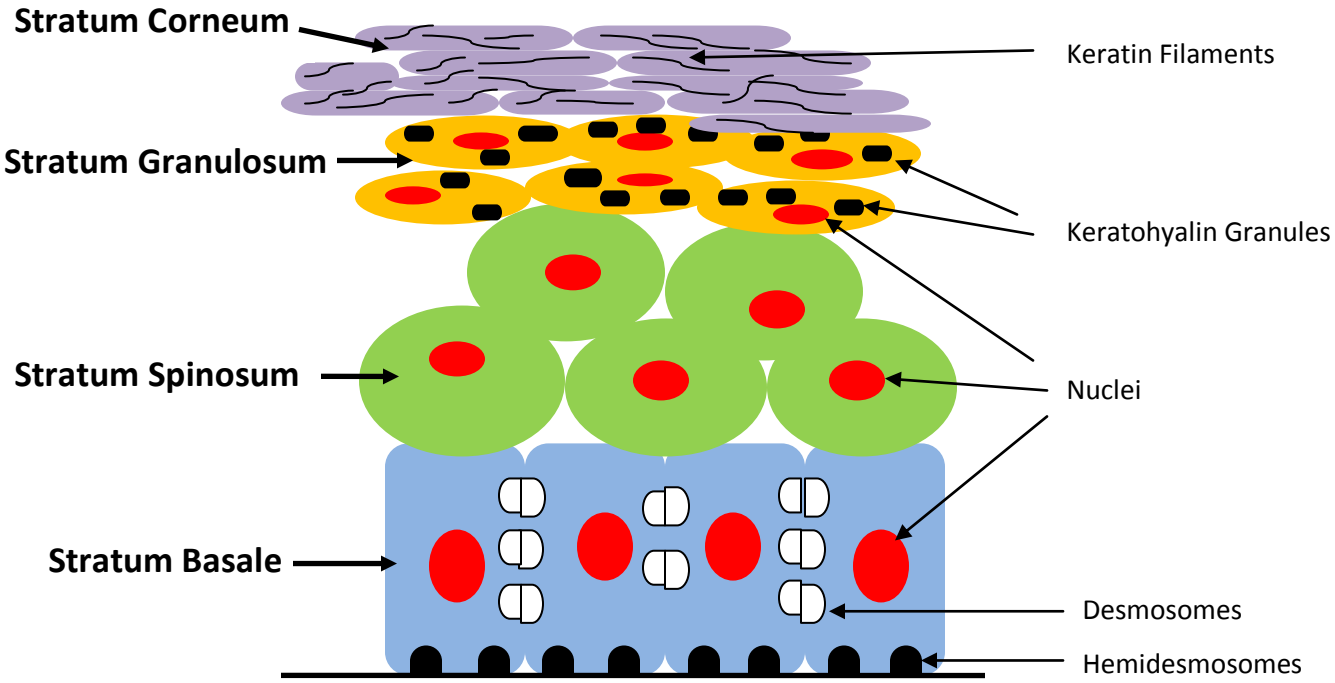


**Figure 2.1. Illustrative schematic of the oral mucosa showing the principal cells and structures which constitute the oral lining above the basal lamina. The cell layers near the basal side appear more cuboidal; as they migrate toward the apex, they become more squamous and undergo apoptosis and keratinization.**

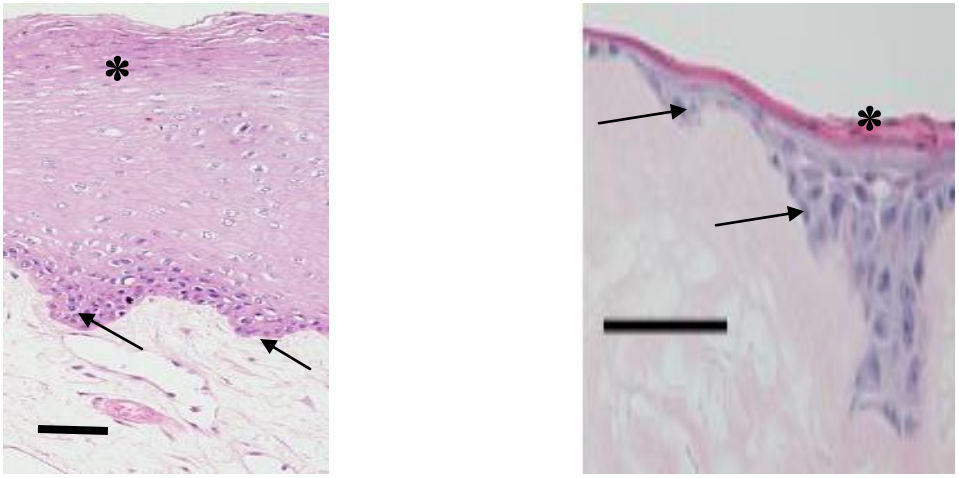

**(a)** **(b)**

**Figure 2.2. Histology of natural oral mucosa tissue (a) and EVPOME device (b). In both cases, there is a basal layer of actively dividing and differentiating cells (arrows), followed by a uniformly keratinized surface (asterisk). Scale bars represent 100μm.**

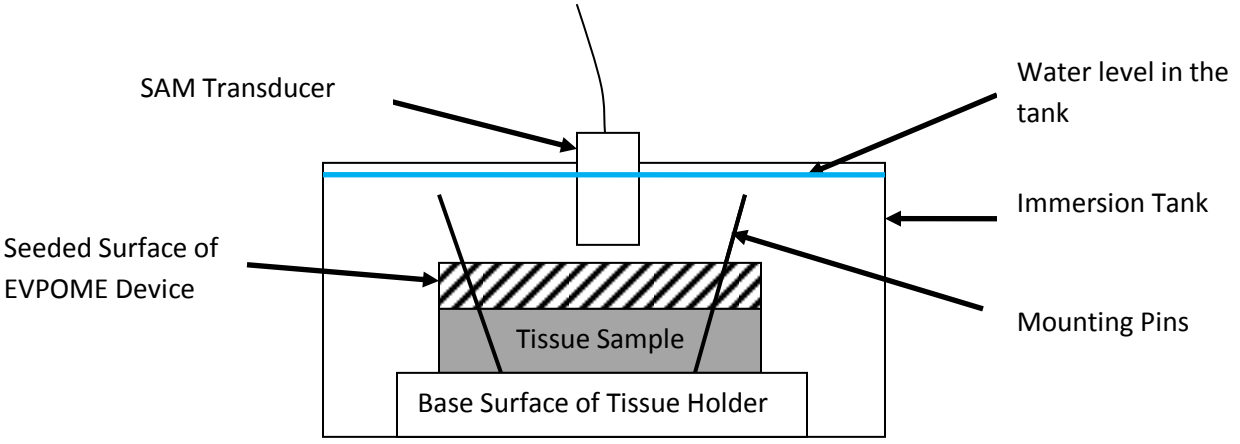


**Figure 2.3A. Illustrative set-up of the SAM, showing principal features for the scan. The tissue specimens (ie: AlloDerm® and EVPOME) are mounted on the tissue holder using either pins or adhesive. The devices are then immersed in degassed, deionized water with the scanning transducer placed directly over them. The focal length is then adjusted for each sample being scanned the surfaces of the AlloDerm® and EVPOME at different days post-seeding showing difference in the acoustic reflections off of the surface of the apical surfaces for each of the devices. Note: the sizes of the devices, tank, transducer, and other objects are not to scale.**

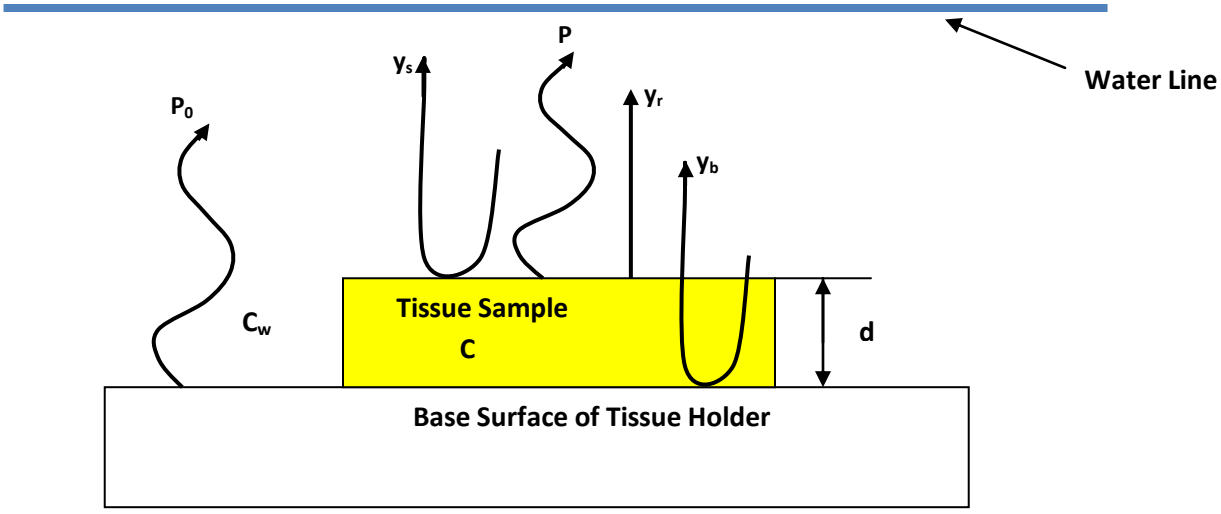


**Figure 2.3B. Set-up: 61 MHz Transducer is aimed directly above the tissue stage; coupling medium is deionized water.**

- **P0= Specular reflection off base surface**
- **P = Specular reflection off tissue sample**
- **yr = received signal**
- **ys = reflection from the surface of the specimen**
- **yb = reflection from the bottom of the specimen**
- **Cw= Sound speed in water**
- **C = Sound speed in tissue**
- **d= Tissue thickness**

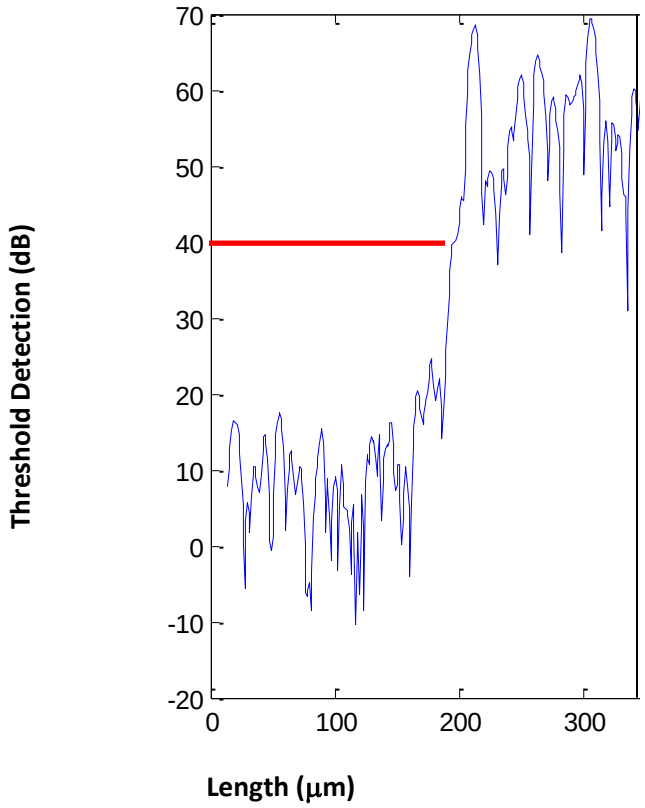


**Figure 2.4. Plot diagram of the SAM, showing the detection of the device surface (red line) after setting the threshold detection safely above the signal of the water.**

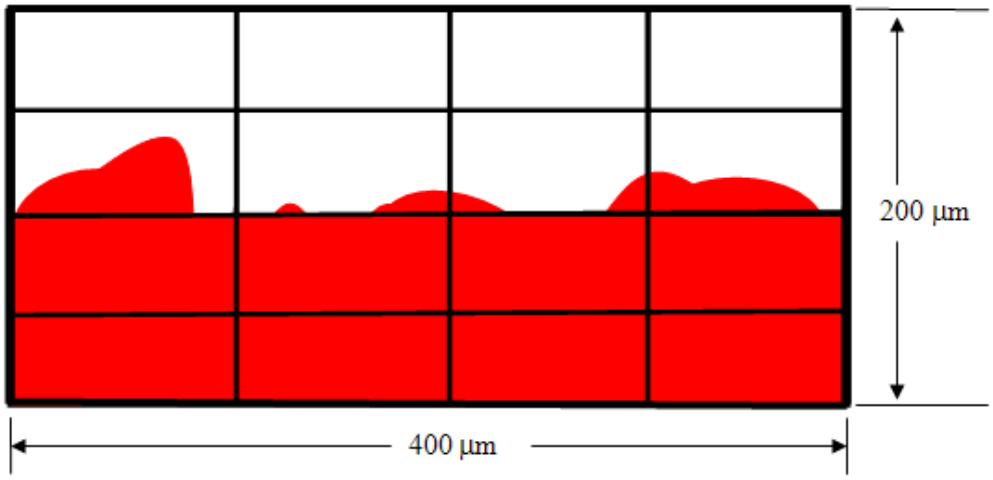


**Figure 2.5. Illustrative set-up used to quantify the surface irregularities for both the AlloDerm® and EVPOME images. A known area (80,000 $\mu m^2$) of each micrograph was divided into 16 even segments - 4 rows, 4 columns; each segment being 5000$\mu m^2$ in area. The number of times the foreground (device, shown in red) and background (empty slide, shown in white) appear in each segment were then quantified for each row. The numbers for all rows were then added up, giving the total counts for the entire area. Illustration is not to scale.**

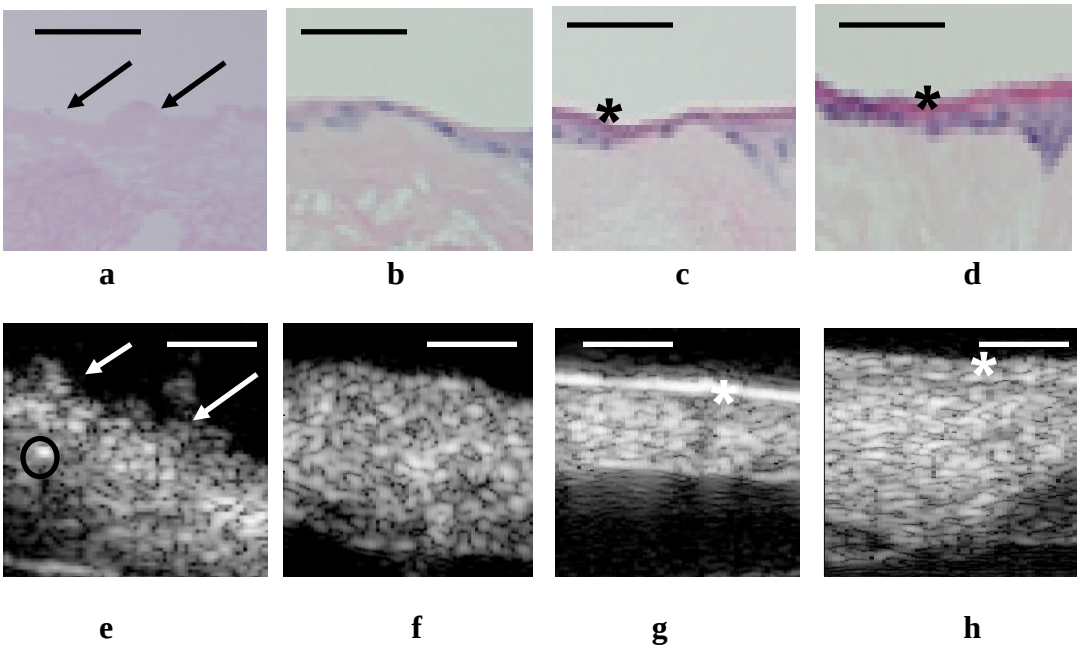


**Figure 2.6. Representative AlloDerm® and EVPOME images from the respective histology scans (a-d) and SAM images (e-h). Histology micrographs of AlloDerm® (a) and EVPOME at 4 days (b), 7 days (c), and 14 days (d) post-seeding. Note the presence of surface irregularities on the AlloDerm® surface (arrows) compared to the smoother surface of the EVPOME (asterisk); this is more evident at 7 and 14-days post-seeding. These findings are confirmed by the representative SAM 2D B-scan images of AlloDerm® (e) and EVPOME at 4 days (f), 7 days (g), and 14 days (h) post-seeding. The bright spots indicate backscatter and are approximately 20-30μm in diameter (circled). There is also the presence of surface irregularities on the AlloDerm® (arrows). EVPOME images at 7 days and 14 days post-seeding show greater reflectivity off of the surface and decreased irregularities (asterisks). Scale bars are 100μm.**

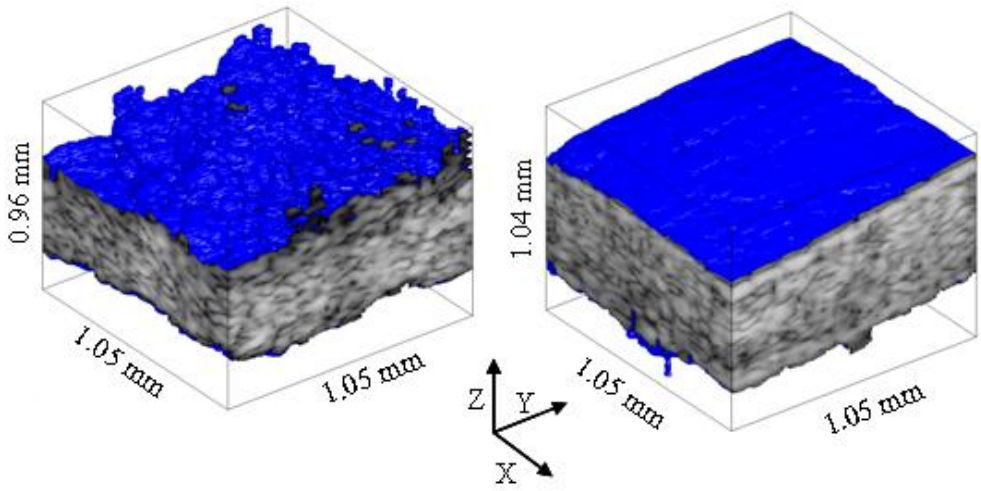


**a** **b**

**Figure 2.7. 3D SAM representations of the AlloDerm®, EVPOME at 11-days post-seeding (a and b, respectively) with the apical sides is on top, showing differences in the scatter characteristics on the apical surface The blue rendering is taken at the set threshold of the tissue: everything above and below the threshold value are rendered grayscale and transparent, respectively. Because of greater surface irregularities on the AlloDerm® specimen, there is an increase in the amount of acoustic scatter, evident by the higher presence of grayscale on its surface. By contrast, there is significantly less scatter on the surface of the EVPOME; evident of the space-filling and keratinization of the cells seeded onto its surface.**

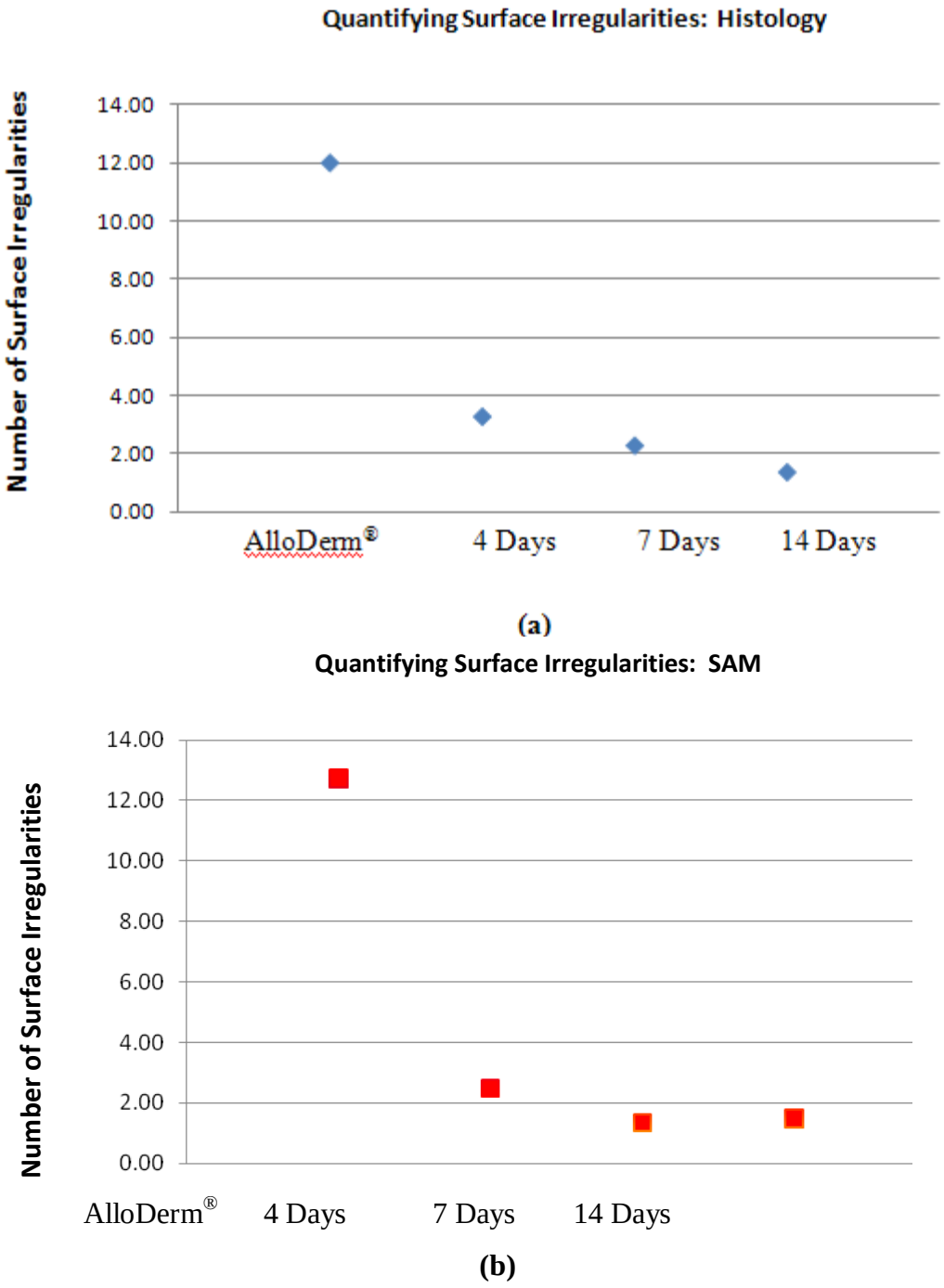


**Figure 2.8. Histology (a) and SAM (b) correlations between counts for AlloDerm® and EVPOME at 4 Days, 7 Days, and 14 Days post-seeding.**

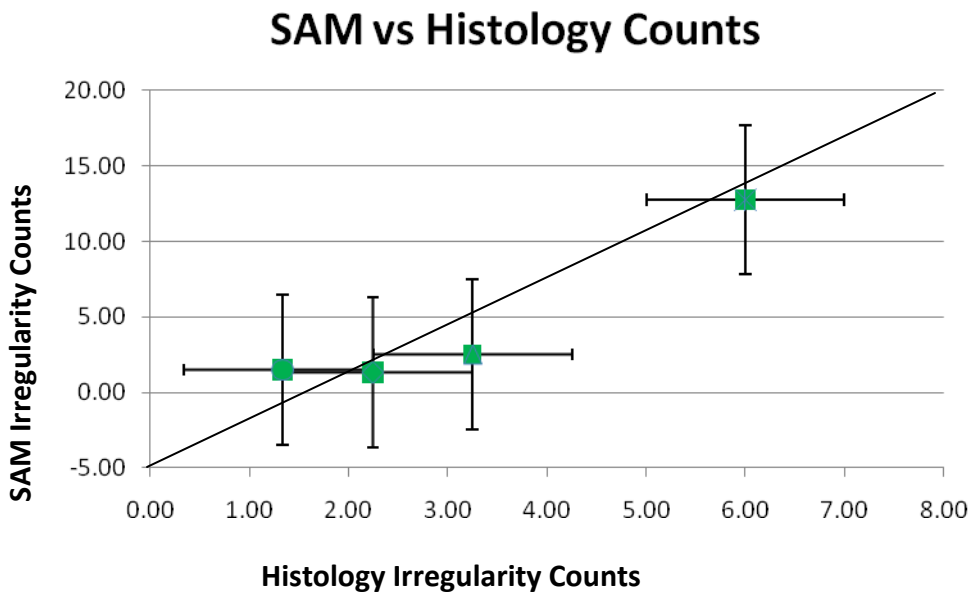


**Figure 2.9. Linear regression analyses for surface irregularity counts on the apical surfaces between both EVPOME at 14, 7, and 4 days post-seeding and AlloDerm®; analyzed from both histology and SAM micrographs. The slope is 1.88, with the intercept at 0.00. The standard error of the mean for the EVPOME ranged between 0.77 for 14 days post-seeding to 1.63 for 4 days; for the AlloDerm®, the standard error was calculated to be 4.24.**

The axial resolution depends on the dimensions of the pressure pulse, which is related to the transducer bandwidth (BW) and system electronics:

$$R_{ax} = \frac{c}{2 \times BW} \quad (1)$$

where $c$ is the sound speed in the tissue and BW is 32MHz. Likewise, the lateral resolution at the focal point can be estimated by:

$$R_{lat} = \lambda \times f/\text{number} \quad (2)$$

where, $\lambda$ is the wavelength (25$\mu$m).

The depth of field (DOF) is calculated by:

$$DOF = 4\,(f/\text{number})^2\ \lambda \quad (3)$$

Due to a small f/number (which provides a tight beamwidth), the DOF is also limited.

Lateral resolution is the resolution orthogonal to the propagation direction of the ultrasound wave.

Acoustic Impedance (Z): The impedance determines the amplitude of the reflected / transmitted waves at the fluid-tissue interface. Complex scattering properties of tissues are due to acoustic impedance interfaces in microstructure of tissues:

$$Z = \rho c \quad (4)$$

$$R = |(Z2-Z1)/(Z2+Z1)| \quad (5)$$

Where Z is the impedance, $\rho$ is the density, and R is the reflection coefficient.

**Table 1. Basic equations of the SAM operating principles: axial and lateral resolutions, DOF, and acoustic impedance.**

# CHAPTER III

# ACOUSTIC MICROSCOPY ANALYSES TO DETERMINE GOOD VERSUS FAILED TISSUE ENGINEERED ORAL MUCOSA UNDER NORMAL OR THERMALLY STRESSED CULTURE CONDITIONS

## 3.1 INTRODUCTION

The development and use of an *ex vivo* produced oral mucosal equivalent (EVPOME) – an engineered human oral mucosa developed for reconstructive intraoral grafting procedures - has demonstrated its clinical efficacy in intra-oral surgical grafts (Izumi, et. al 2003). EVPOME has shown to be an effective soft tissue replacement in cases where patients' oral mucosa was absent or damaged due to disease, injury, or other pathological conditions (Izumi, et. al 2003, Izumi, et. al 2004, Izumi, et. al 2000). Previous studies have shown the efficacy of using scanning acoustic microscopy (SAM) to image and assess the

differentiation of these tissues (Wickline, et. al. 1985, Winterroth, et. al. 2009a). In this study, we tested the ability of SAM to differentiate between seeded EVPOME devices which have undergone periods of elevated thermal incubation (stressed) to those which were incubated continuously at physiological temperature (unstressed).

### 3.1.1 Background on EVPOME for Use in Repair and Replacement

The oral mucosa's histology resembles that of skin: as new cells are formed on the basal lamina, the more matured cells migrate toward the apex, undergoing apoptosis and keratinization as they migrate (Izumi, et. al 2004). This same process occurs in the EVPOME tissues, making it an excellent tissue for repair and replacement of damaged or diseased soft tissue.

We earlier examined and compared the morphologies of AlloDerm® - a commercially available acellular human cadaver dermis (the tissue goes through a cell removal process while retaining biochemical and structural components.), and EVPOME at different stages of development using SAM (Winterroth, et. al. 2009b). By first comparing the morphologies of the oral mucosal tissues – both natural and engineered, we can better understand the physical compositions when it comes to testing for similarities in the tissues' physical properties. We can then quantify the cellular constituents among each of the tissue types and

correlate how each contributes to the physical behavior of their respective tissues. This would assist us in establishing criteria for standardization of manufacture of the engineered tissues as well as criteria for their uses in reconstructive surgery based on their mechanical properties.

### 3.1.2 Background on SAM and the Use of Surface Profilometry

SAM is an effective tool to study both the morphology and non-linear elastic characteristics of natural and engineered oral mucosal tissues. The advantages of using SAM over conventional optical and electron microscopy include being able to image the cells and tissues without doing any preparations which could potentially kill or alter the tissues; this provides a more accurate representation of the tissues' natural properties. We have also shown that SAM can provide evidence as to the degree of differentiation which the cells are undergoing without altering their physical conditions (Izumi, et. al 2000, Matsuyama, et. al. 1989, Olerud, et. al. 1999, Winterroth, et. al. 2009a). In addition, ultrasound imaging systems can indirectly estimate and image elastic properties of tissue using ultrasonic measurements of externally or internally induced tissue motion (Bridal, et. al. 1997).

Other imaging methods which do not require preparing cell/tissue cultures include atomic force microscopy (AFM) (Marchant, et. al. 2002). Although AFM

can provide imaging of the cultures, there are several disadvantages associated with this imaging method. These include the AFM cantilever systems deforming or tearing apart living cells and other biological materials and the force being too great to image cells with sufficient resolution (Marchant, et. al. 2002, Verstraenten, et. al. 2008).

We are currently using SAM to examine and correlate any changes in the radiofrequency (RF) data to the EVPOME (and mucosal cells in general) undergoing differentiation, apoptosis, and keratinization. This will allow us to better understand the physiological processes of these cells as they undergo stratification on the AlloDerm® over time.

#### 3.1.2.1 Profilometry

This is a standard method used to measure a surface's profile, in order to quantify its roughness: the number of surface irregularities of the overlying basement membrane (AlloDerm® without cells) or of the stratified epithelium (EVPOME). The SAM is utilized to check for surface roughness and correlate this to the growth and development of the keratinized layer on the surface: the smoother the surface (as determined by the reflectivity of the SAM), the higher the keratinized surface as the cells differentiate and stratify when migrating up to the surface. Surface profilometry will also provide evidence as to the degree of

differentiation which the cells are undergoing without chemically affecting their properties.

## 3.2 MATERIALS AND METHODS IN DEVELOPING AND EXAMINING THERMALLY STRESSED EVPOME

### 3.2.1 EVPOME Preparation –Stressed and Unstressed

The protocol for harvesting human oral mucosal tissue was approved by a University of Michigan Internal Review Board. All individuals signed informed consent before the tissue samples were procured. A keratinized oral mucosa sample was taken from an out-patient at the University of Michigan Oral and Maxillofacial Surgery Clinic. The methods for preparation have been described in greater detail previously (Cohn, et. al. 1997b, Endo, et. al. 2010). Briefly, oral mucosa keratinocytes were enzymatically dissociated from the tissue sample, and a primary cell culture was established and propagated in a chemically-defined, serum- and xenogeneic products- free culture medium, with calcium concentration of 1.2mM. The AlloDerm® was soaked in 5 $\mu g/cm^2$ human type IV collagen at 4°C overnight prior to seeding cells to assist the adherence of cells, then approximately 1.5 x $10^5$ cells/$cm^2$ of oral keratinocytes were seeded onto the type IV collagen pre-soaked AlloDerm®. The composites of the keratinocytes and the AlloDerm® were then cultured, in the submerged condition, for 4 days to form a continuous epithelial monolayer. After 4 days, the equivalents were raised to an air-liquid interface to encourage epithelial stratification and cultured for another 7 days, resulting in a fully-differentiated, well-stratified epithelial layer on

the AlloDerm®. At Day 11 post-seeding, EVPOME samples were collected for SAM imaging.

On Day 9 post-seeding, one set of EVPOME devices was incubated at 43°C for 24 hours, then switched back to 37°C for another 24 hours (thermally stressed). Another set of EVPOMES were kept at 37°C up through Day 11 post-seeding (non-stressed). The total seeding times for both conditions were equal. 3 specimens were used for each study set: an unseeded AlloDerm®, an unstressed control, and a thermally stressed EVPOME.

### 3.2.2 SAM Apparatus Set-up and Imaging, Tissue Preparations and Analyses

Details of the scanning and ultrasound system are similar to those described elsewhere (Cohn, et. al. 1997a, Cohn, et. al. 1997b, Holland, et. al. 1997). EVPOME samples were immersed in deionized water and imaged with a single element fixed focus transducer, producing ultrasonic B-scans. The transducer has an approximate frequency of 61 MHz, the element is 3 mm in diameter and focused to a depth of 4.1 mm, giving an f/number of approximately 1.4. The transducer was fastened to an optical mount and the angular position was adjusted until the ultrasonic beam was normal to the deflecting plate. We scanned the surfaces of the EVPOME, showing the acoustic signal between the interface of the sample and water on the sample's apical side. DC stepper

motors accurately positioned the transducer above the specimen. B-scan images were obtained by stepping the transducer element laterally across the desired region. At each position, the transducer fired and an RF A-line was recorded. After repeated firings at one position, the transducer moved to the next, where the image was constructed from A-lines acquired at all lateral positions. Because low f/number, single element transducers have a short depth of field, a composite B-scan image was generated from multiple scans at different heights. Ultrasonic images were created using confocal image reconstruction. The spacing was determined by the step sizes along each of the axes: 15 μm scanning step size in both the transverse and horizontal directions; a lateral resolution ($R_{lat}$) of 37μm; an axial resolution ($R_{ax}$) of 24μm; a depth of field of 223μm. Z-axis was sampled at 300 mega samples/second. $R_{ax}$ is the resolution in the direction of propagation and is determined by the length of the ultrasound pulse propagating in the tissue; $R_{lat}$ is the resolution orthogonal to the propagation direction of the ultrasound wave. The tissue surface was determined by thresholding the magnitude of the signal at the first axial incidence of a value 20 - 30dB safely above noise; a typical A-line is illustrated in Figure 3.1. Four sets of scans were performed, each set containing a thermally stressed and unstressed specimen. An unseeded AlloDerm® specimen was also scanned as a control. All specimens were imaged for approximately 30 minutes, thus minimizing the risk for contamination to occur.

Surface profilometry was determined by first finding the instance of threshold value, fitting and subtracting the planar surface, then calculating root-mean-squared (RMS) height (Endo, et. al. 2010). The RMS value was computed over the surface and therefore a function of x and y. Because the surface height is z, its function is z(x,y). It has a two-dimensional sum and is divided by nx and ny inside the square root:

$$RMS = \sqrt{\sum_{n} \frac{z(x,y)}{nx + ny}} \quad (1)$$

where *n* is number of *x* and y samples.

### 3.2.2.1 Histology

EVPOME (both the stressed and unstressed samples) were fixed with 10% formalin, embedded in paraffin, cut in 5μm sections, stained with hematoxylin and eosin. The histology of the EVPOME samples were then examined under a Nikon Ti-U inverted microscope (Nikon Optical, Tokyo, Japan) using brightfield light.

#### 3.2.2.2 Statistical Analyses

Both one-way analyses of variance (ANOVA) and linear regression analyses were performed on the surface characteristics for both categories of EVPOME cultures. The RMS values with their standard deviation values were compared between the stressed and unstressed EVPOME specimens and to an unseeded AlloDerm® control specimen.

## 3.3 RESULTS

For the thermally stressed devices, the apical sides showed similar surface irregularities to those of the 2D B-scans of unseeded AlloDerm® devices (Figure 3.2a). Comparing the B-scans taken of EVPOME at 11 days post-seeding (Figure 3.2b), there is a distinct reflection off of the surface which is not found in the unseeded AlloDerm®; a result of the seeded keratinocytes differentiating (Wickline, et. al. 1985, Winterroth, et. al. 2009a). The histology images of these same devices - AlloDerm® and EVPOME at 11-days post seeding (Figures 3.2c and 3.2d, respectively), verifies this finding as the keratinized layer in the latter image shows a smooth surface, with less surface irregularities compared to the former image (Wickline, et. al. 1985).

The SAM 2D B-scans showed higher reflectivity on the surfaces for the non-stressed devices (Figures 3.3a-b) than those of the stressed (Figures 3.3c-d). This is typical to the results we had obtained from our previous study to examine the morphological differences between the AlloDerm® device and EVPOME at different stages of post-seeding (Wickline, et. al. 1985). This was confirmed by examining the device sections using standard optical microscopy to compare non-stressed (Figures 3.3e-f) and stressed (Figures 3.3g-h) devices. Further, the scans for the stressed devices displayed a darkened region between two more brightly reflected regions (Figure 3c); an indication that the keratin layer had partitioned from the surface of the device. We validated this by comparing the histological images of the same device (Figure 3.3g), which confirmed our findings. For one of the thermally stressed devices the irregular surface of the AlloDerm® device is visible, but no keratinized layer; the likely result of the keratin completely sloughing off from the surface (Figure 3.3d). The histology from this latter device showed the keratin layer more fractionated and partitioning from the surface to a greater degree than other stressed devices (Figure 3.3h); this validates our claim of the keratin sloughing from the device.

Filtering any existing artifacts in the RMS processing showed uniformity within the non-stressed devices. This again validated the findings from our previous studies: the space-filling properties of the keratinocytes on the devices (Wickline, et. al. 1985, Winterroth, et. al. 2009a).

The surface profilometry images for all scans performed on each device displayed higher degrees of variation for the stressed devices compared to the non-stressed ones (Figure 3.4). The images displaying red and blue in certain regions show greater variations in the surfaces; this is particularly the case for the thermally stressed specimens. The classification is based on fitting the planar surface of each representative sample and subtracting the difference. Therefore, the more changes in colors represent greater irregularities in the surface of the specimen. The unstressed devices' scans showed minimal variation in the RMS height values; either low or high (Figures 3.4a-b). By contrast there are greater changes in these RMS values in the scans for the stressed devices (Figures 3.4c-d). There was some variation found in the unstressed device scans; a result of the way in which the device was mounted to the bottom of the water tank (we also took this into account when examining the stressed device scans). This compares with the 2D B-scan, histology, and C-scan profilometry images produced by scanning the unseeded AlloDerm® control (Figures 3.5 a-c, respectively).

Examining the 2D B-mode images found irregularities caused by the tissue with respect to the placement of the transducer which caused the increased RMS heights. For the non-stressed device scans, there was one scan from each sample which produced relatively higher RMS results than the others.

This is noticeable in both the SAM surface profilometry images (Figures 3.4a3 and 3.4b1) and in the 2D B-scans (Figure 3.6) of the devices. Consequently, the standard deviations were comparatively greater for the non-stressed devices than the stressed group, while the mean values remained lower for the non-stressed group. The compendium of RMS values between the thermally stressed and unstressed EVPOME devices shows significant values: the RMS heights for the stressed devices are 4-5 times greater than the unstressed devices, with the unseeded AlloDerm® control mean displaying RMS value approximately 2.5 times greater than the unseeded EVPOMEs (Figure 3.7).

## 3.4 ANALYZING THERMAL EFFECTS ON EVPOME SPACE FILLING PROPERTIES BASED ON SAM

Ultrasonic profilometry does not detect cells on the thermally stressed EVPOMEs filling in the irregularities on the surfaces compared to the unstressed EVPOMEs. The decrease in the RMS values for the unstressed device is evidence of the proliferation/differentiation by the seeded cells on the EVPOME surface; in contrast the thermally stressed cells show little to no activity. The latter case indicates SAM's ability to measure physiological activity by measuring the degree of ultrasonic scatter. These initial results show that ultrasonic

characterization may have the potential to monitor EVPOME development during its manufacturing process: SAM could be utilized in a sterile environment such as a laminar hood and its applicability to monitor *in vitro* cell and tissue growth over specified time periods (ie: 24 hours) exists. Comparing similarities on SAM 2D B-mode images of the unstressed EVPOME to earlier studies' images of EVPOME at 11 days post-seeding (Izumi, et. al. 2004, Izumi, et. al, 2000) provided the best evidence to select the correct devices.

The two outliers in the non-stressed devices are likely the result of their mounting prior to performing the scan and not any error in the SAM detection and imaging. Nevertheless, they present a serious challenge towards properly imaging and accurately identifying the structural characteristics of the devices and any other subsequent cells, tissues, and other biological devices examined using SAM: in the specific case of the sample being observed, there was a significant slope caused by inadvertently positioning the sample in the manner described. A similar case involving an optical micrograph would be having the tissue specimen slightly thicker on one end, which could lead to the image being slightly out of focus on one side. Although we are able to correct for this error through filtering and background subtraction and analyses, improving methods for mounting the devices during the SAM scans must take effect. This is to minimize any potential errors in calculating RMS heights caused by the devices buckling or tilting.

Although SAM identified differences in cell and tissue development on the 11-day EVPOMEs, we cannot conclude that the devices are devoid of surface irregularities, regardless of the amount of keratinization present: neither acoustic nor optical microscopy can show that the EVPOMEs are consistently uniform across their entire surfaces. This was verified by the aforementioned outliers seen in the SAM scans of both thermally unstressed devices.

This study provides strong supplemental evidence to demonstrate SAM as a method to objectively quantify cell and tissue development and differentiation. In addition, it provides insight on mature EVPOME's characteristics when subjected to an elevated temperature. Subsequent studies will further examine these differentiation characteristics through continuous ultrasound monitoring of *in vitro* EVPOME devices under aseptic conditions.

Future Considerations will examine the use of apparent integrated backscatter (AIB) to further demonstrate and quantify cell development using SAM. AIB is a measure of the frequency-averaged (integrated) backscattered power contained in some portion of a backscattered ultrasonic signal; it has been used extensively to study soft tissues (Cohen, et. al. 1982, Endo, et. al. 2010, Kolios, et. al. 2002, Zuber, et. al. 1999).

## REFERENCES


Bridal, S. L., P. Fornes, P. Bruneval, and G. Berger. Parametric (integrated backscatter and attenuation) Images Constructed using Backscattered Radio Frequency Signals (25-56 MHz) from Human Aaortae In Vitro. *Ultrasound in Med. & Biol.* 1997.23: 215-229.

Cohen, R.D., J.G. Mottley, J.G. Miller, P.B. Kurnik, and B.E. Sobel. Detection of Ischemic Myocardium In Vivo through the Chest Wall by Quantitative Ultrasonic Tissue Characterization. *Amer. J. Cardiol*. 1982. 50: 838-843.

Cohn, N.A., Emelianov, S.Y., Lubinski, M.A., O'Donnell, M. An Elasticity Microscope. Part I: Methods. *IEEE Trans. Ultrason. Ferr. Freq. Ctrl.* 1997. 44(6): 1304-1319.

Cohn, N.A., Emelianov, S.Y., O'Donnell, M. An Elasticity Microscope. Part II: Experimental Results. *IEEE Trans. Ultrason. Ferr. Freq. Ctrl.* 1997. 44(6): 1320-1331.

Endo T, W.J. Finger, M .Kanehira, A . Utterodt, and M. Komatsu. Surface Texture and Roughness of Polished Nanofill and Nanohybrid Resin Composites. *Dent Mater J.* 2010. 29(2): 213-23.

Holland, M.R., Hall, C.S., Lewis, S.H., Handley , S.M., Finch-Johnston, A.E., D'Sa, A.P., Perez, J.E., Miller, J.G. Comparison of integrated backscatter values obtained with acoustic densitometry with values derived from spectral analysis of digitized signals from a clinical imaging system. *J. Amer. Soc. Echocardio.* 1997. 10(5): 511-517.

Hollman, K.W., Emelianov, S.Y., Neiss, J.H., Jotyan, G., Spooner, G.J.R., Juhasz, T., Kurtz, R.M., O'Donnell, M. Strain Imaging of Corneal Tissue With an Ultrasound Elasticity Microscope. *Cornea.* 2002. 21(1): 68-73.

Insana, M. F. and T. J. Hall. Parametric Ultrasound Imaging from Backscatter Coefficient Measurements - Image-Formation and Interpretation. *Ultrason. Img*. 1990. 12: 245-267.

Izumi, K., Feinberg, S.E., Iida, A., Yoshizawa, M. Intraoral Grafting of an *Ex Vivo* Produced Oral Mucosa Equivalent: A Preliminary Report. *Int. J. Oral Maxillofac. Surg.* 2003. 32: 188–197.

Izumi, K., Song, J., Feinberg, S.E. Development of a Tissue-Engineered Human Oral Mucosa: From the Bench to the Bed Side. *Cells Tissues Organs.* 2004. 176:134–152.

Izumi, K., Terashi, H. Marcelo, C.L., Feinberg, S. E. Development and characterization of a tissue-engineered human oral mucosa equivalent produced in a serum-free culture system. *J. Den. Res*. 2000. 79: 798-805.

Kolios, M.C., Czarnota, G.J., Lee, M., J.W. Hunt, and M.D. Sherar. Ultrasonic spectral parameter characterization of apoptosis. *Ultrasound Med. Biol*. 28: 589–597, 2002.

Marchant RE, Kang, I., Sit, P.S. Zhou, Y., Todd, B.A. , Eppell, S.J. Lee, I. Molecular Views and Measurements of Hemostatic Processes using Atomic Force Microscopy. *Curr Protein Pept Sci.* 2002.3(3):249-74.

Matsuyama, T., St. Goar, F.G., Tye, T.L., Oppenheim, G., Schnittger, I., Popp, R.L. Ultrasonic Tissue Characterization of Human Hypertrophied Hearts *In Vivo* with Cardiac Cycle-Dependent Variation in Integrated Backscatter. *Circul.* 2003. 80: 925-934. 1989.

Olerud, J. E. , Obrien, W.D. , Riedererhenderson, M.A. , Steiger, D.L., Debel, J.R., Odland, G. F. Correlation of Tissue Constituents with the Acoustic Properties of Skin and Wound. *Ultrasound Med. Biol*. 1999. 16: 55-64,

Taggart, LR., Baddour, R.E., Giles, A., Czarnota, G.J., Kolios, M.C. Ultrasonic Characterization of Whole Cells and Isolated Nuclei. *Ultrasound in Med. & Biol*. 2007. 33(3): 389–401.

Verstraeten V.L., Lammerding, J. Experimental Techniques for Study of Chromatin Mechanics in Intact Nuclei and Living Cells. *Chromosome Res*. 2008.16(3):499-510.

Wickline, S. A., Thomas, L.J. , Miller, J.G., Sobel, B.E., Perez, J. E. The Dependence of Myocardial Ultrasonic Integrated Backscatter on Contractile Performance. *Circulation*. 1985. 72: 183-192.

Winterroth, F., Hollman, K.W., Izumi, K., Feinberg, S.E., Fowlkes, J.B., Hollister, S.J. Examination and Comparisons of EVPOME/ AlloDerm® Compositions with Natural Mucosal Tissues Using Scanning Acoustic Microscopy. *Society for Biomaterials 2009 Annual Meeting and Exposition*. 2009.

Winterroth, F., Fowlkes, J. B., Kuo, S., Izumi, K., Feinberg, S.E., Hollister, S. J., Hollman, K. W. High-Resolution Ultrasonic Monitoring of Cellular Differentiation in an *Ex Vivo* Produced Oral Mucosal Equivalent (EVPOME). *Proc. IEEE Bioultrasonics Conference.* 2009.

Zuber, M., Gerber, K., Erne, P. Myocardial Tissue Characterization in Heart Failure by Real-Time Integrated Backscatter. *Eur. J. Ultrasound*. 1999. 9: 135–143.

## FIGURES

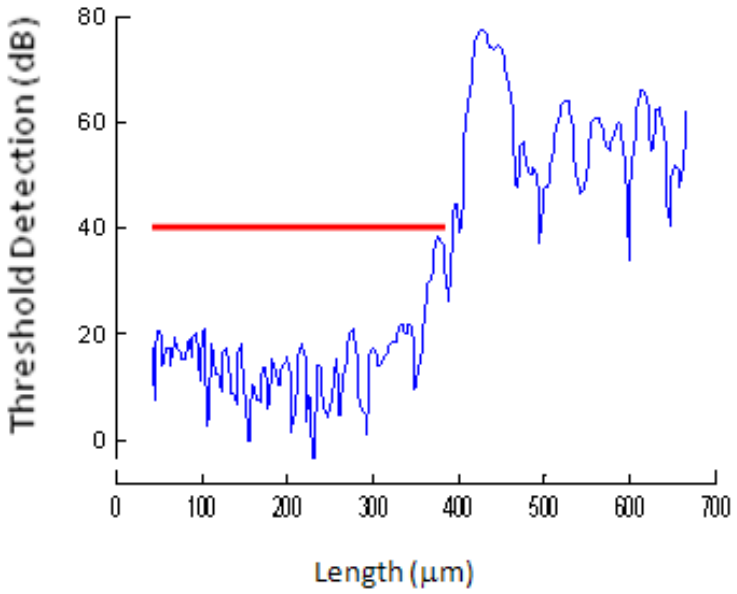


**Figure 3.1. Plot diagram of the SAM, showing the detection of the device surface (red line) after setting the threshold detection safely above the signal of the water.**

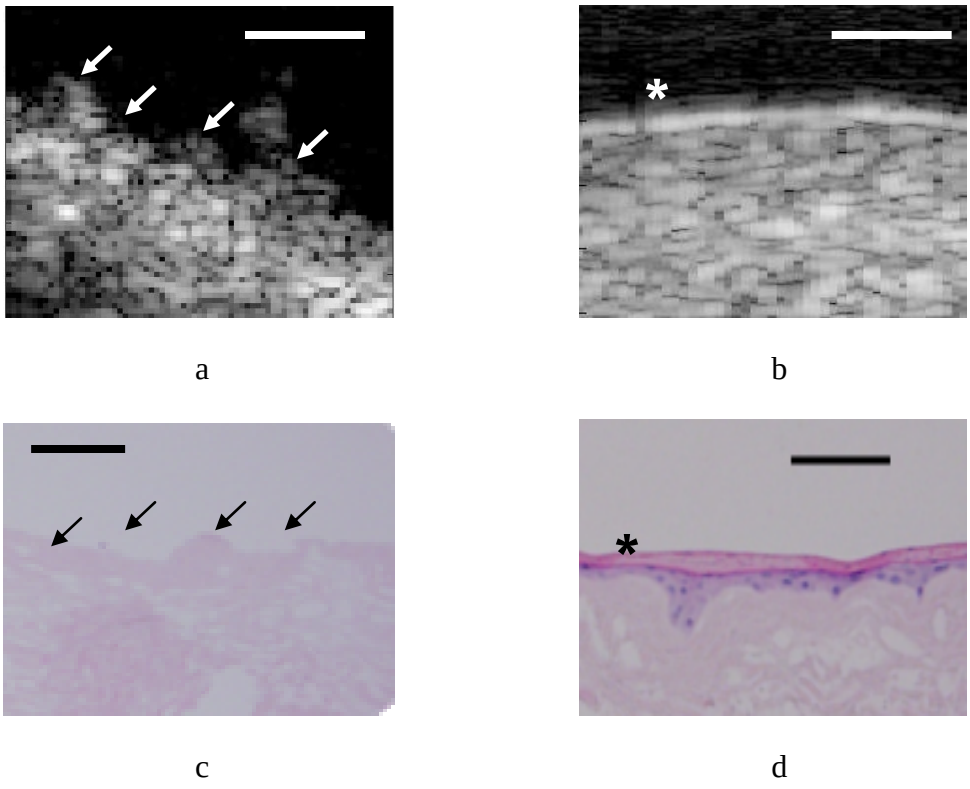


**Figure 3.2. 2D B-scan images of the untreated AlloDerm® device (a) and EVPOME at 11 days post seeding (b). Surface irregularities (arrows) are clearly present on the AlloDerm® compared to the EVPOME; the latter shows a brighter surface reflection (asterisk), the result of the differentiating keratinocytes. The corresponding histology images for the untreated AlloDerm® device (c) the EVPOME at 11 days post seeding (d) also shows a high number of surface irregularities (arrows) on the former compared to the keratinized layer (asterisk) on the EVPOME surface. Scale bars represent 100 μm.**

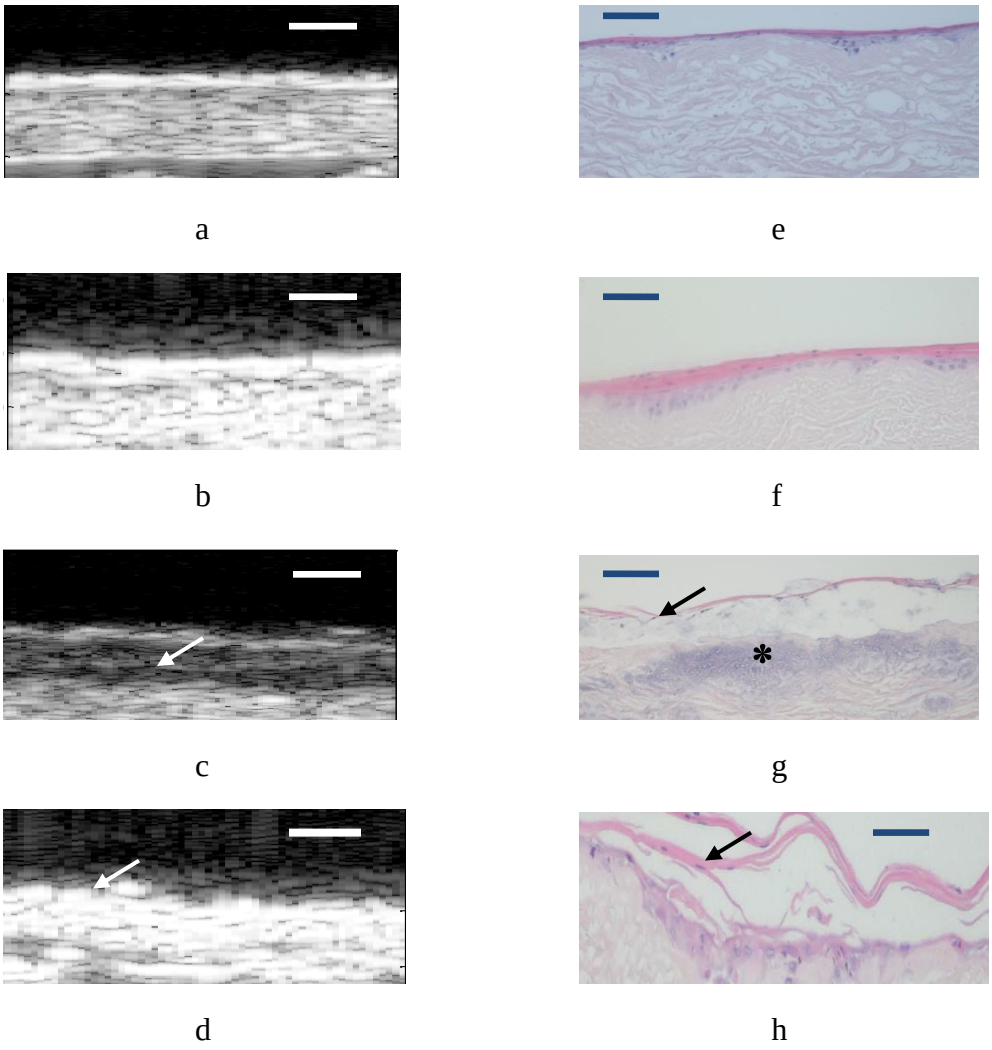


**Figure 3.3. 2D B-scan composites of the EVPOME devices for both the thermally unstressed (a-b) and stressed (c-d) groups. The corresponding histology micrographs of both unstressed (e-f) and stressed devices (g-h) compare the conditions of the keratinized surfaces for both imaging modalities. Comparing image c with g, there is a clear partitioning (arrows) between the keratinized layer and the device due to the heat stress; evident in the darkened region of the B-scan image (arrow). For image d, the irregular surface of the AlloDerm® device is visible (arrow), but no keratinized layer; the likely result of the keratin layer sloughing off from the device surface. For image g, the blue staining on the device (asterisk) is a result of excessive hematoxylin used in their preparation and not a result of the thermal treatment. Device surfaces are at the top of each image. Scale bars represent 100 μm.**

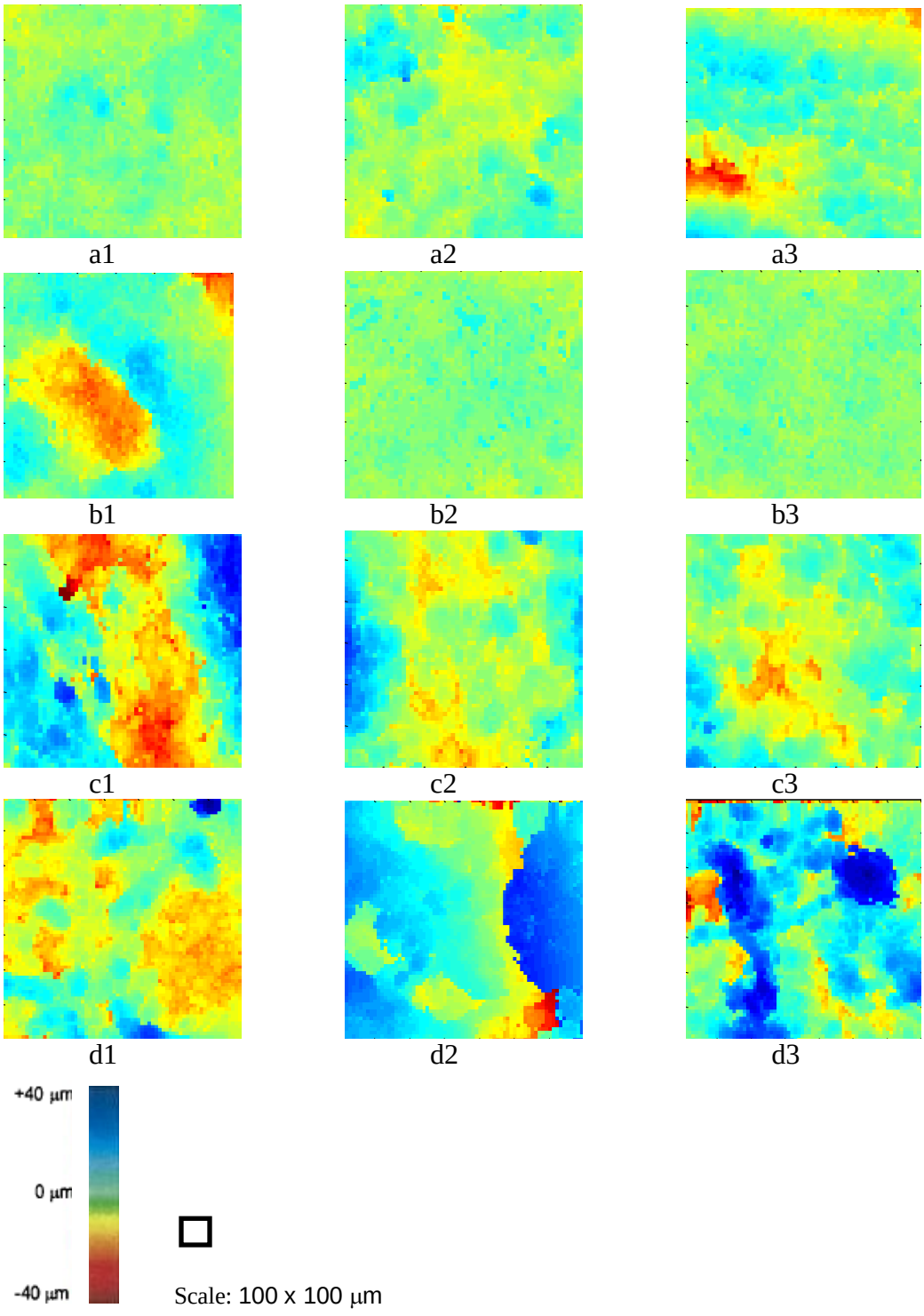


**Figure 3.4. RMS profilometry images for each scan performed on the thermally non-stressed (a-b) and stressed (c-d) devices. For the latter, there is higher variation in the surface features – presumably from the thermal stress fractionating the keratinized layer. With the non-stressed devices, there is little variation in the surface profiles, characteristic of the uniformity of the keratin layer on their surfaces.**

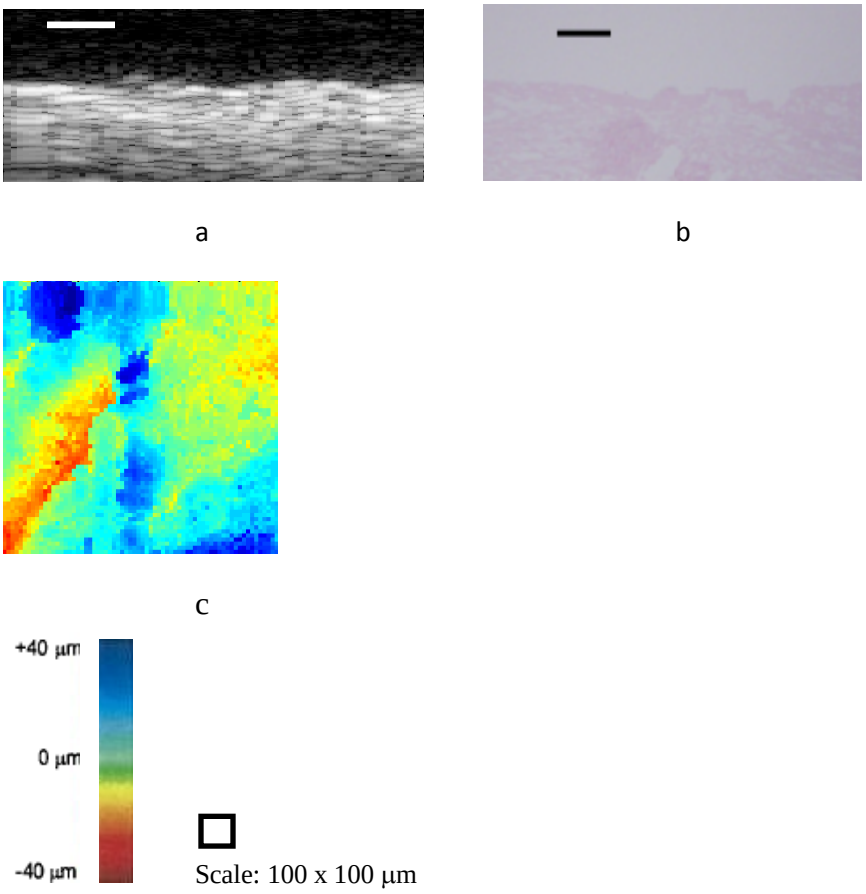


**Figure 3.5. SAM 2D B-scan (a), histology micrograph (b), and C-scan profile (c) of an unseeded AlloDerm® device. Scale bars represent 100 µm.**

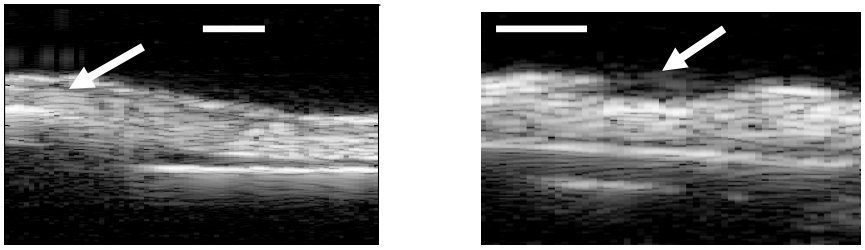

**Figure 3.6. 2D B-scans of non-stressed devices showing surface irregularities (arrows) in these two selected scan areas of the devices - due to positioning the devices. This resulted in higher (outlier) RMS values when processing the SAM scans and consequently, higher variations. Scale bars are 100 μm.**

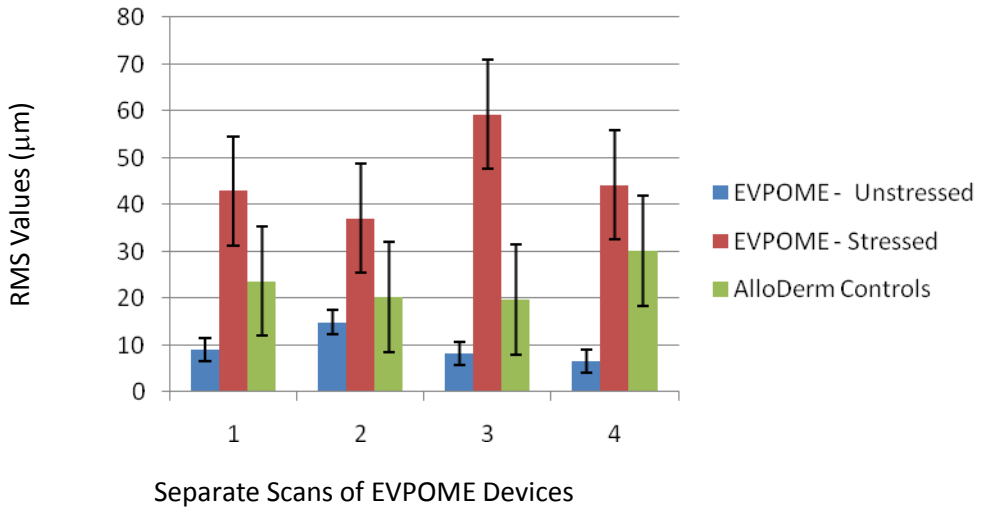


**Figure 3.7. Comparative RMS heights for EVPOME devices, both unstressed, stressed, and the unseeded AlloDerm®. Values provided are from each separate set of SAM scans.**

# CHAPTER IV

# ULTRASONIC ANALYSES ALGORITHM ON AN EX VIVO PRODUCED ORAL MUCOSAL EQUIVALENT AFTER UNDERGOING A THERMAL STRESS TEST

## 4.1 REPRESENTATION OF FILTERING AND ANALYSES ALGORITHM ON SAM EVPOME IMAGES

This study examines using scanning acoustic microscopy (SAM) coupled with filtering and an analyses algorithm to effectively study the surface characteristics of engineered oral mucosal tissues. The advantages of using SAM over conventional optical microscopy include being able to image the cells and tissues without doing any preparations which could potentially kill or alter the tissues; this provides a more accurate representation of the tissues' natural

properties (Cohn et. al 1997a). It will also provide evidence as to the degree of differentiation which the cells undergo without chemically affecting their properties (Kolios et. al. 2002, Saijo, et. al. 2004).

Previously, we used SAM to compare changes in the radiofrequency (RF) data in *ex vivo* produced oral mucosal equivalent (EVPOME) specimens undergoing differentiation, apoptosis, and keratinization by studying the reflectivity off their surfaces and analyzing the degree of surface irregularities. We then compared these results to EVPOME specimens which underwent standard histological preparation and examination under optical microscopy: a strong linear correlation was found between the optical and SAM images when quantifying these surface characteristics. We also used SAM to study changes in RF data between seeded EVPOME devices which have undergone periods of elevated thermal incubation (stressed) to those which were incubated continuously at physiological temperature (unstressed) (Winterroth et. al. 2011). By correlating changes in the RF data to the EVPOME (and natural tissue cells in general) undergoing differentiation, apoptosis, and keratinization, we can better understand the physiological processes of these cells as they evolve.

For this study, we examined and compared the surface acoustic profile characteristics (ultrasonic profilometry) between two EVPOME specimens: one

underwent a thermal elevation for 24 hours (stressed) while the other was an unstressed control. Ultrasonic profilometry uses an analysis algorithm to remove any major artifacts from the scanned specimens – which could potentially alter the image of the scanned surface; it is a promising method to analyze tissue types and their respective characteristics on the basis of acoustic transmission and scatter properties (Matsuyama et. al. 1989, Zuber et. al. 1999).

## 4.2 CALCULATIONS OF EVPOME SURFACE PROFILES

The 2D B-scans from the SAM and their comparative histology images show a clear partitioning of the keratin layer from the apical surface of the specimens under stressed conditions. Comparing the B-scans taken of EVPOME at 11 days post-seeding, there is a distinct reflection off of the surface (Figure 4.1a) – a result of the seeded keratinocytes differentiation - which is not found in the stressed EVPOME specimen (Figure 4.1b). The histology images of these same specimens- AlloDerm® and EVPOME at 11-days post seeding (Figures 4.1c and 4.1d, respectively) - verify these findings as the keratinized layer in the latter image shows a smooth surface, with less surface irregularities compared to the former image.

Removing any tilt (which potentially occurs when mounting and positioning the specimens) lowers the measured RMS heights for all specimens but it

maintains the mean difference between the stressed and non-stressed specimens in SAM C-scans of their surface (Figure 4.2a); the same is true when adding the weak filter (Figure 4.2b). However, adding the weak filter seems to slightly increase standard deviation; the filter parameters may require further adjustments. B-scans taken along the transverse axis of the stressed specimen where the surface variations are the highest show significant changes in the surface at the point where there is a significant increase in the RMS height (Figure 4.3), accounting for the higher variation in the RMS value for the stressed specimen. This is verified by calculating the mean values for the height variations between the stressed and non-stressed specimens and determining their respective standard errors in all the study sets performed (Figure 4.4). The error bars represent the percent standard deviation of the mean. Because there are more RMS variations in the stressed specimens, there would be the likelihood for higher error. There is also the likelihood of the tissue samples tilting during their mounting process which would contribute to the increased RMS profiles, for both stressed and non-stressed specimens.

## REFERENCES


Cohn, N.A., Emelianov, S.Y., Lubinski, M.A., O'Donnell, M. An Elasticity Microscope. Part I: Methods. *IEEE Trans. Ultrason. Ferr. Freq. Ctrl.* 44(6): 1304-1319. 1997.

Cohn, N.A., Emelianov, S.Y., O'Donnell, M. An Elasticity Microscope. Part II: Experimental Results. *IEEE Trans. Ultrason. Ferr. Freq. Ctrl.* 44(6): 1320-1331. 1997.

Izumi, K., J. Song, and S.E. Feinberg. Development of a Tissue-Engineered Human Oral Mucosa: From the Bench to the Bed Side. *Cells Tiss. Org.* 176:134–152, 2004.

Kolios, M.C., Czarnota, G.J., Lee, M., Hunt, J.W., Sherar, M.D. Ultrasonic Spectral Parameter Characterization of Apoptosis. *Ultrasound in Med. Biol*., 28(5): 589–597. 2002.

Matsuyama, T., St. Goar, F.G., Tye, T.L., Oppenheim, G., Schnittger, I., Popp, R.L. Ultrasonic Tissue Characterization of Human Hypertrophied Hearts *In Vivo* with Cardiac Cycle-Dependent Variation in Integrated Backscatter. *Circul.* 80: 925-934. 1989.

Saijo, Y., Miyakawa, T., Sasaki, H., Tanaka, M., Nitta, S. Acoustic Properties of Aortic Aneurysm Obtained with Scanning Acoustic Microscopy. *Ultrasonics*. 42: 695–698. 2004.

Winterroth, F., Fowlkes, J. B., Kuo, S., Izumi, K., Feinberg, S.E., Hollister, S. J., Hollman, K. W. High-Resolution Ultrasonic Monitoring of Cellular Differentiation in an *Ex Vivo* Produced Oral Mucosal Equivalent (EVPOME). *Proc. IEEE Bioultrasonics Conference.* 2009.

Winterroth, F., Lee, J., Kuo, S., Fowlkes, J.B., Feinberg, S.E., Hollister, S.J., Hollman, K.W. Acoustic Microscopy Analyses to Determine Good Versus Failed Tissue Engineered Oral Mucosa Under Normal or Thermally Stressed Culture Conditions. *Ann. Biomed. Engineer* 2011. 39(1): 44-52.

Zuber, M., Gerber, K., Erne, P. Myocardial Tissue Characterization in Heart Failure by Real-Time Integrated Backscatter. *Eur. J. Ultrasound*. 9: 135–143. 1999.

## FIGURES

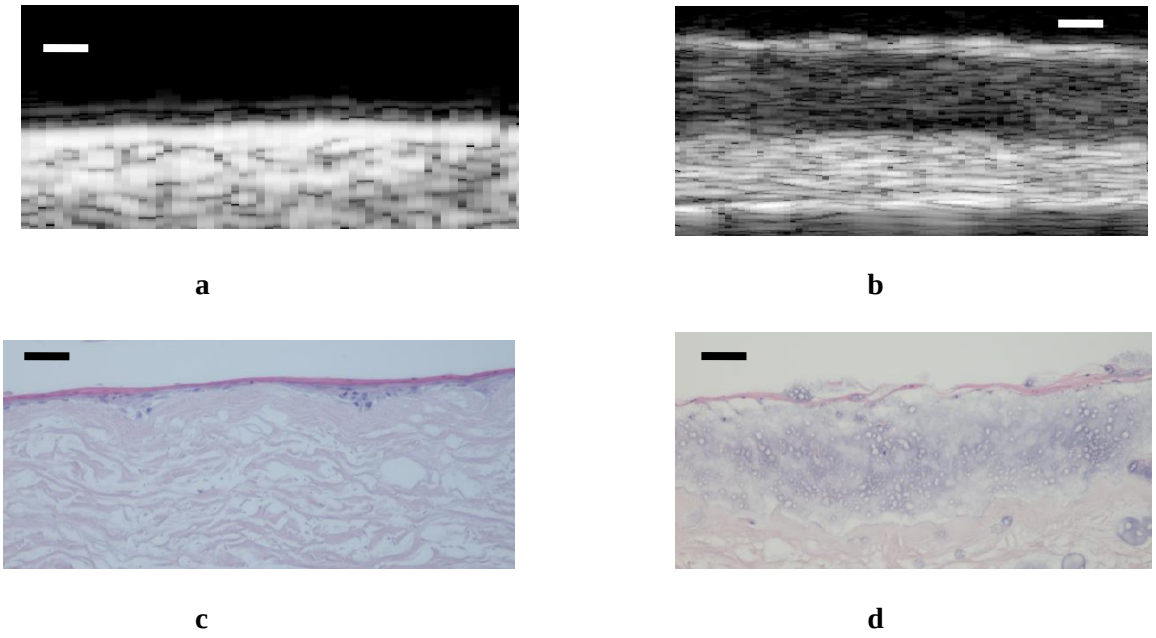


**Figure 4.1. SAM 2D B-Scans of EVPOMEs under unstressed (a) and stressed (b) conditions. Note the differences in the reflectivity on the surfaces (arrows). The histology images of the unstressed (c) and stressed (d) devices verify these findings: the keratinized layer (arrow) and the artifacts in the partitioned area (asterisk). The scale bars represent 100μm.**

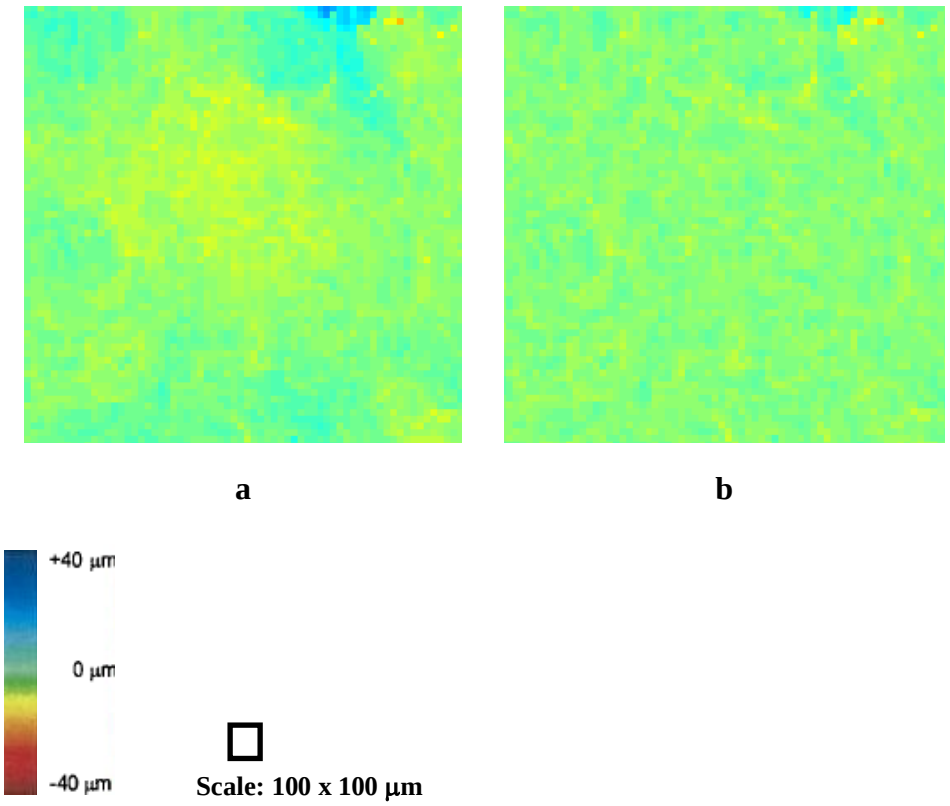


**Figure 4.2. SAM C-scans of an unstressed EVPOME specimen. The images result from taking the image and removing any tilt (a), followed by fitting the planar surface and subtracting the result (b).**

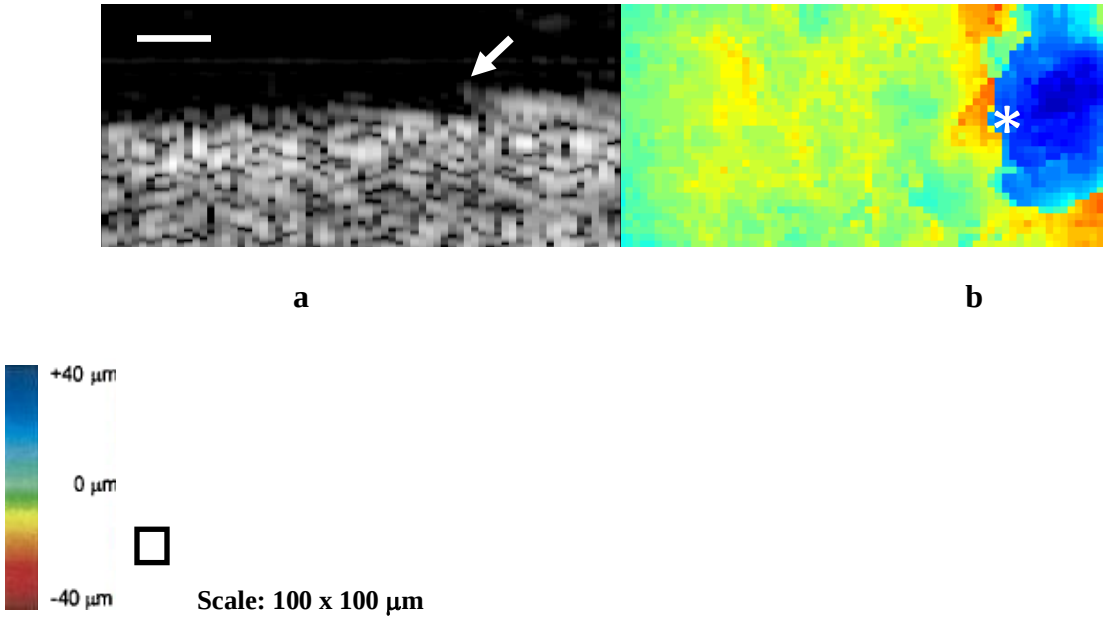


**Figure 4.3. SAM 2D B-scan of the thermal stress scaffold (a) showing an elevated surface irregularity (arrow) produced in the C-scan (b) at the same region (asterisk), the RMS height being approximately 40 μm. The scale bar on the B-scan is 100 μm.**

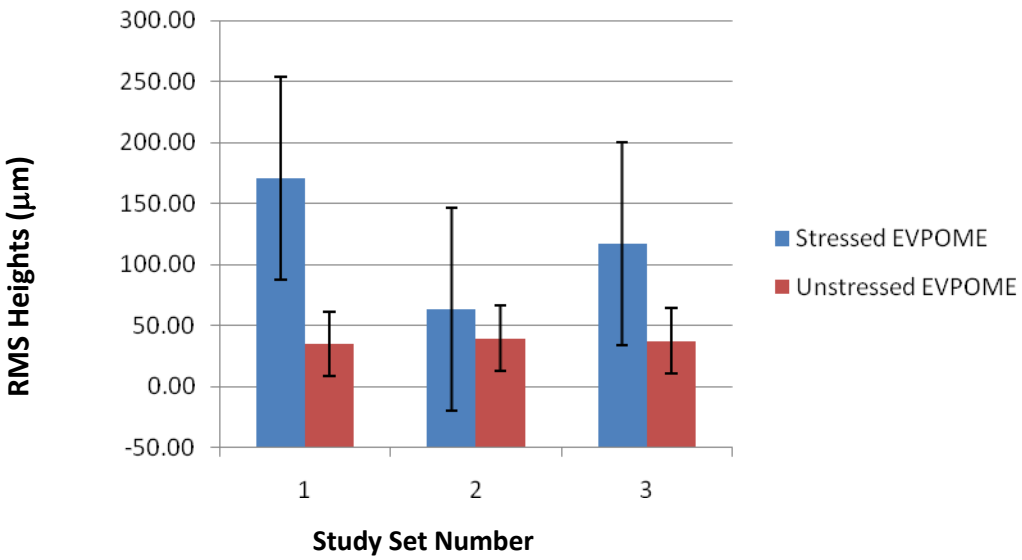


**Figure 4.4. RMS variations in height for the stressed and unstressed EVPOME specimens for each set of studies conducted. The standard deviation of the scaffold as a percentage of the mean is 70.71.**

# CHAPTER V

# ULTRASONIC PROFILOMETRY AND STRESS – STRAIN ANALYSES ON NATURAL AND ENGINEERED ORAL TISSUES AFTER MECHANICAL DEFORMATION TESTING

## 5.1 INTRODUCTION

This study examines using scanning acoustic microscopy (SAM) as an effective tool to study both the mechanical properties and non-linear elastic characteristics of natural and engineered oral mucosal tissues. The advantages of using SAM over conventional optical and electron microscopy include being

able to image the cells and tissues without doing any preparations which could potentially kill or alter the tissues; this provides a more accurate representation of the tissues' natural properties (Cohn et. al. 1997a, Cohn 1997c). We used SAM as a method to examine the elastic properties, specifically stress-strain models on both natural oral mucosal tissues. In addition, further mechanical studies were conducted on two engineered tissue specimens: the commercially available acellular cadaveric dermis, AlloDerm® (LifeCell Corp., Branchburg, NJ, USA) and an in-house designed *ex vivo* produced oral mucosal equivalent (EVPOME).

### 5.1.1 Background on Oral Mucosal Anatomy

The oral mucosal epidermis is composed of a keratinized stratified squamous epithelium. Its cells, keratinocytes, are arranged into 4 (thin skin) or 5 (thick skin) layers. The outermost layer is always composed of non-living, highly keratinized (cornified) cells that function to reduce water loss (Warner et. al. 1988). After keratinocytes leave the germinal layer, they undergo a specialized form of cell death known as anoikis. Anoikis is initiated when cells detach from their surrounding environment and loose communication with it (Tortora et. al. 1993). In keratinocytes, this programmed cell death is accompanied by the accumulation of keratin to the exclusion of all other products and organelles (Broekaert et. al 1988, Holland et. al. 1997, Moll et. al. 2008, Norlén et. al. 2004, Norlén et. al. 2006).

### 5.1.2 Background on the Human Dermis and its Comparison to AlloDerm®

The dermis is the thick layer of connective tissue to which the epidermis is attached. Its deepest part continues into the subcutaneous tissue without a sharply defined boundary. Its thickness is for this reason difficult to determine but 1-2 mm is a good estimate for human skin. Figure 1 illustrates the histology of the human dermis and its principal components. The dermis may be divided into two sublayers (again without a sharp boundary):

3. The papillary layer: consisting of loose, comparatively cell-rich connective tissue, which fills the hollows at deep surface (dermal papillae) of the epidermis. Capillaries are frequent. Collagen fibers appear finer than in the reticular layer.
4. The reticular layer: appearing denser and containing fewer cells. Thick collagen fibers (5-10 µm) often aggregate into bundles (up to 100 µm thick). The fibers form an interlacing network, although their predominant direction is parallel to the surface of the skin. A preferred orientation of the collagen fibers is not visible in the sections, but the main orientation of the fibers differs in skin from different parts of the body. Usually, their main orientation will follow the "lines of greatest tension" in the skin (Kraissl lines). This is of some surgical importance since incisions parallel to these lines will heal faster and with less formation of scar tissue.

### 5.1.3 Background on EVPOME

The development and use of an *ex vivo* produced oral mucosal equivalent (EVPOME) has demonstrated its clinical efficacy in intra-oral surgical grafts (Hotta et. al. 2007, Izumi et. al 2003). In addition, oral mucosa tissues have been clinically reported to be suitable for transplantation to treat vaginal agenesis (Lin et. al. 2003). The oral mucosa's histology resembles that of skin: as new cells are formed on the basal lamina, the more matured cells migrate toward the apex, undergoing apoptosis and keratinization they migrate (Izumi et. al. 2003); this same process occurs in the EVPOME tissues. Figure 1 provides an illustration comparing the EVPOME device with natural oral mucosa tissue; In both cases, there is a basal layer of actively dividing and differentiating cells, followed by a uniformly keratinized apical layer. What is still unknown is EVPOME's effectiveness as a substitute tissue replacement for other soft tissues such as dermal, vaginal, or urethral; they have not been tested for non-linear elastic characteristics. Although the oral mucosa's histology resembles that of human epidermis and both tissue types are derived from ectodermal tissues, similarities in their physical properties have yet to be compared.

### 5.1.4 Background on SAM

Although SAM has been used to study the morphology and density of skin tissue under both normal and pathological conditions (Barr et. al 1991), it has not

been applied toward understanding its elastic properties. Further no studies have yet examined the elastic parameters of oral tissues, both natural and engineered.

Previously, we used SAM to compare any changes in the RF data to the EVPOME and natural human oral mucosal cells in general undergoing differentiation, apoptosis, and keratinization (Winterroth et. al 2009). The spectral analysis results from SAM can be compared to histological images of the EVPOME tissues at different stages of growth and development. By correlating changes in the RF data to the EVPOME (and mucosal cells in general) undergoing differentiation, apoptosis, and keratinization, we can better understand the physiological processes of these cells as they evolve.

The transducer's parameters are: 15 μm in the transverse direction; a lateral resolution ($R_{lat}$) of 37μm; an axial resolution ($R_{ax}$) of 24μm; a depth of field of 223μm. The Z-axis was sampled at 300 megasamples/second. $R_{ax}$ is in the direction of propagation and is determined by the length of the ultrasound pulse propagating in the tissue; $R_{lat}$ is orthogonal to the propagation direction of the ultrasound wave.

### 5.1.5 Background on Small Tissue Compression Device and Testing

This set-up is derived from the experiments originally performed by Erkamp (Erkamp et. al. 1998) in which a cylindrical sample was indented while

mounted on top of a glass slide (Figure 5.2 a-b). The system consisted of an in-house built manual compressor using cylindrical pistons of different known surface areas for indentation and electronic scale for measuring the degree of force applied with each compressive step applied by the piston. To obtain the Young's modulus, the slope of force–displacement response was transformed to Young's modulus using a conversion factor. This factor was obtained experimentally and validated by finite element (FE) modeling. Preliminary results of canine kidney tissue were presented and reasonable reproducibility was concluded.

Further studies (Samani et. al. 2003) applied FE analysis for the linear relation required to transform the indentation force–deformation slope to the Young's modulus of tissue specimens, specifically soft tissue specimens. In both Samani and Erkamp, a piston load leading to indentation in the tissue, leading to elastic deformation with the area of indentation ($\Delta$) in the same direction as the indentation forces (F). FE modeling of the object would lead to the object behaving according to Hooke's Law:

$$\mathbf{F = KX} \qquad \mathbf{(1)}$$

where K is the stiffness matrix and X is the nodal displacement.

The system to measure elastic moduli of soft tissue is an in-house built compressor using a cylindrical piston of known length and volume to indent the tissue sample at steps of a known length, registering as a change in mass (in

grams) on an electronic scale (Ohaus Scout Pro, Pine Brook, NJ. USA.) This compressor set up is illustrated in Figure 5.2a and 5.2b. The tissue sample is cylindrical in shape with an area (A) slightly larger than that of the piston. The piston is mounted directly over the center of the sample and pushes on the sample, producing a known amount of force. This force plus knowing the degree of surface displacement provides the stiffness characteristic for the given samples. In addition, stress-strain relationships are derived for each specimen based on the following equations:

Gram to Newton conversion was applied to obtain the appropriate force for each step using the following equation:

$$F = [(gr/1000)*9.80665] \qquad (2)$$

where gr is the piston load in grams registered by the scale.

The compressive stress ($\sigma$) was obtained by dividing the given force by the area of the piston:

$$\sigma = F/A \qquad (3)$$

The stretch ratio ($\lambda$) was measured as

$$\lambda = \frac{\Delta l}{l_0} \qquad (4a)$$

where $\Delta l$ is the change in the thickness of the specimen $l_0$ is the original specimen length. This is further applied to the 1-term Ogden model where the strain energy density is given by:

$$W = \frac{\mu}{\alpha} (\lambda_\alpha^1, \lambda_\alpha^2, \lambda_\alpha^3 - 3) \qquad \textbf{(4b)}$$

where $\mu$ and $\alpha$ are the material constants and $\lambda_\alpha^1$, $\lambda_\alpha^2$, and $\lambda_\alpha^3$ are the principal stretches.

Poisson's ratio ($\nu$) defines transverse contraction strain ($\varepsilon_{trans}$) to longitudinal extension strain ($\varepsilon_{long}$) in the direction of the stretching force. The tensile deformation is considered positive and the compressive deformation is considered negative:

$$\nu = - \varepsilon_{trans} / (\varepsilon_{long}) \qquad \textbf{(5)}$$

Finally, Young's modulus (E) was obtained as the ratio of stress/strain:

$$E = \sigma/\varepsilon \qquad \textbf{(6)}$$

The elastic modulus measures the stiffness of the material.

Poisson's ratio is related to elastic modulus K (the bulk modulus), G (shear modulus), and E by the following:

$$\nu = \frac{(3K - 2G)}{(6K + 2G)} \qquad \textbf{(7)}$$

$$E = 2G(1 + \nu) \qquad (8)$$

Given a volume which remains constant under deformation, Equation 6 can be revised as the following:

$$E = \frac{(FL^2)}{(\Delta LV)} \qquad (9)$$

where L and V are the piston length and volume, respectively and $\Delta L$ is the length change in the piston due to the applied force F.

Specimens used for this study include natural porcine mucosal, and epidermal tissues; engineered specimens were the aforementioned AlloDerm® and EVPOME at 11 days post-seeding – previously determined as the optimal growth time for proper keratinization to occur (Izumi et. al. 2003).

For the indentation experiments shown in Figure 5.2, the piston causes displacements of equal $\Delta L$ over the given indentation area of the tissue.

In the case of the EVPOME the additional presence of the seeded material on the surface contributes to elastic changes corresponding to Hookean principles of two materials in series:

$$\frac{1}{k_{eq}} = \frac{1}{k_1} + \frac{1}{k_2} \qquad (10)$$

where $k_1$ and $k_2$ are the two spring constants (namely, the seeded cellular material and the AlloDerm® scaffold) for the specimen and the seeded materials and $k_{eq}$ is the equivalent spring constant for the specimen.

Because of the large stress-strain deformations occurring, particularly with the AlloDerm® and the non-linear hyperelasticity of the deformation for both engineered and natural tissues, we assume they behave as Ogden hyperelastic models (Bathe 1996). Under Neo-Hookean principles, the engineered biomaterials are incompressible as they exhibit a change in their surface area when subjected to compression forces, but their volume remains constant (Erkamp et. al 1998, Samani et. al. 2003). The high water content in these tissues accounts for this incompressibility.

Earlier SAM studies between AlloDerm® and EVPOME showed significant differences in their reflectivity (Winterroth et. al. 2009) and in their surface irregularities as the EVPOME evolved and developed a stratified surface, filling in the surface roughness (Winterroth et. al. 2010). Additional studies subjecting EVPOME to a thermal stress test showed its surface characteristics comparable to an unseeded AlloDerm® device (Winterroth et. al. 2011).

The in-house SAM system has previously been used to obtain elastic properties - specifically, stress-strain parameters, and consequently, Young's modulus in different soft tissues, including porcine cornea (Cohn et. al. 1997b, Hollman et. al. 2002). Currently, there have been no studies to examine the elastic properties of either natural or engineered mucosal tissues, therefore it has

been difficult to prognosticate or assess what effects would result from any compression testing. We therefore used skin tissues for comparisons as they have been studied for compressive properties (Harrison et. al 2006) and exhibit similar morphology to the mucosal tissues since they are derived from the same embryological tissues.

For this study, we examined the structures of engineered and natural oral tissues and natural skin tissues using SAM, followed by testing their mechanical deformation properties using the cylindrical compressor. In addition, we used SAM with a built-in compressor to test for stress-strain relationships on these same tissues. These experiments are essential to learn how ultrasound can aide in understanding the physical properties of soft tissues, particularly the engineered soft tissues and their adaptability to the human body.

## 5.2 MATERIALS AND METHODS

### 5.2.1 Preparation of Natural Tissues

Fresh porcine tissue was obtained from a local abattoir and the oral tissues – buccal mucosa, gingival, and upper palate - were surgically excised and immersed in degassed, deionized water for SAM imaging. Similarly, porcine skin tissues were obtained and prepared in this manner – in this case, the epidermis was surgically excised from the subcutaneous tissues and latter discarded.

### 5.2.2 Preparation of AlloDerm® and EVPOME Devices

The protocol for harvesting human oral mucosal tissue was approved by a University of Michigan Internal Review Board. Details of the AlloDerm® and EVPOME development are similar to those described elsewhere (Izumi et. al. 2004). Briefly, oral mucosa keratinocytes were enzymatically dissociated from the tissue sample, and a primary cell culture was established and propagated in a chemically-defined, serum- and xenogeneic products-free culture medium, with a calcium concentration of 1.2 mM. The AlloDerm® specimens were soaked in 5 $\mu g/cm^2$ human type IV collagen overnight prior to seeding cells to assist the adherence of cells, then approximately $2.0 \times 10^5$ cells/$cm^2$ of oral keratinocytes (cell lines: DPG3, JXP2) were seeded onto the type IV collagen pre-soaked AlloDerm®. The morphologies of the keratinocytes at seeding and 24-hours post-seeding are shown in Figure 3. The composites of the keratinocytes and the AlloDerm® were then cultured, in the submerged condition, for 4 days to form a continuous epithelial monolayer. At 4 days, samples of the EVPOME were collected while in the submerged condition for SAM imaging. After 4 days, the equivalents were raised to an air-liquid interface to encourage epithelial stratification and cultured for another 10 days, resulting in a fully-differentiated, well-stratified epithelial layer on the AlloDerm®.

For the last set of experiments, 2 additional AlloDerm® and EVPOME specimens were prepared; these were the thermally stressed specimens. For

the thermally stressed AlloDerm® and EVPOME specimens: on Day 9 post-seeding, one of each specimen was incubated at 43°C for 24 hours, then switched back to 37°C for another 24 hours. The total incubation times were equal for all specimens.

### 5.2.3 SAM Set-Up and Imaging

Details for the set up of the SAM have been detailed previously (Cohn 1997a, Cohn 1997b, Hollman et. al. 2002). Briefly, AlloDerm®, EVPOME, and natural mucosal tissue samples were immersed in deionized water and imaged with a single element fixed focus transducer, producing ultrasonic B-scans. The transducer has an approximate frequency of 50 MHz, the element is 3 mm in diameter and focused to a depth of 4.1 mm, giving an f/number of approximately 1.4. The transducer was fastened to an optical mount and the angular position was adjusted until the ultrasonic beam was normal to the deflecting plate. We scanned the surfaces of the EVPOME, AlloDerm®, and keratinized oral mucosa (palate) and non-keratinized oral mucosa (buccal mucosa), showing the acoustic signal between the interface of the sample and water on the sample's apical side. DC stepper motors positioned the transducer above the specimen. B-scan images were obtained by stepping the transducer element laterally across the desired region. At each position, the transducer fired and an RF A-line was recorded. After repeated firings at one position, the transducer moved to the next position, where the image was constructed from A-lines acquired at all lateral

positions. Because of low f/number, single element transducers have a short depth of field; a composite B-scan image was generated from multiple scans at different heights. The SAM set up is illustrated in Figure 5.3 both as a schematic illustration (Figure 5.3a) and a photograph (Figure 5.3b), with the differences in the acoustic patterns as they reflect off of the tissue boundaries (surface and base) (Saijo 1991, Hollman et. al. 2002), including the phase shift in the sound waves when reflecting off the tissue as opposed to the base surface of the holder, the reflections off the surface and bottom of the tissue, and the sound speed through water and tissue. The tissue surface was determined by thresholding the magnitude of the signal at the first axial incidence of a value safely above noise, approximately 20-30 dB. All of the tissue specimens were imaged by SAM before and after the compression testing by the cylinder compressor. 2D B-scan images of the EVPOME and unseeded AlloDerm® are shown in Figure 5.4a-b, along with their histology counterparts (Figure 5.4c-d).

### 5.2.4 Mechanical Compression Testing Using SAM

The mechanical compressor was positioned over the tissues to be scanned. The compressor consists of a metal plate approximately 2cm$^2$ with a 2mm open slit running along the middle of the plate (Figures 5.5a-d). The transducer was positioned over the slit and the focused until the scatter from the

tissue was recorded. Changes in acoustic signals between compressor plate and the tissue were easily obtained because of differences in their height and scatter properties. Once the signal for the tissues was captured, the plate was positioned over a selected area of the tissue and lowered until it made direct contact with the tissue, without causing any compression to the tissue: the compressor plate was retracted one step size from first contact with the tissue to minimize this.

### 5.2.5 SAM 3D Deformation Image and Motion Processing

To image strain, confocal images of the different tissue specimens were taken before and after deformation. Before measurements, the tissues were in slight contact with the deformation plate. Two surface deformation steps of 50 μm were then applied, capturing ultrasound data at no deformation and at each step. Speckle was tracked between these images with a correlation-based algorithm (O'Donnell et. al. 1994, Lubinski et. al. 1996, Lubinski et. al. 1999).

### 5.2.6 Mechanical Testing Using Cylindrical Compressor

Additional compression testing was performed on both unseeded AlloDerm® and EVPOME (11-days post-seeding) specimens by removing each specimen from an aqueous environment, measuring their thickness with an electronic caliper (Mituyo Corp., Japan) and placing it under an in-house built

compression unit with cylindrical pistons which were either 55.40 $mm^2$ or 28.26 $mm^2$ in area. A digital scale was placed directly beneath the specimen, tares to the weight of the specimen, and recorded changes in the weight for each successive step (10μm) that the cylindrical piston was applied to the specimen. Further details of the mechanical set-up and its applications and calculations are described under the Introduction and illustrated in Figure 5.2. All stress levels were measured as Pascals in relation to strain levels of known compression steps length. These same methods were performed on all natural skin and oral mucosal tissues obtained from a local abattoir.

### 5.2.7 Statistical Analyses and Fitting Models

Both one-way analyses of variance (ANOVA) and linear regression analyses were performed to determine the root mean square (RMS) values for the individual specimens. Mathematical fitting models of the tissues (stressed and unstressed AlloDerm® and 11 days post-seeding EVPOME specimens), specifically 1-term Ogden models were performed and analyzed using a program developed using MatLab (MathWorks, Inc. Natick MA., USA).

## 5.3 RESULTS

In the SAM 2D B-scan for the tissues as well as the AlloDerm® and EVPOME devices, the transducer is positioned at the top of the image, pointing

downward. The top bright echo indicates the boundary between the coupling medium (water) and the apical surface of the AlloDerm®. Below this, the tissue device appears as uniform speckle. Some bright spots indicate backscatter and are approximately 30μm in diameter. Post-compression RMS values between the AlloDerm® and EVPOME (11 days post-seeding) are similar to those in previous studies where they were not subjected to any compression: there is a significantly higher value (up to 4x greater) in the AlloDerm® specimens than their EVPOME counterparts (Figure 5.6).

### 5.3.1 3D Deformation Scans

The degree of tissue displacement noted by the SAM compression test showed similar characteristics between the skin and oral tissues (namely, the palate and buccal) and the EVPOME. The RMS values for each set of datasets at each compression level were compared among the tissue groups: in each case, there is an initial decrease in the RMS value between compression steps – usually steps 1 through 3 - for each tissue. Afterwards, there is a slight elevation in RMS, although it does not restore to the initial values prior to the compression tests. By contrast, the unseeded AlloDerm® device shows higher RMS variance from the compression scans (Figure 5.7a-b).

### 5.3.2 Mechanical Compression Testing

The AlloDerm® specimen from the first compression tests was not subjected to any water exposure, hence it was placed directly from a dry environment to the mechanical compression. In the second case, it was immersed in a container of deionized water for approximately 10 minutes prior to the mechanical compression tests.

In all tests, the unseeded AlloDerm® specimens all exhibited the fastest deformations with each successive step from the cylinder (Figure 5.8a); an indication of higher stiffness properties.

The EVPOMEs at 11 days post-seeding exhibited similar behavior to that of porcine buccal mucosa: both showed limited stress with increasing strain. Between 5 – 8 steps (50 – 80 μm) of compression, a threshold would be reached for both tissue types, resulting in successively increasing stress levels with each successive change in strain.

Porcine skin also exhibited similar characteristics as the buccal and EVPOME, but resisted higher load levels: increased stress would occur between steps 12-16 (120 – 160 μm) of compression. Afterwards, a threshold was crossed and the skin exhibited increased stress with each successive strain change similar to the buccal and EVPOME.

Porcine palate demonstrated the highest resistance to stress among all the tissue types. Applying compression force from the piston greater than 50 steps (> 500 μm) showed little increase in stress and the total increase in stress

at greater than 90 steps (> 900 μm) was less than half of the stress exhibited by the other tissues. A compendium of the stress-strain behavior for each of the tested tissues is listed in Figure 5.8b.

Because the porcine buccal and EVPOME (11 days post-seeding) specimens both exhibited similar stress-strain relationships under the mechanical compressor, SAM 2D B-scans were compared for both tissues (Figure 5.9). In the latter case, there is a significantly higher reflectivity off of the surface; evidence of the keratinized layer that was examined in earlier studies (Chapters II and III). Although the buccal shows less reflectivity off its surface, its similar behavior to EVPOME (and to a lesser degree, the skin and palate tissues) demonstrates a similar stratified tissue composition which will be analyzed in upcoming studies.

### 5.3.3 Mechanical Testing and Examination of Stressed and Unstressed EVPOME and AlloDerm® Specimens

The RMS values varied highly within the AlloDerm® specimens, both stressed and unstressed and for the stressed EVPOME specimen (Figure 5.10) along with visible variations within the SAM B-Scans (Figure 5.11a-b) and their histology images (Figure 5.11c-d) for these specimens. Although for the mechanical compression testing, the results between the stressed and unstressed AlloDerm® specimens were very similar, there was a significant change when comparing the Hookean models between the seeded and

unseeded specimens, but not between themselves in the stressed/unstressed states. Both EVPOME specimens exhibited similar stress-strain curves when subjected to the compressor, regardless of their stressed/unstressed states (Figure 5.12a), along with similar elastic modulus (Figure 5.12b). Both AlloDerm® specimens demonstrated stiffer properties similar to the earlier compressor results (Figure 5.7a): higher deformations at each successive change in their original length.

The high similarity in Hookean behavior between the EVPOMEs – either stressed or unstressed – suggests the cellular constituents in the EVPOMEs behave alike regardless of whether they are fully attached to the AlloDerm® surface. This finding mandates use of SAM to examine the specimens' elastic properties at each of the layers in the EVPOME (both stressed and unstressed) using the compression data and speckle tracking methods. Further work here will allow us to analyze which components in the tissues contribute most to the changes in stress-strain models observed.

### 5.3.4 Examination of Stressed and Unstressed EVPOME and AlloDerm® Specimens using Fitting Program for 1-term Ogden Models

The AlloDerm® stress coefficients for the thermally stressed and unstressed specimens are very similar ($\mu$ = 4.77 KPa and 4.78 KPa, respectively), but different for both EVPOMEs. The EVPOMEs' stress coefficients are different among themselves with stressed $\mu$ = 0.22 KPa and unstressed $\mu$ = 1.99 KPa. The fitting models worked well for all datasets (Figure 5.13). Basically, we acquired the same fit with the stressed/unstressed

AlloDerm®, but the stressed/unstressed EVPOME showed much different nonlinear behavior as per the Ogden model fit. The unstressed EVPOME appeared to be actually closer to the nonlinear mechanics of the AlloDerm®.

## 5.4 DISCUSSION

Difficulties with the 61MHz transducer (a problem with the coupling between the crystal and the wiring caused poor RF lines and subsequent scans) forced us to switch to a 50MHz transducer for the final phase of the mechanical testing experiments. Although the RF signal was substantially improved over the 61MHz transducer, the image resolution was significantly lower in quality than in the previous B-scans and C-scans from the 61MHz transducer (before it experienced the hardware problems). Although the image resolution was lower on these tested specimens than in the previous experiments, it still provided accurate measurements between the tissue types when examining their surface profilometries and testing their stress-strain properties

Comparing the unseeded AlloDerm® specimens to any of the oral tissues using acoustic imaging, we have seen major differences on the surfaces characteristic of their reflectivity between the unseeded device and the mature EVPOME (Winterroth et. al. 2009). In this study, we show that the presence of cells (particularly in a stratified pattern) provides changes not in the reflectivity of the cells, but further in the elasticity of the tissues. Even the minimal presence of

cells – including seeded layers that are rather poorly developed – still demonstrate resistance to stress at increasing strain deformations.

In the case of the buccal tissue, there is no keratinization on their surfaces (Amelink et. al.2008, Moll, et. al. 2008); this takes into account the lower reflectivity on the surface of these tissues compared to fully mature EVPOME when performing acoustic scans to each (Figure 5.9). However, the mechanical behavior for both is comparable: the degree of cell stratification, not keratinization appears to affect the mechanical properties in so far as the stress-strain relationship is concerned (Figures 5.7b and 5.8b). In this case, the second EVPOME was poorly developed with little keratinization occurring, yet displayed similar stress-strain relationships to a properly mature EVPOME – this in spite of poor development as seen in both the SAM and histology micrographs (Figure 5.11).

Because of the tissues' incompressibility, the change in volume remains essentially constant; this is likely due to their high water content, particularly the tissues within the oral cavity. Both the natural and EVPOME tissues exhibited similar stress-strain characteristics – an example of the tissues' incompressibility. The unseeded AlloDerm® device alone shows high changes in stress with each successive change in compression step length, which shows strong evidence of the stratified cells acting to reduce stiffness in the devices. Comparing the components of the AlloDerm® scaffold to that of a fully differentiated EVPOME, with the focus on stratified cells; this is evident from the poorly developed and

keratinized EVPOME exhibiting similar stress-strain behavior as EVPOME that was properly differentiated.

The amount of stratified cell layers within the tissue types appears to play a significant role in degree of stiffness each tissue displays; this is evident in the low stress-strain mechanics observed when testing the porcine palate on the mechanical compressor. (Figure 5.8). This certainly warrants examining these same tissue types using the SAM system to analyze which cell layers (or combination of layers) contributes the most to such mechanical behavior.

### 5.4.1 Analyses of Thermal Stressed/Unstressed Specimens

Doing a comparison among devices that were thermally stressed and unstressed (both for AlloDerm® and EVPOME) there were similarities in compression results among the AlloDerm® and stressed EVPOME. The similar stress-strain behavior from the mechanical compressor in both stressed and unstressed EVPOME suggested the cellular debris present on the surface of the stressed specimen exhibits a spring constant similar to the unstressed control (in spite of its thermally elevated state). Despite high variations in the SAM RMS profiles, the mechanical compression tests between stressed and unstressed EVPOME collectively show no significant changes in Hookean behavior. Further studies here to test elasticity of the individual layers of the mature EVPOME using the SAM compressor and speckle tracking methods may delineate what

particular properties in the EVPOME's seeded material contributes most to these similarities.

### 5.4.2 Further Comparisons between SAM and the Mechanical Compressor on Elastic Properties of Natural and Engineered Tissues

The analyses of stressed/unstressed EVPOMEs using 1-term Ogden models shows significant changes in the stress-stretch relationships between the two specimens; the unstressed EVPOME actually displaying mechanical behavior similar to the AlloDerm® specimens while the stressed EVPOME had a much different non-linear behavior. This behavior in the stressed EVPOME is the likely effect of the thermal stress application on the active keratinocytes and acellular keratin layer. Exactly what properties in the EVPOME are affected by the thermal increase remains unknown. Furthermore, why the unstressed EVPOME showed the lowest stress coefficients yet exhibited tissue mechanics similar to the two AlloDerm® tissues warrants additional tests. Future studies must include using SAM and the mechanical compressor to evaluate stress-strain on EVPOME tissues during their development at each successive day to determine at which exact day or days the specimens evolve sufficiently to show the observed changes in the Hookean stress-strain relationships and 1-term Ogden model's behavior.

The first set of studies in the immediate future are comparing the elastic properties of the tissues tested – both natural and engineered – using 1-term

Ogden and Neo-Hookean models to examine and compare their stress coefficients to stretch relationships. This will be followed by compiling the SAM data to evaluate which cell and tissue groups contributed most to the mechanical behavior observed in the mechanical compression studies.

Subsequent additional microscopy studies (using acoustic, optical, and possibly transmission electron microscopy) will be applied to analyze which sub-cellular constituents are present at each day of EVPOME development and how they – either individually or in succession – contribute to the changes in linear elasticity observed.

## REFERENCES


Amelink, A., Kaspers, O.P., Sternborg, H.J.C.M., van der Wal, J.E., Roodenburg, J.L.n., Witjes, M.J.H. Non-Invasive Measurement of the Morphology and Physiology of Oral Mucosa by use of Optical Spectroscopy. *Oral Oncol.* 2008. 44: 65-71.

Barr, R.J., White, G.M., Jones, J.P., Shaw, L.B., Ross, P.A. Scanning Acoustic Microscopy of Neoplastic and Inflammatory Cutaneous Tissue Specimens. *J. Invest. Dermatol.* 1991. 96: 38-42.

Bathe, K-J. *Finite Element Procedures.* NJ: Prentice-Hall. 1996. 1037pp.

Broekaert, D., Van Oostveldt, P.. Nuclear Differentiation During Epidermal Keratinization. *Arch. Dermatol. Res.* 1988. 280:188-189.

Cohn, N.A., Emelianov, S.Y., Lubinski, M.A., O'Donnell, M. An Elasticity Microscope. Part I: Methods. *IEEE Trans. Ultrason. Ferr. Freq. Ctrl.* 1997. 44(6): 1304-1319.

Cohn, N.A., Emelianov, S.Y., O'Donnell, M. An Elasticity Microscope. Part II: Experimental Results. *IEEE Trans. Ultrason. Ferr. Freq. Ctrl.* 1997. 44(6): 1320-1331.

Cohn, N.A. An Elasticity Microscope for High Resolution Imaging of Tissue Stiffness Using 50MHz Ultrasound. University of Michigan Ph.D. Dissertation. 1997. 195pp.

Erkamp RQ, Wiggins P, Skovoroda AR, Emelianov SY, O'Donnell M. Measuring the Elastic Modulus of Small Tissue Samples. *Ultrasonic Imaging*. 1998 Jan;20(1):17-28.

Harrison, C.A., Gossiel, F., Layton, C.M., Bullock, A.J., Johnson, T., Blumsohn, A., MacNeil, S. Use of an *In Vitro* Model of Tissue-Engineered Skin to Investigate the Mechanism of Skin Graft Contraction. Tiss. Engin. 2006. 12(11): 3119-3133.

Holland, M.R., Hall, C.S., Lewis, S.H., Handley , S.M., Finch-Johnston, A.E., D'Sa, A.P., Perez, J.E., Miller, J.G. Comparison of integrated backscatter values obtained with acoustic densitometry with values derived from spectral analysis of digitized signals from a clinical imaging system. *J. Amer. Soc. Echocardio.* 1997. 10(5): 511-517.

Hollman, K.W., Emelianov, S.Y., Neiss, J.H., Jotyan, G., Spooner, G.J.R., Juhasz, T., Kurtz, R.M., O'Donnell, M. Strain Imaging of Corneal Tissue With an Ultrasound Elasticity Microscope. *Cornea.* 2002. 21(1): 68-73.

Hotta, T., Yokoo, S., Terashi, H., Komori, T. Clinical and Histopathological Analysis of Healing Process of Intraoral Reconstruction with Ex Vivo Produced Oral Mucosa Equivalent. *Kobe J. Med. Sci.*, 2007. 53(1): 1-14.

Hughes, T.J.R. *The Finite Element Method: Linear Static and Dynamic Finite Element Analysis.* Mineola, NY: Dover Publications. 2000. 682pp.

Izumi, K., Feinberg, S.E., Iida, A., Yoshizawa, M. Intraoral Grafting of an *Ex Vivo* Produced Oral Mucosa Equivalent: A Preliminary Report. *Int. J. Oral Maxillofac. Surg.* 2003. 32: 188–197.

Izumi, K., Song, J., Feinberg, S.E. Development of a Tissue-Engineered Human Oral Mucosa: From the Bench to the Bed Side. *Cells Tissues Organs.* 2004. 176:134–152.

Kolios, M.C., Czarnota, G.J., Lee, M., Hunt, J.W., Sherar, M.D. Ultrasonic Spectral Parameter Characterization of Apoptosis. *Ultrasound in Med. Biol*. 2002. 28(5): 589–597.

Kolios, M.C., Taggart, L., Baddour, R.E., Foster, F.S.., Hunt, J.W., Czarnota, G.J., Sherar, M.D. An Investigation of Backscatter Power Spectra from Cells, Cell Pellets, and Microspheres. *IEEE Ultrasonics Symposium*. 2003. 752-757.

Lin, W.C., Chang, C.Y.Y., Shen, Y.Y., Tsai, H.D. Use of Autologous Buccal Mucosa for Vaginoplasty: A Study of Eight Cases. *Human Reproduction*. 2003. 18(3): 604-607.

Lubinski MA, Emelianov SY, Raghavan KR, et al. Lateral Displacement Estimation Using Tissue Incompressibility. *IEEE Trans UFFC* 1996. 43:247–56.

Lubinski MA, Emelianov SY, O'Donnell M. Speckle Tracking Methods for Ultrasonic Elasticity Imaging Using Short Time Correlation. *IEEE Trans UFFC* 1999. 46:82–96.

Moll, R., Divo, M., Langbein, L. The Human Keratins: Biology and Pathology. *Histochem. Cell Biol.* 2008. 129: 705-733.

Norlén, L., Ashraf Al-Amoudi, A. Stratum Corneum Keratin Structure, Function, and Formation: The Cubic Rod-Packing and Membrane Templating Model. *J. Investig. Dermatol*. 2004. 123: 715–732.

Norlén, L. Stratum Corneum Keratin Structure, Function and Formation – A Comprehensive Review. *Int. J. Cosmet. Sci*. 2006 Dec;28(6):397-425.

O'Donnell M, Skovoroda AR, Shapo BM, et al. Internal Displacement and Strain Imaging Using Ultrasonic Speckle Tracking. *IEEE Trans UFFC* 1994. 41:314–25.

Saijo, Y., Miyakawa, T., Sasaki, H., Tanaka, M., Nitta, S. Acoustic Properties of Aortic Aneurysm Obtained with Scanning Acoustic Microscopy. *Ultrasonics*. 2004. 42: 695–698.

Saijo, Y., Tanaka, M., Okawai, H., Dunn, F. The Ultrasonic Properties of Gastric Cancer Tissues Obtained with a Scanning Acoustic Microscope. *Ultrasound in Med. & Biol.* 1991. 17(7): 709-714.

Samani A., Bishop J., Luginbuhl C., Plewes D.B. Measuring the Elastic Modulus of Ex Vivo Small Tissue Samples. *Phys Med Biol*. 2003 Jul 21;48(14):2183-98.

Tortora, G.J. & Grabowski, S.R. *Principles of Anatomy and Physiology (7th Edition)*. 1993. HarperCollins College Publisher, New York.

Warner, R.R., Myers, M.C., Taylor, D.A. Electron Probe Analysis of Human Skin: Determination of the Water Concentration Profile. *J. of Invest. Dermatol.* 1988. 90: 218–224.

Winterroth, F., Fowlkes, J. B., Kuo, S., Izumi, K., Feinberg, S.E., Hollister, S. J., Hollman, K. W. High-Resolution Ultrasonic Monitoring of Cellular Differentiation in an *Ex Vivo* Produced Oral Mucosal Equivalent (EVPOME). *Proc. IEEE Bioultrasonics Conference.* 2009.

Winterroth, F., Hollman, K.W., Feinberg, S.E., Kuo, S., Izumi, K., Hollister, S.J., Fowlkes, J.B. Examination and Characterization of Human Mucosal Tissue Differentiation Using Scanning Acoustic Microscopy. *Ultrasound Med. Biol*. 2010 (In Press)

Winterroth, F. Lee, J., Kuo, S. J., Fowlkes, J.B., Feinberg, S.E., Hollister, S.J., Hollman, K.W. Acoustic Microscopy Analyses to Determine Good vs. Failed

Tissue Engineered Oral Mucosa Under Normal or Thermally Stressed Culture Conditions. *Ann. Biomed. Engineer.* 2011. 39(1): 44.

Zuber, M., Gerber, K., Erne, P. Myocardial Tissue Characterization in Heart Failure by Real-Time Integrated Backscatter. *Eur. J. Ultrasound*. 1999. 9: 135–143.

## FIGURES

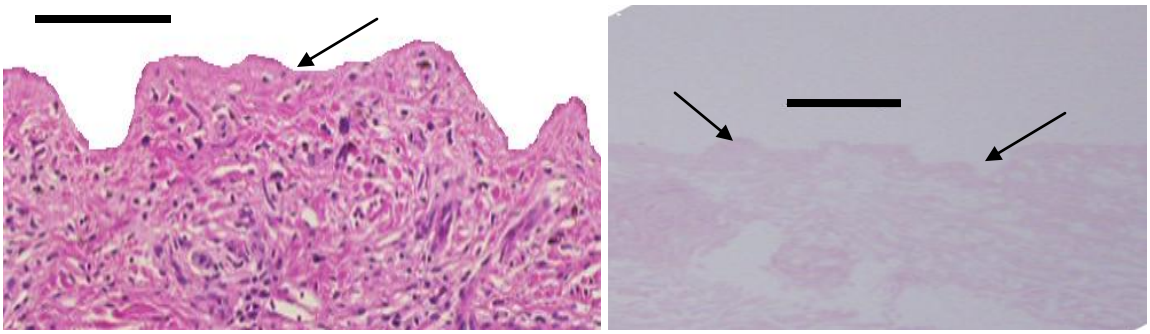

**a** **b**

**Figure 5.1. Illustration of the human dermis (b), showing principal components. Like the oral mucosa, the dermis is comprised of basal cells which differentiate into stratified squamous cells as they migrate upward toward the apex (arrows). By comparison, the AlloDerm® specimen (b) has the same structural components, but completely lacks the cells which fill in its dermal matrix (arrow). Scale bars equal 100μm.**

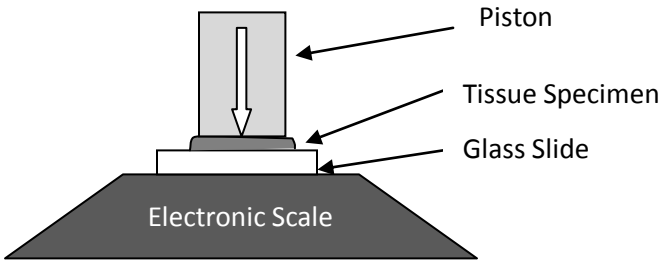


**Figure 5.2a. Schematic side view of the compression system used to measure indentation of soft tissue samples. The large white arrow shows the motion direction of the piston.**

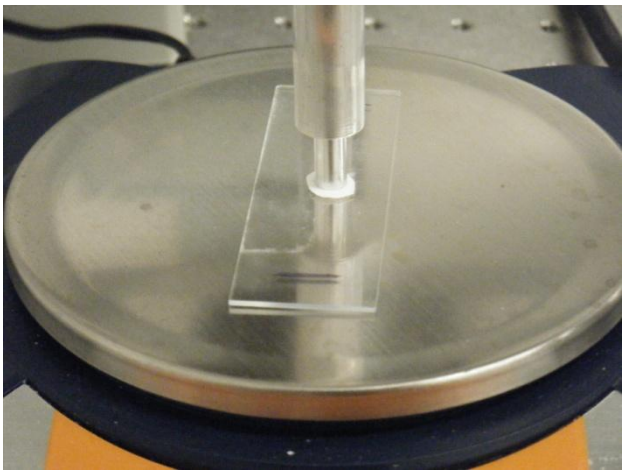

**Figure 5.2b. Photograph of the compression system testing a tissue specimen placed on top of a glass slide.**

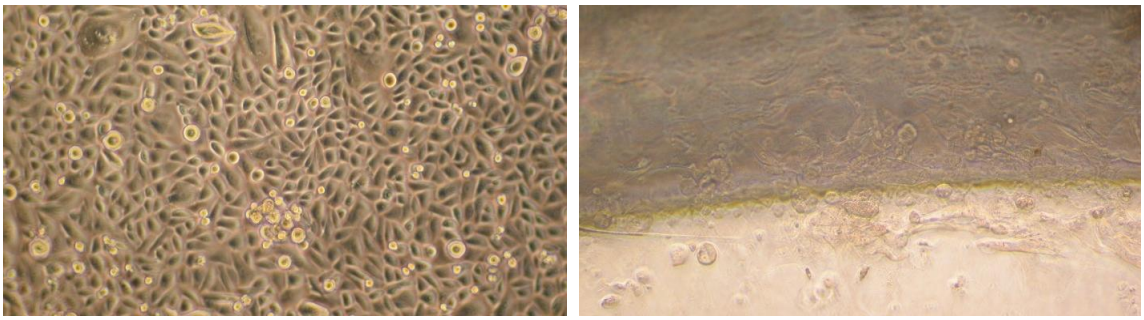

**a** **b**

**Figure 5.3. Oral keratinocytes on the EVPOME plate at 24-hours post seeding (a) and 96-hours post-seeding (b). The degree of differentiation is clearly evident in the morphologies between the two: in the former image, the cells appear rounder (either circular or tear-shaped). In the latter, the cells are more elongated and adhering to the plate. There are also far less cells present as the majority have bonded to the surface of the AlloDerm® specimen.**

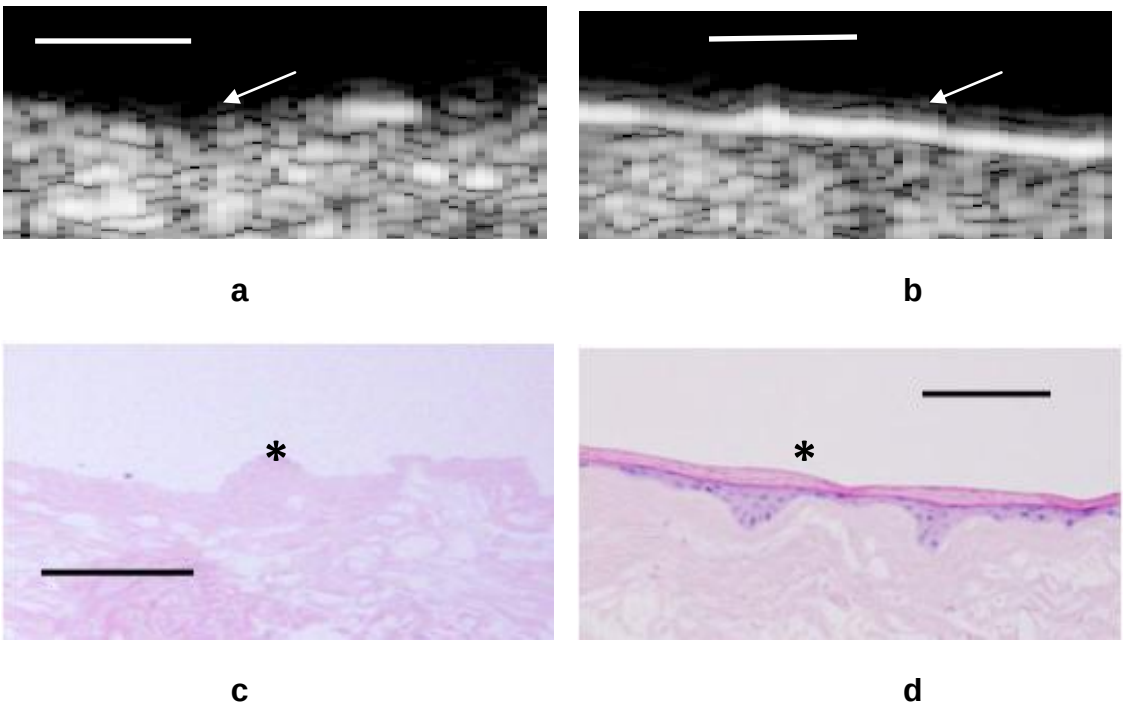


**Figure 5.4 a-d. SAM 2D B-Scans between the unseeded AlloDerm® scaffold (a) and the EVPOME 11-days post-seeding (b), followed by their histological counterparts (c and d). In the 2D B-Scans, there is a greater reflectivity off of the surface of the EVPOME compared to the AlloDerm® specimen (arrows); indicative of the space-filling/keratinization activity of the oral keratinocytes which were seeded onto its surface. This is verified in the histological micrograph comparing the two specimens (asterisk). Scale bars equal 100 μm.**

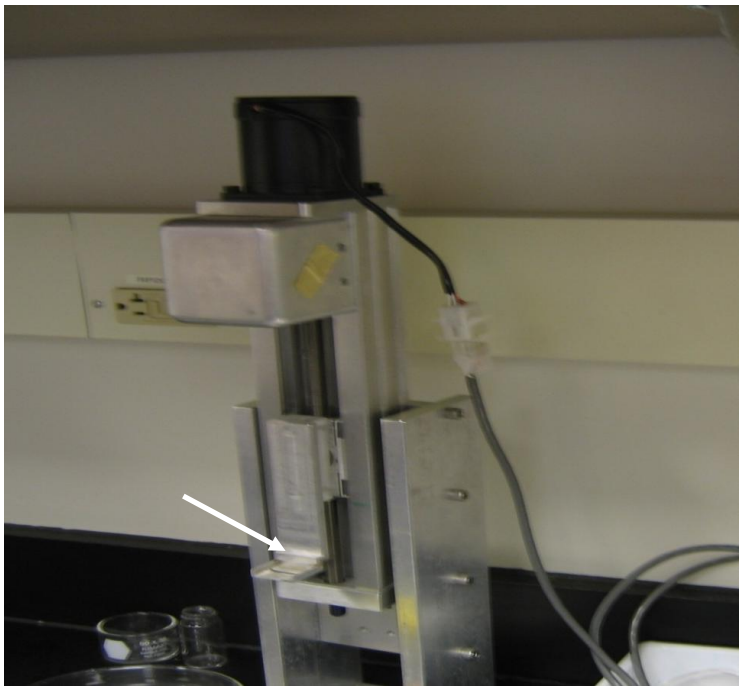

**Figure 5.5a. Photograph of the compressor set up for the SAM with the compression platform (arrow). The tissue samples are to be loaded directly beneath the platform. The platform can then induce recorded compression-rarefaction levels while the SAM transducer mounted directly over the platform will record deformation characteristics**.

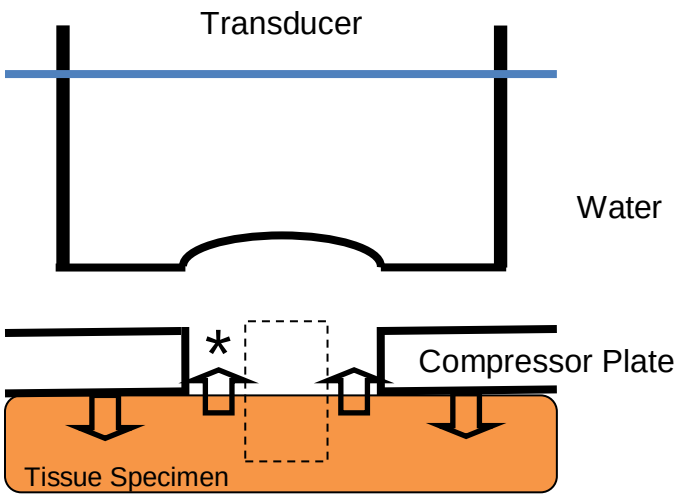


**Figure 5.5b. Illustrative set-up of the SAM for strain imaging. Deformations were caused by a compressor plate with a slit in the center (asterisk). The large open arrows indicate motion of the outer surface of the tissues. The imaging area is represented by the dotted box.**

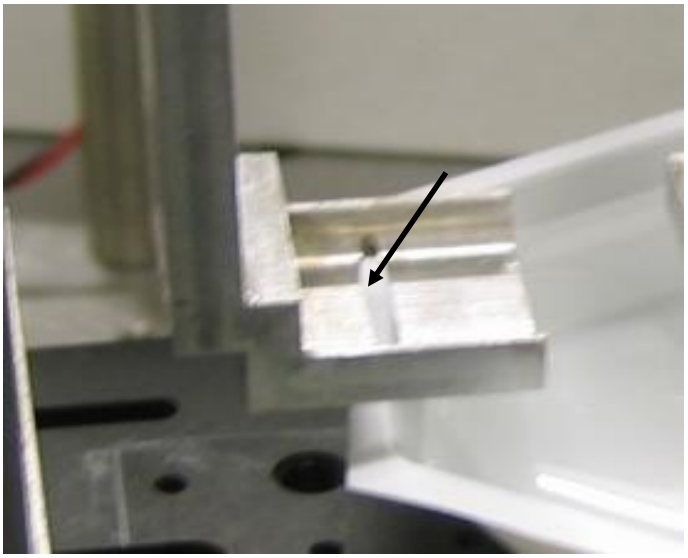

**Figure 5.5c. Photograph of the compressor set up for the SAM with the compression platform (arrow). The tissue samples are to be loaded directly beneath the platform. The platform can then induce recorded compression-rarefaction levels while the SAM transducer mounted directly over the platform will record deformation characteristics.**

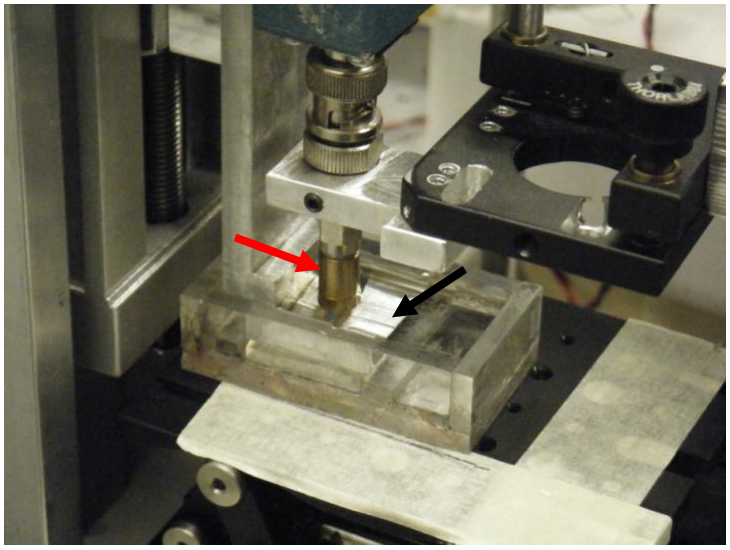

**Figure 5.5d. Photograph of SAM set-up for strain imaging, with the transducer (red arrow) and compressor plate (black arrow) mounted over a tissue specimen.**

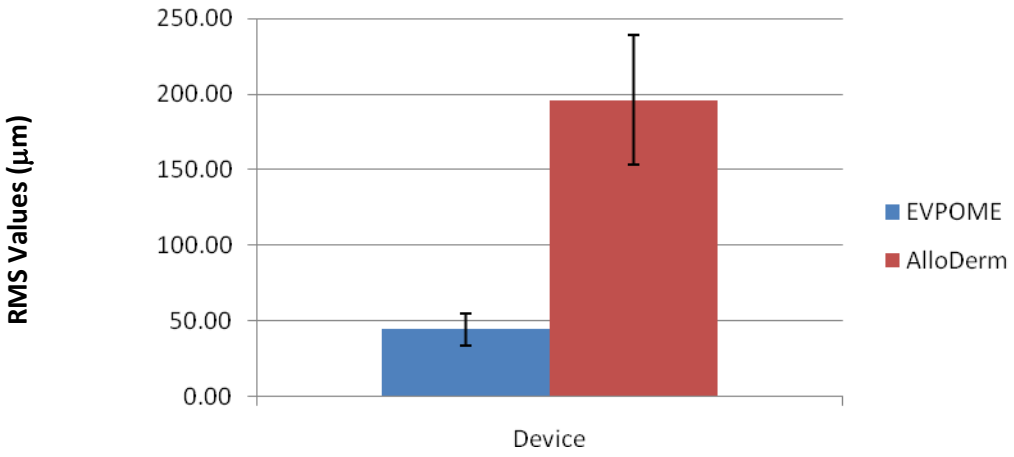


**Figure 5.6. General RMS values between the AlloDerm® and EVPOME at 11 days post-seeding after being subjected to SAM compression steps.**

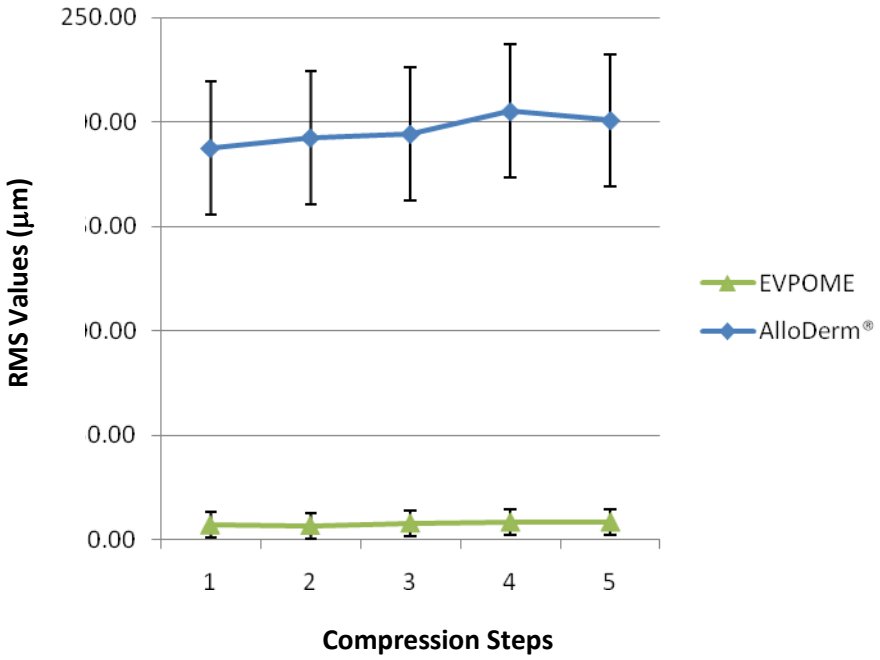


**Figure 5.7a. SAM mechanical compression tests showing RMS values at different compression steps between AlloDerm® and EVPOME (11 days post-seeding).**

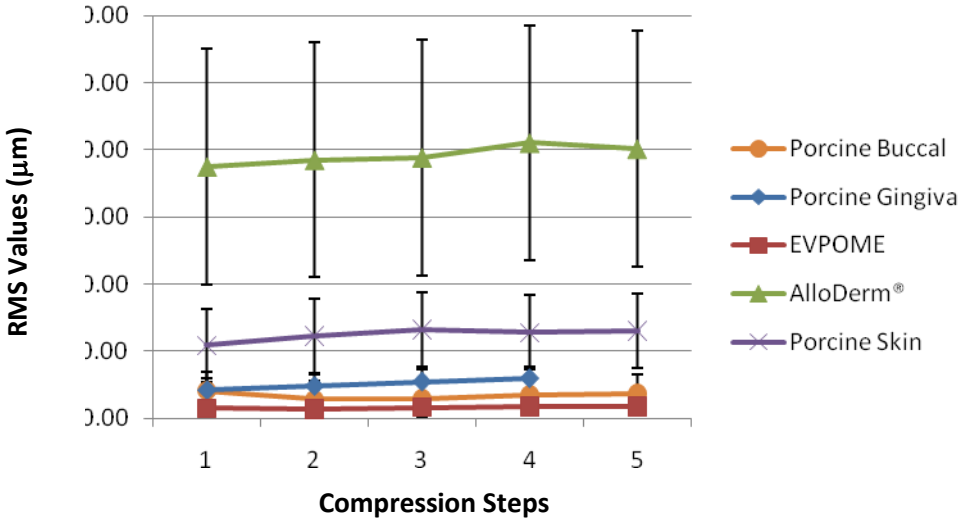


**Figure 5.7b. Collective SAM mechanical compression tests showing RMS values at different compression steps between AlloDerm® ,EVPOME (11 days post-seeding), and natural porcine soft tissues: skin, buccal, and gingiva.**

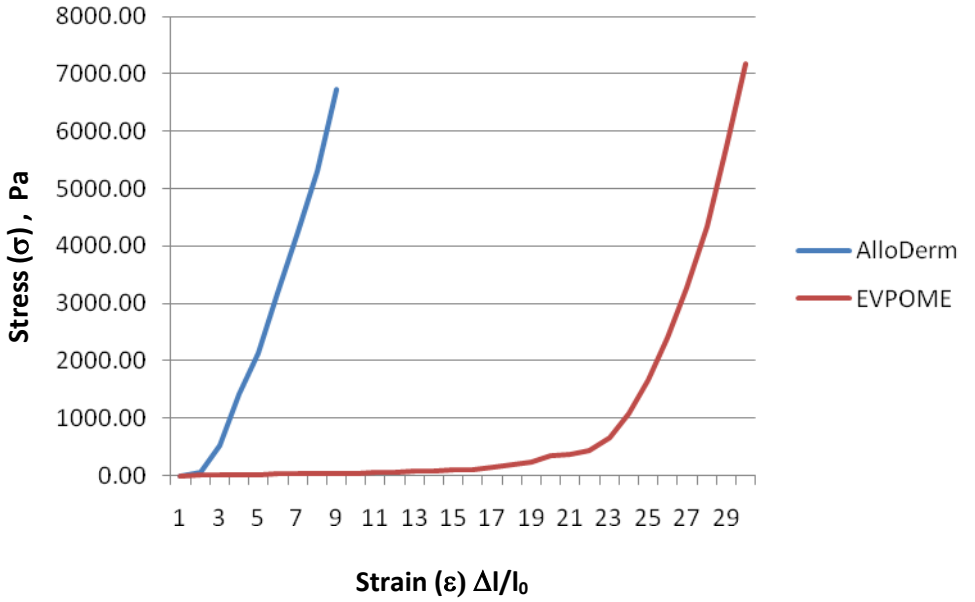


**a**

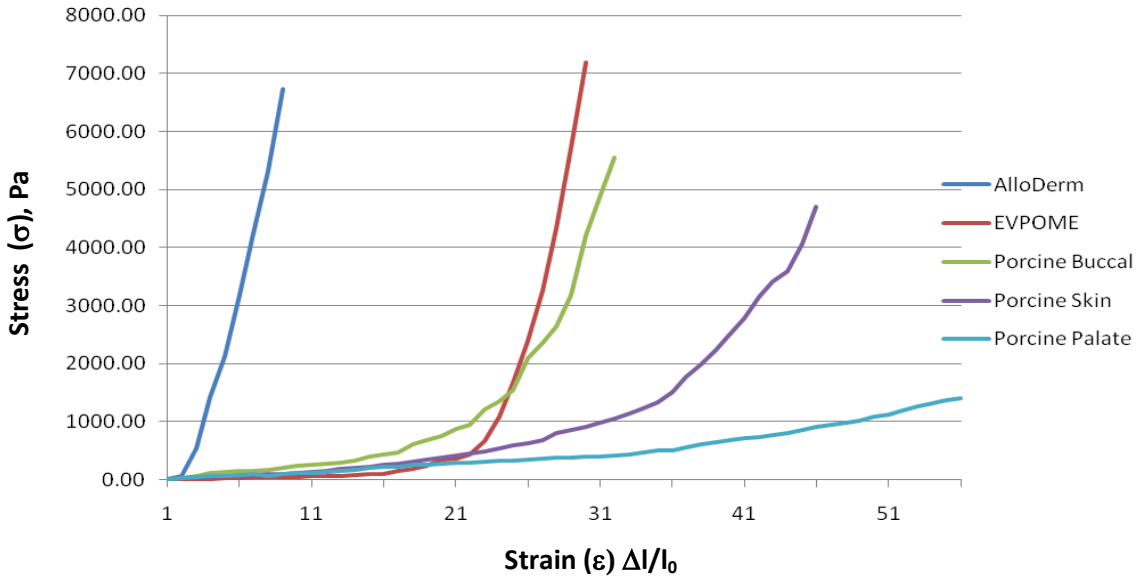


**b**

**Figure 5.8. Stress-strain relationships comparing AlloDerm® and EVPOME (a) and collectively for all tissue types, including porcine buccal, skin, and palate (b). All tissues exhibited stress deformation at increasing stress levels: EVPOME showing similar characteristics with buccal and skin.**

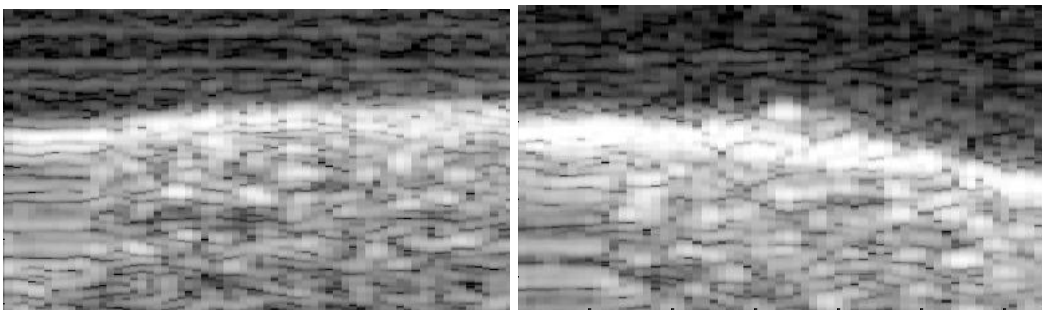

**a** **b**

**Figure 5.9. 2D B-scans of porcine buccal tissue (a) and EVPOME 11 d post seeding (b). Note the higher reflectivity off of the latter surface which correlates with the presence of keratinization. The mechanical behavior of both the buccal and EVPOME are similar when subjected to the piston compressor.**

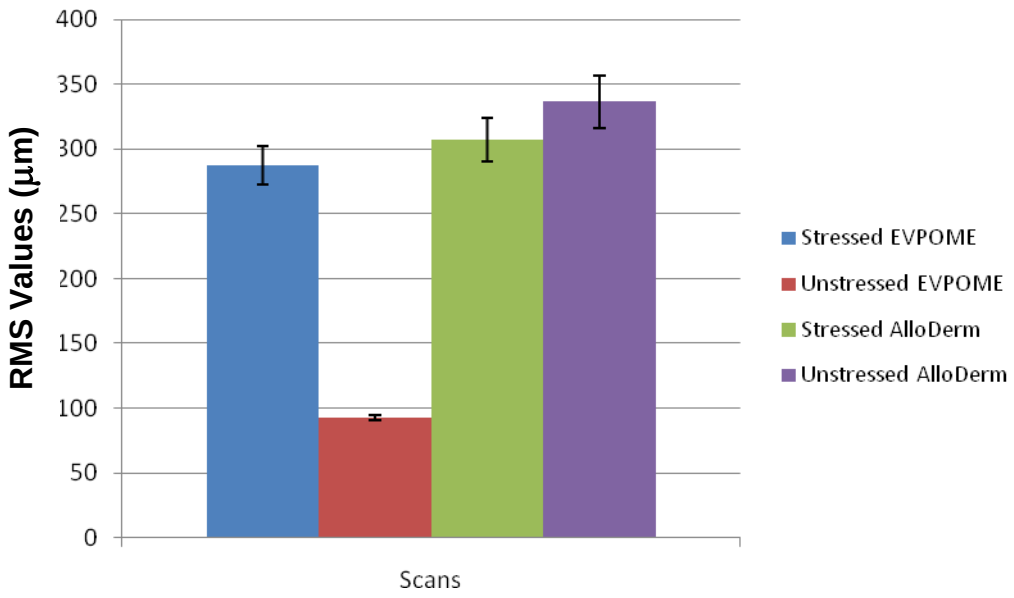


**Figure 5.10. SAM RMS profiles for the EVPOME specimens, both stressed and unstressed (F1 and F2, respectively) and the unseeded AlloDerm®, both stressed and unstressed (FC1 and FC2, respectively). Note the high variations in three of the four specimens, with greater degrees of standard deviation.**

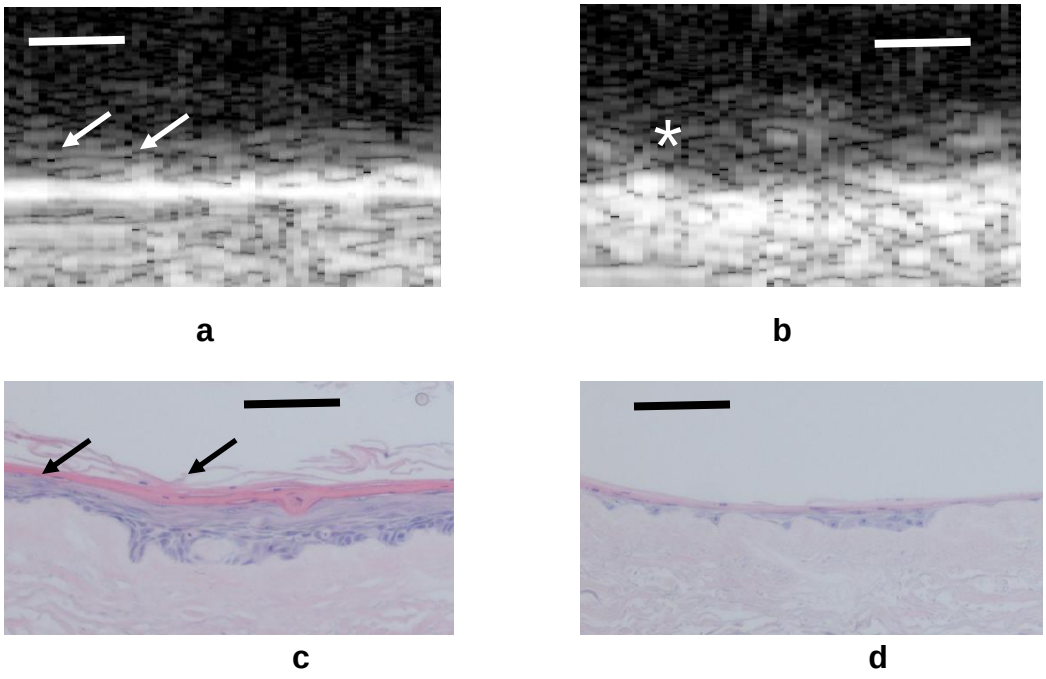


**Figure 5.11 a-d. Comparative 2D B-scans (a-b) and histology (c-d) images between EVPOME (11 days post-seeding) that was properly developed and keratinized (a and c), EVPOME that was poorly evolved and differentiated (b and d). The keratin levels in the properly developed specimens are significantly greater in the staining and reflectivity (arrows). The lower acoustic reflection in the surface of the poorly developed EVPOME is a result of the reduced keratin layer on the surface (asterisk). Scale bars equal 100 μm.**

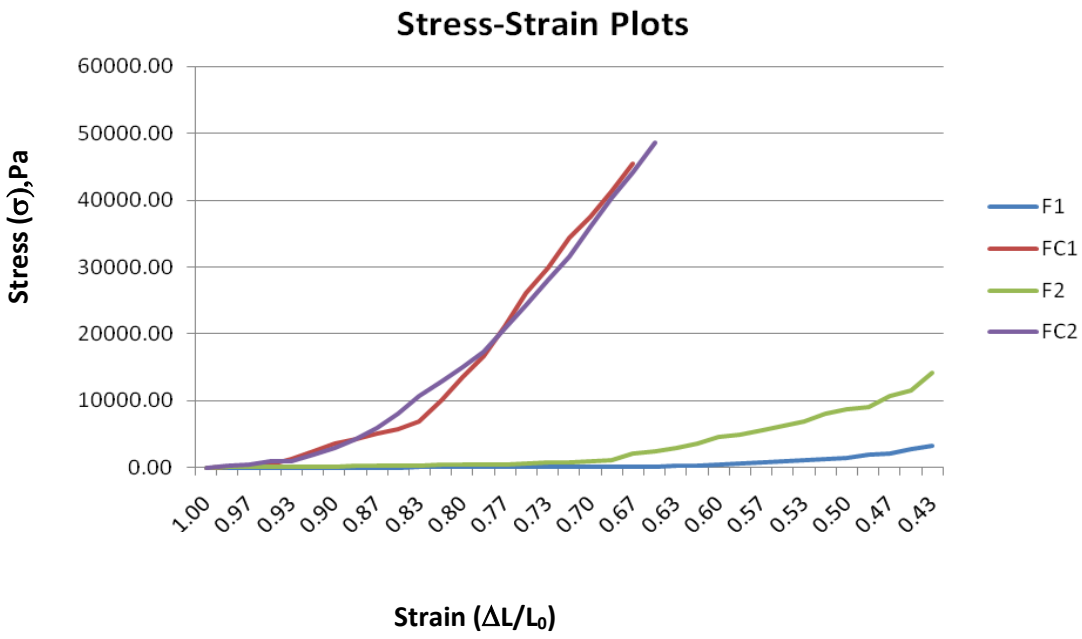


**Figure 5.12a. Stress-strain relationships comparing stressed and unstressed EVPOME (F1 and F2, respectively) and stressed and unstressed AlloDerm® (FC1 and FC2, respectively). All tissues exhibited stress deformation at increasing stress levels: EVPOME at both stressed and unstressed levels exhibited similar behavior. The AlloDerm® specimens exhibited similar stiffness properties regardless of being placed in an elevated thermal environment.**

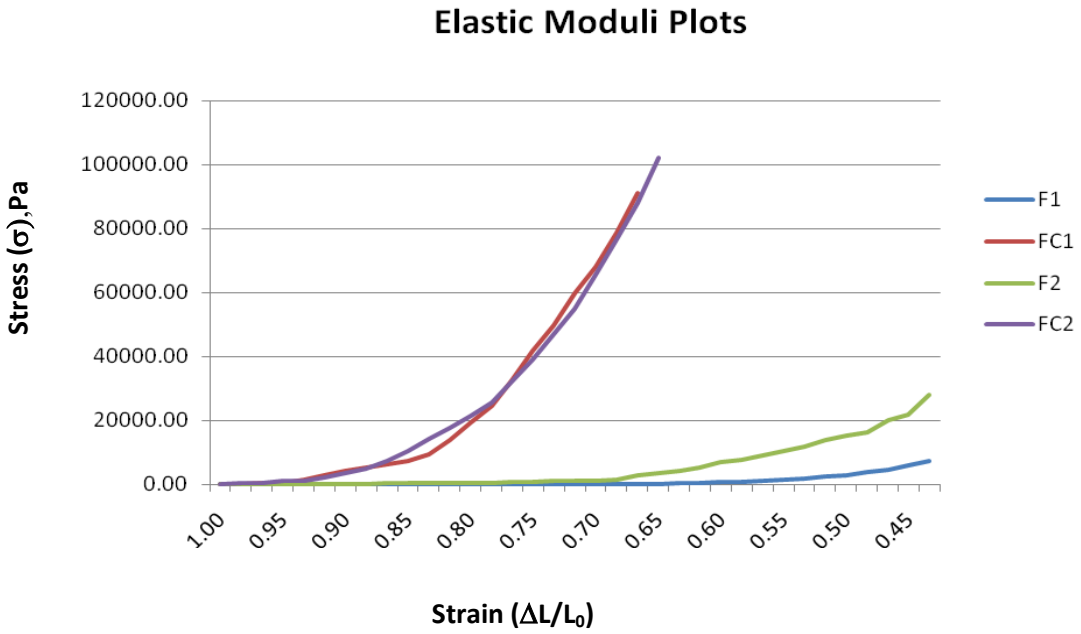


**Figure 5.12b. Elastic modulus relationships comparing stressed and unstressed EVPOME (F1 and F2, respectively) and stressed and unstressed AlloDerm® (FC1 and FC2, respectively). All tissues exhibited elastic characteristics at increasing stress levels: EVPOME at both stressed and unstressed levels exhibited similar behavior. The AlloDerm® specimens exhibited similar elastic properties regardless of being placed in an elevated thermal environment.**

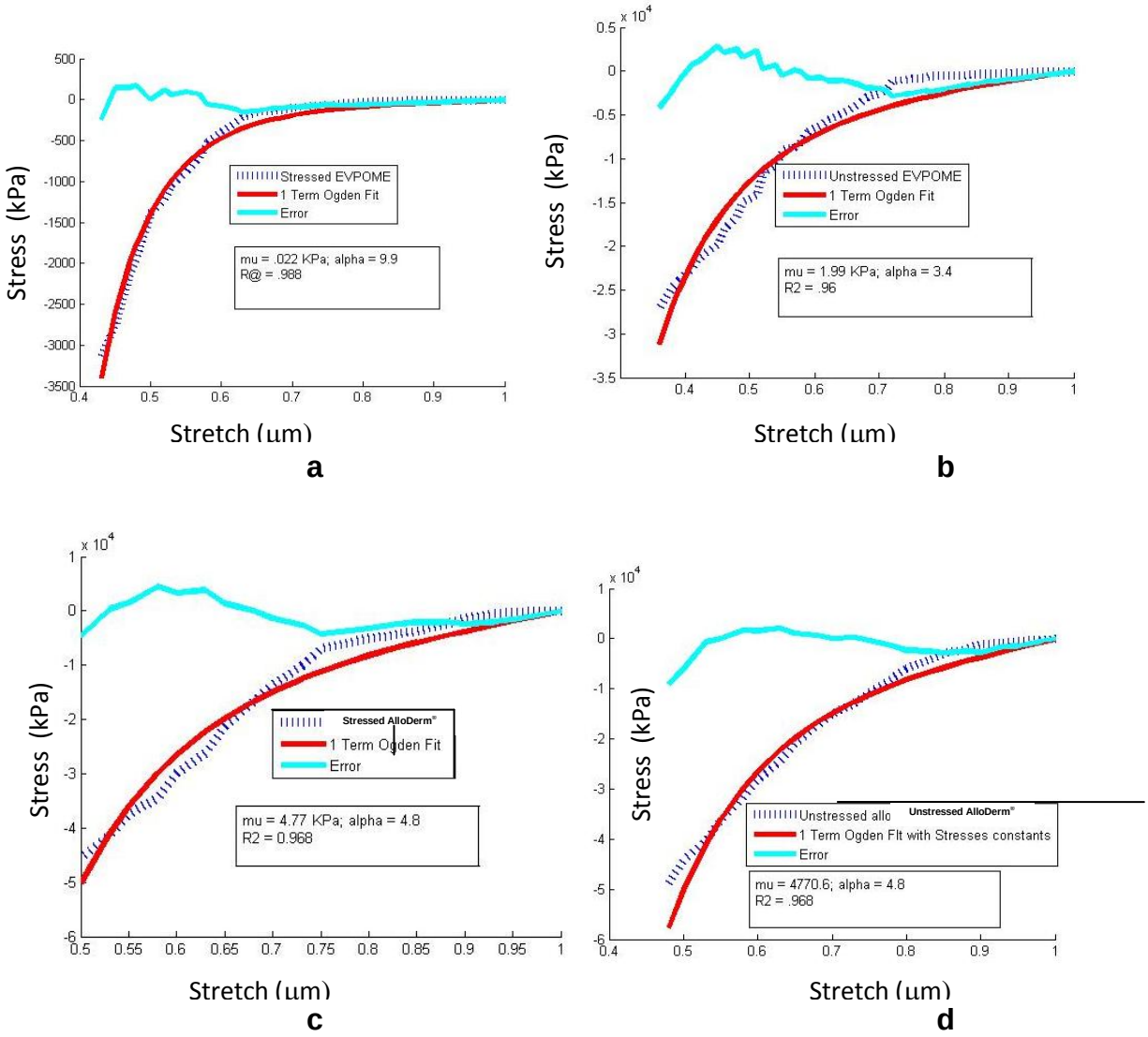


**Figure 5.13. 1-term Ogden fitting models comparing the stress-to-stretch ratios between stressed and unstressed EVPOMEs (a and b) and the stressed unstressed AlloDerm® (c and d). Included are the ratios, the 1-term Ogden fit, and the degree of error.**

# CHAPTER VI
# CONCLUSIONS AND FUTURE DIRECTIONS

This work describes applications of an in-house constructed scanning acoustic microscopy (SAM) to examine the morphologies of an *ex vivo* produced oral mucosa equivalent (EVPOME) and the unseeded AlloDerm® device and compare them to histology counterparts, to quantify and compare the mean surface irregularities on AlloDerm® and on developing and fully mature EVPOME from both SAM and histology images. Additional studies use SAM to examine the surface characteristics of EVPOME which have undergone thermally stressed conditions compared to unstressed controls. Examining the stiffness properties of the AlloDerm® - the degree of stress as a result of increasing strain – and comparing it to EVPOME and natural mucosal tissues are also considered.

We demonstrated in this dissertation some of the physical and morphological characteristics of an engineered oral mucosal tissue implant to repair and/or replace native tissues. Many patients in need of soft tissue transplants have suffered from disease, congenital defects, and injuries. Soft tissue transplantation is an established and successful procedure that represents the causal and curative therapy for many of these diseases and conditions which lead to soft tissue failures (Izumi et al 2004, Hotta et al 2007).

Aside from the providing the background information on the SAM and different tissues examined, there were four main criteria which were studied in the development of this dissertation:

1. Quantifying the degree of surface irregularities on the tissue specimens, and statistically correlating the quantifying methods used, both with SAM and optical microscopy.
2. Using SAM to study the surface characteristics of AlloDerm® and EVPOME, specifically the latter after undergoing a thermal stress test.
3. Continuing the thermal stress studies on the AlloDerm® and EVPOME tissue specimens, specifically using an analyses algorithm to fit and subtract their planar surfaces.
4. Examining the elastic properties of AlloDerm® and EVPOME using both SAM and an in-house constructed compressor to measure internal displacement and strain.

The versatility of the oral mucosa for soft tissue transplantation has been successfully implemented in vaginoplasty (Lin et. al. 2003). Both biological and physical tests are required to determine mucosal tissue adaptability to the body (not just in the oral cavity) and for successful long-term durability of the tissues within the transplanted area. SAM has been demonstrated as an effective method to examine cell/tissue properties and test for mechanical effects, namely in the EVPOMEs. Details of the preparation and development of the EVPOME were discussed under Chapters II and III.

The medical need for soft tissue replacements stems from damage and deficiencies in soft tissues. In addition to the aforementioned military BI statistics, there are further requirements for use of engineered soft tissues for replacement/corrections resulting from disease, congenital genetic defects, and accidents. Because buccal tissue has been clinically reported as a suitable transplant to treat vaginal defects, it offers potential as a surrogate for other ectoderm - derived soft tissue problems. Likewise, an engineered oral mucosal tissue implant has the clinical potential to repair and/or replace tissues; therefore, it can act as an excellent surrogate for natural oral tissues. Soft tissue transplantation is an established and successful procedure that represents the causal and curative therapy for many diseases and conditions resulting in soft tissue failures.

As EVPOME is derived from a foundation containing AlloDerm®, it contains similar concentrations of matrix components seen in human dermis.

EVPOME contains an additional seeding of oral mucosal cells on the surface of the AlloDerm® matrix; what eventually becomes the basal lamina of the EVPOME. This addition of cells has been shown experimentally to significantly affect the tissue's structural and elastic properties. Further, we've come to better understand how to physically regulate changes in the mature EVPOME tissues, namely through the aforementioned thermal stress.

Oral mucosal tissues' physical properties are shown to be very much like the skin. Further, testing on the morphologies and elasticity between the skin, oral tissue, and EVPOME showed similar stress-strain curves. In contrast, the unseeded AlloDerm® scaffold by itself showed higher stiffness properties (based on the results from the piston compressor studies) as it exhibited faster and greater stress behavior with increasing strain than any of the tissues, including the mature EVPOME. This latter result was concluded to be a characteristic of the stratified squamous cells which make up the surfaces of the developed tissues. In the case of the thermally stressed EVPOME, we saw similar surface profilometry C-scans and stiffness properties to those of the AlloDerm®.

SAM 2D B-scans of the mature EVPOME, skin, and palate tissues show similar bright reflectivity on the surfaces, a result of their keratinized surfaces. By contrast, the surfaces of the AlloDerm® scaffold and buccal tissue – neither having a keratinized surface – had lower surface reflection from the SAM. However, the buccal tissue showed similar stress-strain curves during the mechanical compression testing, owing to its stratified tissue composition; a

similar composition to the EVPOME, skin, and palate. We concluded that these stratified surfaces – regardless of them being keratinized or not - contributed to the overall mechanical behavior of the tissues.

Thermal Stress Examinations

EVPOMEs have been clinically demonstrated to have a high adaptability restorative ability when surgically implanted into patients (Izumi et al 2003, Izumi et al 2004). To examine their conditions when subjected to an altered physical environment, EVPOMEs were subjected to the thermal stress tests, followed by examining their surface profilometries (Winterroth et. al. 2011a) and mechanical behaviors (Winterroth et. al. 2011b).

Advantages of Using SAM as a Biomedical Tool

The in-house built SAM used in our experiments has shown to produce images with resolution similar to a standard optical microscope; images produced between 50-61 MHz, but capable of increasing up to 100 MHz. However, because the images come from an acoustic signal, contrast arises from variation in the acoustic properties of the material and features may be revealed that are not visible in an optical microscope. In cells and tissues, such changes in acoustic features may derive from different densities among anatomical tissues. The advantages to using SAM include its potential to measure such minute differences, providing a better understanding of the comparisons between tissues

- such as those derived from the same tissue sources but found in different anatomical areas.

Ultrasound imaging can indirectly estimate and image tissues' elastic properties based on externally or internally induced internal tissue motion (Cohn et. al. 1997a, Cohn et. al. 1997b, Hollman et. al. 2002). SAM was developed to image tissue stiffness at high resolution. The hypotheses tested on this experimental system demonstrate the potential to develop a real-time, clinical system. These were critical initial tests toward such a development to understand the structure and function of cells and tissues. Further compression tests using the in-house constructed cylindrical piston compressor validated the SAM elasticity results for the engineered and natural tissue specimens.

The thermally stressed EVPOMEs show similar characteristics to the unseeded AlloDerm® scaffold: high surface variations and stiffness properties. Additional experiments to regulate EVPOME's physical environment in order to better understand its robustness is discussed under the section on future studies.

We tested the elastic properties of all the tissues based on the 1-term Ogden model as it is ideal for testing materials that are non-linearly elastic, isotropic, incompressible and generally independent of strain rate (Bathe). Many biological tissues (in this case, skin and oral mucosa) fit the criteria of such hyperelastic materials. The Ogden material model was used in these studies to simulate the behavior of non-linear tissues, particularly the relation between an

imposed displacement and the resulting reaction force can be used to identify these material parameters using a mixed numerical-experimental approach.

The slopes of the linear portion of the viscous stress-strain curves were 5.37, 7.05 and 4.35 for human skin, AlloDerm® and processed dermis, respectively. Fibril lengths calculated from the slopes of the viscous stress-strain curves in the region of strain above 0.4 are listed in Table 1 and are 54.8 nm, 63.7 nm and 48.8 nm for human skin, AlloDerm® and processed dermis, respectively.

One of the principal challenges encountered in this research involved studying the elasticity of the mucosal tissues – both natural and engineered. Because there are no previous stress-strain models for either natural or engineered oral mucosal tissues to which to compare our studies, we examined the stress-strain models of skin. This was followed by performing the same stress-strain analyses on the different oral tissues, AlloDerm®, and finally EVPOME at 11-day post-seeding; these were then compared to existing skin elasticity models for accuracy of methods. Skin was the preferred tissue to make these comparisons since it is morphologically similar to the oral mucosal tissues – being derived from the same ectoderm tissues during embryologic development.

Future Studies

There are numerous experiments which need to be performed to better assess the physical and biological properties of the tissues studied in this dissertation. First and foremost are using Ogden and Hookean models to examine and compare the individual tissues' stress to stretch relationships.

Other experiments to be performed in the near-future include SAM 3D deformation imaging and motion processing (to image strain, confocal images of the different tissue specimens will be taken before and after deformation). Before measurements, the tissues will be in slight contact with the deformation plate. Two surface deformation steps of 50 μm will then be applied, capturing ultrasound data at no deformation and at each step. Speckle is to be tracked between these images with a correlation-based algorithm (Lubinski et al 1999).

Additional future applications for SAM include the aforementioned possibility of monitoring EVPOME growth and development under aseptic conditions. The non-destructive/non-invasive qualities of ultrasound serve as a vehicle to image and assess biological materials more accurately as they appear *in vitro*. Finally, long-term studies will consider SAM imaging and monitoring cell and tissues *in situ* to better understand and assess their functions in living systems. Such cases would provide strong support for SAM as an effective tool for any biological/medical laboratory involved in microscopy.

Other potential uses of SAM include examining the elastic properties of mucosal tissues – this time to include vaginal and uterine tissues – and to further compare both natural and engineered tissue elastic characteristics. Such objectives involve producing high-resolution strain images of the aforementioned mucosal tissues and EVPOME. These elastic properties can then be compared and potentially validated to stress-strain tests on the same tissues using the in-house piston compressor.

Based on the experiments performed using SAM detailed under Chapters II-IV, new tests will be performed to correlate the evolution and differentiation of EVPOME determined through analyzing changes in its cellular morphology. These would include examining and comparing how the cells and tissues look over certain time points (ie: 1-day, 2-days, 4-days, 7-days, and 11-days post-seeding); all work performed under sterile conditions on the same specimen to insure accuracy in its development. Subsequent tests – including mass spectrometry and possibly chromatography and Western blotting – are to verify the SAM experiments: quantify subcellular materials which contribute to the elastic properties of the tissues, including elastin and collagen.

Long-term research to better understand the soft tissues' physical and biological properties require studying these principal factors:

1. Examining whether regenerated mucosal tissues come close to mimicking natural tissues

2. Determining what the cell turnover rates are in the skin and comparing them to the oral cavity

3. Examining the normal mucosal tissues of the uterus and comparing the deformation characteristics

4. Considering the mechanical properties of other comparable soft tissues (ie: ureter, vaginal mucosal tissues)

These same factors can and should be applied to other surrogate tissue models and scaffolds for examination using SAM. This non-invasive and non-destructive imaging method has the additional yet-untested potential to examine engineered tissue implants adaptability and differentiation *in vivo*. This aim is currently beyond the scope of this dissertation, but clearly future studies should examine the possibility of using SAM to study bioengineered implants in animal models; the current in-house SAM is designed to accommodate small rodent species such as mice and rats when the appropriate protocols for performing these experiments are in place.

## REFERENCES


Bathe, K-J. *Finite Element Procedures.* NJ: Prentice-Hall. 1996. 1037pp.

Cohn, N.A., Emelianov, S.Y., Lubinski, M.A., O'Donnell, M. An Elasticity Microscope. Part I: Methods. *IEEE Trans. Ultrason. Ferr. Freq. Ctrl.* 1997. 44(6): 1304-1319.

Cohn, N.A., Emelianov, S.Y., O'Donnell, M. An Elasticity Microscope. Part II: Experimental Results. *IEEE Trans. Ultrason. Ferr. Freq. Ctrl.* 1997. 44(6): 1320-1331.

Hollman, K.W., Emelianov, S.Y., Neiss, J.H., Jotyan, G., Spooner, G.J.R., Juhasz, T., Kurtz, R.M., O'Donnell, M. Strain Imaging of Corneal Tissue With an Ultrasound Elasticity Microscope. *Cornea.* 2002. 21(1): 68-73.

Hotta, T., Yokoo, S., Terashi, H., Komori, T. Clinical and Histopathological Analysis of Healing Process of Intraoral Reconstruction with *Ex Vivo* Produced Oral Mucosa Equivalent. *Kobe J. Med. Sci.*, 2007. 53(1): 1-14.

Izumi, K., Feinberg, S.E., Iida, A., Yoshizawa, M. Intraoral Grafting of an *Ex Vivo* Produced Oral Mucosa Equivalent: A Preliminary Report. *Int. J. Oral Maxillofac. Surg.* 2003. 32: 188–197.

Izumi, K., Song, J., Feinberg, S.E. Development of a Tissue-Engineered Human Oral Mucosa: From the Bench to the Bed Side. *Cells Tissues Organs.* 2004. 176:134–152.

Lin, W.C., Chang, C.Y.Y., Shen, Y.Y., Tsai, H.D. Use of Autologous Buccal Mucosa for Vaginoplasty: A Study of Eight Cases. *Human Reproduction*. 2003. 18(3): 604-607.

Lubinski, M.A., Emelianov, S.A., O'Donnell, M. Speckle Tracking Methods for Ultrasonic Elasticity Imaging Using Short-Time Correlation. *IEEE Trans. Ultrason, Ferroelect. Freq. Cont.* 1999. 46(1): 82-96.

Winterroth, F., Lee, J., Kuo, S., Fowlkes, J.B., Feinberg, S.E., Hollister, S.J., Hollman, K.W. Acoustic Microscopy Analyses to Determine Good vs. Failed Tissue Engineered Oral Mucosa Under Normal or Thermally Stressed Culture Conditions. *Annals Biomed. Eng.* 2010. 39(1): 44-52.

Winterroth, F., Hollman, K.W., Feinberg, S.E., Kuo, S., Izumi, K., Hollister, S.J., Fowlkes, J.B.. Examination and Characterization of Human Mucosal Tissue Differentiation Using Scanning Acoustic Microscopy. *Ultrasound in Medicine and Biology.* 2011. (Submitted).